Title
RESULTS OF SPECTRAL AND ANGULAR SKY RADIATION MEASUREMENT PROGRAM

Authors
Martin, Mario
Berdahl, Paul.

Publication Date
1982-07-01

UC-59
LBID-592

Lawrence Berkeley Laboratory
UNIVERSITY OF CALIFORNIA

ENERGY & ENVIRONMENT DIVISION

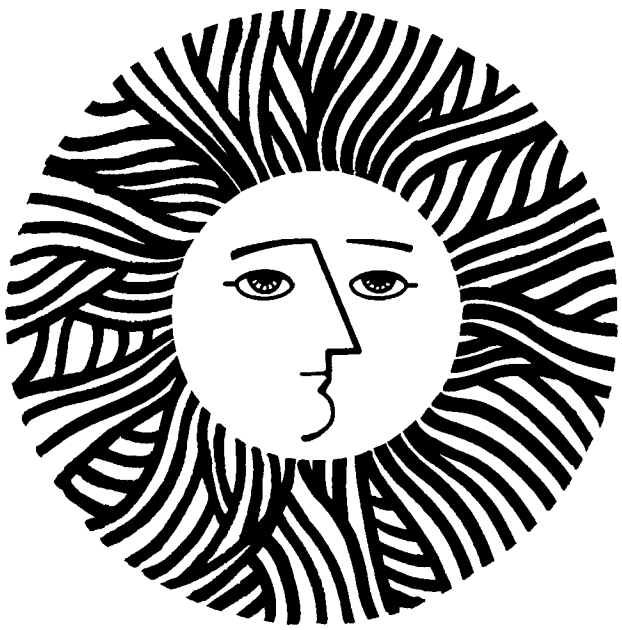

DISCLAIMER

RESULTS OF SPECTRAL AND ANGULAR SKY RADIATION MEASUREMENT PROGRAM*

Marlo Martin and Paul Berdahl
Lawrence Berkeley Laboratory
University of California
Berkeley, California 94720

Abstract

Results are analyzed and plotted from a series of more than 50 thousand spectral infrared sky radiation measurements made in 6 U.S. cities over a 1-1/2 year period. The data has been edited to arrive at monthly averages for 42 spectral and angular sky emissivity components under both clear sky and all sky conditions. An empirical sky emissivity equation has been developed and validated to allow one to disaggregate the total sky emissivity ε_r, as would be measured by a pyrgeometer, into its spectral and angular components. Such information is of special relevance to the performance of radiative cooling systems, especially those designed to make use of angular and/or spectral selectivity to enhance their performance.

*This work was supported by the Assistant Secretary for Conservation and Renewable Energy, Office of Solar Heat Technologies, Passive and Hybrid Solar Energy Division of the U.S. Department of Energy under Contract No. DE-AC03-76 SF00098.

1. Introduction

The heat balance of the earth is determined by two heat sources and one heat sink. The sources are incident absorbed solar radiation and the relatively smaller amount of heat generated in the core of the planet by nuclear reactions. The only heat sink available is in the form of thermal infrared radiation from the earth's surface and atmosphere into outer space. The net radiative heat loss from an object at the earth's surface is given by the difference between the outward radiated flux and the inward fluxes due to emissions from the atmosphere and radiation from outer space. Since the radiative temperature of interstellar space is low (approx. $4^{o}K$) it effectively contributes nothing to the inward flux. The outward flux from a radiator of known emissivity can be simply determined if its surface temperature is known, by means of the Stefan-Boltzman equation:*

$$R_r = \varepsilon_r \sigma T_r^4$$

where $\sigma = 5.67 \times 10^{-8} Wm^{-2}K^{-4}$, T_r is expressed in degrees Kelvin, and ε_r is a constant lying between 0 and 1.

It is apparent that a complete quantitative description of the radiative cooling rate from a surface exposed to the sky depends on an accurate knowledge of the incident radiative flux from the atmosphere. The atmosphere consists of a mixture of gases and particulates, only some of which are strong emitters in the thermal infrared region of the spectrum (approximately 5 to 40 micrometer wavelengths). Droplets of

*For simplicity, we are assuming that ε_r is independent of wavelength and angle, as is often the case. Equation 1 is not sufficiently general to apply to selective radiators.

water, as found in clouds, fog, and maritime haze, act essentially like blackbody radiators for which the outward flux is related to the droplet temperature by Equation 1 with $\varepsilon_r = 1$. Dry particulates generally have a low emissivity and do not contribute strongly to the atmospheric radiation unless they form nucleation centers for the condensation of water vapor [1].

Infrared emission also occurs strongly from carbon dioxide and water vapor molecules. The radiation has a spectral dependence characteristic of the molecule, and the intensity of emission depends on the air temperature in the vicinity of the molecule. Although the concentration of CO_2 does not vary appreciably through the atmosphere, the amount of water vapor present generally decreases with altitude, as does the temperature. The downward radiation from the atmosphere thus depends strongly on the vertical temperature and water vapor profiles, and on the presence and temperature of clouds. For a review of infrared optical properties of atmospheric constituents, see chapter 5 of Reference 2.

The spectral dependence of sky radiation for a typical clear sky summer condition is shown in Figure 1, based on earlier work by our group [1,3]. The curve labeled 0^o represents the radiation incident from the zenith direction. The peak of radiation centered at about 7 micrometers is associated with an emission band from water vapor molecules, and that at 15 micrometers is largely due to carbon dioxide emission. The small peak at 9.6 micrometers is attributable to atmospheric ozone. In addition, the entire region shown in Figure 1 has a radiation contribution due to continuum water vapor emission which is

important in determining the overall shape of the sky radiation spectrum, especially within the 8 to 13 micron window region [4]. As the zenith angle increases toward the horizon (90^o) the instrument measures radiation emitted preferentially along a path in the lower atmosphere having higher temperatures and relatively large concentrations of water vapor.

In this paper we report on detailed spectral measurements of the sky radiation taken in six U.S. locations; Tucson, AZ, San Antonio, TX, St. Louis, MO, Gaithersburg, MD, West Palm Beach, FL, and Boulder City, NV. The radiometers used in this study were developed at Lawrence Berkeley Laboratory to measure the incident sky radiation through a 2^o field of view at five zenith angles (0^o, 20^o, 40^o, 60^o, 80^o). At each angular position, the incident radiation was recorded through seven infrared filters for which the transmission characteristics are presented in Figure 2. The "no filter" channel actually represents the spectral radiation passing through a coated germanium lens. The remaining six channels will be referred to in terms of their central wavelengths or their pass bands; 8.8 μm, 9.6 μm, 11 μm, 8-14 μm, 15 μm, and 17-22 μm.

During the course of approximately 1-1/2 years of measurements readings were taken at half hour intervals. Analysis of the resulting data base yielded a total of 57 months of good data from among the six locations. Radiation measurements were averaged over each month for all seven filter channels and for each of the five zenith angles. This data is plotted as a function of the total sky emissivity in a series of graphs presented in section 4.

Sky radiation data can be expressed in a number of ways which are essentially equivalent, but differ in their ease of interpretation. The sky radiance $R_s(\lambda, \theta)$ which is a function of wavelength λ and zenith angle θ is the quantity most directly related to the net radiative heat flux at any time. This quantity is not expressed by means of an equation similar to Eq.1 because the sky does not radiate as a blackbody, as can be seen from the typical radiation profiles of Figure 1. An effective "sky temperature" T_s can be defined as being the temperature of a blackbody for which the emitted radiative flux is the same as for the sky:

$$R_s = \sigma T_s^4 \tag{2}$$

where R_s is the measured incident flux containing all thermal wavelengths from the sky. The objections to using an effective sky temperature are twofold; first, the concept of temperature refers to a body in thermal equilibrium in a well defined state, whereas the sky consists of a gradation of layers at different temperatures, whose spectral emissivity changes as a function of altitude. Due to the partial transparency of the air layers, the observer in reality "sees" a weighted average of temperatures from each layer which is a function of the wavelength. The second objection is more pragmatic in nature. The "sky temperature" as defined in Equation 2 fluctuates strongly with the ambient air temperature T_a throughout the day [3]. The changes in apparent emissivity of the sky can thus be masked to a great extent by ambient air temperature changes. In this report we choose to express the sky radiation data in terms of the spectral and angular sky emissivity $\varepsilon_s(\lambda,\theta)$, which is defined to yield the spectral sky radiance

$$R_s(\lambda,\theta) = \epsilon_s(\lambda,\theta)B_a(\lambda). \tag{3}$$

Here $B_a(\lambda)$ is the Planck function evaluated with the ambient air temperature T_a (^oK). The temperature T_a is to be measured in the conventional meteorological fashion at a height of 1 to 2 meters above the ground. The Planck function is given explicitly by

$$B_a(\lambda) = 2hc^2\lambda^{-5}\left[\exp\left(\frac{hc}{\lambda k_B T_a}\right)-1\right]^{-1}, \tag{4}$$

where h is Planck's constant (6.626×10^{-34} Js), k_B is Boltzmann's constant (1.381×10^{-23} J K^{-1}), and c is the speed of light (2.998×10^8 m s^{-1}).

Under clear sky conditions, the value $\epsilon_s(\lambda,\theta)$ remains practically constant throughout the day. Multiplication by the factor containing T_a allows the incident radiance to be calculated readily, since air temperatures are available for most locations. The total incident sky radiation received by a horizontal surface is obtained by integration of equation (3) over all wavelengths and zenith angles.

$$R_s = 2\pi\int_o^\infty d\lambda B_a(\lambda)\int_o^1 \cos\theta \; d\cos\theta \epsilon_s(\lambda,\theta). \tag{5}$$

The total sky emissivity ϵ_s may be defined by

$$R_s = \epsilon_s \sigma T_a^4, \tag{6}$$

analogous to Eq.(3). Equations (5) and (6) can be used to express the total sky emissivity in the form

$$\epsilon_s = \frac{\int_o^\infty d\lambda B_a(\lambda)\int_o^1 \cos\theta \; d\cos\theta \epsilon_s(\lambda,\theta)}{\int_o^\infty d\lambda B_a(\lambda)\int_o^1 \cos\theta \; d\cos\theta} \tag{7}$$

which shows that ϵ_s is a weighted average of $\epsilon_s(\lambda,\theta)$.

2. Description of Measurements

2a) Overview

The basic spectral sky radiance measurements were made with a radiometer developed by at Lawrence Berkeley Laboratory. Preliminary discussions of the instrumentation and portions off the measured data have been presented elsewhere [3, 5-11]. Measurements of the radiance in seven spectral bands at each of 5 zenith angles were obtained at half hour intervals. Immediately following these measurements a blackbody reference radiation source was viewed through each of the filter channels. The total thermal infrared sky radiance was also measured with an Eppley pyrgeometer. Auxiliary information recorded at the same time included: mirror temperature, blackbody temperature, several reference voltages, and conventional meteorological observations of air and dewpoint temperatures with radiation-shielded, aspirated sensors. A rain sensor recorded the presence or absence of precipitation. During periods when rain was falling, no radiance measurements were performed. The data thus obtained was stored in random access memory of the on-site microcomputer system which also controlled the operation of the radiometer. Data was transferred to the Lawrence Berkeley Laboratory computer system by telephone at intervals of one to three days. This arrangement for data transfer was particularly useful because equipment failures could usually be identified in a few day's time. The raw radiance data thus acquired was processed by a computer program which produces calibration constants for each day of normal radiometer operation, for each filter channel. This program also makes corrections for the small amount of thermal radiance produced by the viewing mirror. The data was then subjected to various automated quality control checks to flag

suspicious or erroneous data, as explained more fully below. Finally, the data was edited manually to identify unforeseen problems and to ensure that good data was not inadvertently deleted by the quality control procedures.

The resulting "prime" data set is summarized in Table 1. The six locations at which measurements were made are located in the southern United States, with the majority of the data collected during the warm months in which air conditioning may be required. The data set contains 50,000 half hourly observations of the 35 spectral radiances measured. Of these observations, 31,000 were obtained during clear sky conditions and 19,000 were obtained with clouds present. (The measured radiances were used to detect the presence of clouds, using the methodology developed earlier in this project [3]). Observations prevented by rain numbered 1300. The data collected is sufficiently extensive to give a statistical picture of the spectral and angular distribution of thermal sky radiance in the southern United States.

The following subsections present a more detailed description of the instrumentation and a discussion of the processes of calibration and data editing.

2.b) Instrumentation

The spectral infrared filter radiometer developed for these sky radiance measurements is based on a commercially available instrument, the Barnes Engineering Corporation's model 12-880 radiometer. This instrument includes a gold plated chopper to modulate incoming infrared radiation, a coated germanium lens, a filter wheel, and a pyroelectric

Table 1: Summary of "prime" data set.

Site	Month	Year	Clear sky observations	Cloudy sky observations	All sky observations	Observations prevented by rain	Average air temperature (°C)	Average dewpoint temperature (°C)
TUCSON, AZ	5	1979	303	294	597	(3)	23.5	8.1
TUCSON, AZ	6	1979	732	418	1150	(6)	28.2	4.9
TUCSON, AZ	7	1979	1004	383	1387	(0)	30.7	10.7
TUCSON, AZ	8	1979	677	281	958	(0)	27.9	13.3
TUCSON, AZ	9	1979	816	112	928	(0)	29.4	8.6
TUCSON, AZ	10	1979	1042	135	1177	(0)	23.6	2.2
TUCSON, AZ	11	1979	403	162	565	(4)	15.3	-2.8
TUCSON, AZ	12	1979	768	306	1074	(4)	13.5	-4.1
TUCSON, AZ	1	1980	344	351	695	(13)	12.0	1.5
TUCSON, AZ	2	1980	702	431	1133	(33)	13.9	2.7
TUCSON, AZ	3	1980	941	493	1434	(31)	14.2	-.2
TUCSON, AZ	4	1980	1015	277	1292	(4)	19.0	-1.4
TUCSON, AZ	5	1980	322	109	431	(0)	22.0	1.9
SAN ANTONIO, TX	5	1979	274	340	614	(10)	22.3	15.8
SAN ANTONIO, TX	6	1979	488	300	788	(68)	25.6	18.2
SAN ANTONIO, TX	7	1979	447	439	886	(16)	27.5	22.4
SAN ANTONIO, TX	11	1979	341	303	644	(8)	13.0	3.8
SAN ANTONIO, TX	12	1979	420	581	1001	(14)	12.2	4.4
SAN ANTONIO, TX	1	1980	520	723	1243	(5)	11.7	5.3
SAN ANTONIO, TX	2	1980	291	234	525	(2)	11.2	2.3
SAN ANTONIO, TX	3	1980	254	346	600	(9)	15.4	5.2
SAN ANTONIO, TX	4	1980	477	334	811	(3)	20.5	9.2
SAN ANTONIO, TX	5	1980	580	854	1434	(18)	23.1	18.5
SAN ANTONIO, TX	6	1980	894	545	1439	(1)	28.6	20.9
SAN ANTONIO, TX	7	1980	681	233	914	(1)	29.9	20.6
GAITHERSBURG, MD	6	1979	179	141	320	(11)	20.1	14.0
GAITHERSBURG, MD	7	1979	559	681	1240	(22)	22.7	18.2
GAITHERSBURG, MD	8	1979	558	321	879	(21)	22.4	17.8
GAITHERSBURG, MD	9	1979	676	546	1222	(20)	19.3	15.3
GAITHERSBURG, MD	10	1979	503	479	982	(40)	13.2	9.8
GAITHERSBURG, MD	11	1979	344	235	579	(14)	12.9	7.5
GAITHERSBURG, MD	1	1980	336	714	1050	(37)	.1	-6.8
GAITHERSBURG, MD	2	1980	583	535	1118	(13)	-1.0	-9.6
GAITHERSBURG, MD	3	1980	438	788	1225	(38)	5.1	-2.8
GAITHERSBURG, MD	4	1980	319	354	673	(10)	12.4	3.7
ST. LOUIS, MO	7	1979	520	252	772	(70)	26.2	17.3
ST. LOUIS, MO	8	1979	636	295	931	(70)	26.1	19.4
ST. LOUIS, MO	9	1979	1190	222	1412	(1)	21.4	12.0
ST. LOUIS, MO	10	1979	844	558	1402	(69)	14.8	5.3
ST. LOUIS, MO	11	1979	266	585	851	(70)	6.0	-1.7
ST. LOUIS, MO	12	1979	400	515	915	(70)	3.8	-5.8
ST. LOUIS, MO	4	1980	482	395	877	(70)	14.3	2.5
ST. LOUIS, MO	5	1980	568	259	827	(70)	19.2	7.4
ST. LOUIS, MO	6	1980	772	315	1087	(32)	23.7	13.2
ST. LOUIS, MO	7	1980	762	155	917	(51)	28.5	18.7
ST. LOUIS, MO	8	1980	744	136	880	(9)	28.5	18.3
ST. LOUIS, MO	9	1980	418	123	541	(26)	24.2	16.6
ST. LOUIS, MO	10	1980	852	305	1157	(70)	13.2	3.5
ST. LOUIS, MO	11	1980	415	34	449	(0)	14.4	2.4
ST. LOUIS, MO	12	1980	302	409	711	(70)	4.2	-2.3
WEST PALM BEACH, FL	7	1980	272	161	433	(28)	27.0	23.5
WEST PALM BEACH, FL	8	1980	155	92	247	(51)	27.8	24.0
WEST PALM BEACH, FL	9	1980	268	198	466	(27)	26.8	23.2
BOULDER CITY, NV	6	1980	241	52	293	(0)	29.4	-1.8
BOULDER CITY, NV	7	1980	588	189	777	(14)	31.0	5.7
BOULDER CITY, NV	8	1980	702	58	760	(0)	32.1	5.5
BOULDER CITY, NV	9	1980	207	83	290	(1)	29.3	6.4
TOTAL OR AVERAGE			30835	19169	50004	(1362)	19.1	8.0

detector. The field of view of the radiometer is approximately 2 degrees (full width at half maximum). Infrared bandpass filters were selected to delineate the main features of the "typical" atmospheric spectrum. In particular, the 8.8, 9.6, and 11 micrometer filters were selected to obtain information concerning the distribution of radiation within the 8 to 13 micrometer window. (Compare Figures 1 and 2.)

The instrument is provided with a stepping motor drive to turn the filter wheel through eight positions. One of the positions is an opaque "filter," which is used to monitor the instrument's output offset voltage. A front surface gold plated mirror is mounted at a 45 degree angle on the optical axis of the radiometer. Rotation of this mirror permits the radiometer to view an arc of the sky from the north horizon to the zenith. When the instrument is not actively making measurements, the mirror assembly is rotated to a position which prevents intrusion of dust, rain, and other environmental contaminants. Further protection is provided against dust and rain by a fan which maintains a positive pressure inside the instrument case.

An important feature of the radiometer is the attached blackbody radiation source which is viewed each half hour by the radiometer, as it permits accurate calibrations on a daily basis.

The output voltage of the radiometer is measured by the microcomputer data acquisition system's analog-to-digital converter. For each measured radiance the output voltage is sampled 50 times over a 3 second interval and the average value stored in the computer's memory. The output voltage with an opaque filter in place is measured in a similar fashion and subtracted from the value in memory. These manipulations

have the effect of limiting the noise bandwidth of the measurements.

Four spectral radiometers systems were constructed and initially deployed at Tucson, AZ (August, 1978), San Antonio, TX (September, 1978), Gaithersburg, MD (November, 1978), and St. Louis, MO (June, 1979). As initially constructed, the radiometers could measure only zenith radiances (for budgetary reasons). During the first few months of operation, a number of system improvements were devised, including the ability to scan from the north horizon to the zenith. Calibration techniques were improved, and the scanning mirrors were replaced with evaporated front-surface gold mirrors to reduce the size of the corrections required to account for the mirror emissivity. Thus the "prime" data, measured at multiple zenith angles, begins in May, 1979 as shown in Table 1. The older data will not be discussed further here; however a brief report on this data was presented at the San Jose National Passive Solar Conference [6].

2.c) Calibration and Data Editing

As mentioned previously, the spectral radiometer was calibrated each day using the radiance data obtained by viewing the blackbody cavity radiation source at half hour intervals. The temperature of the source is measured with a thermistor. Once the temperature is known, the blackbody's spectral radiance can be easily calculated, for example by using Eq.4. The source temperature is controlled at about 70 degrees Celsius most of the day but is turned off under microprocessor control and allowed to cool to ambient temperature early each morning. The temperature of the viewing mirror also varies during each day, following the ambient temperature. A least squares fit of measured and calculated

blackbody radiances is performed for each filter channel to determine the calibration constant and the mirror emissivity correction. The variation of temperature of the blackbody during the calibration period substantially improves the accuracy of the calibration. If the residual root mean square radiance error is greater than 0.1 W m^{-2} sr^{-1} $micron^{-1}$, the calibration is aborted and values from the previous day are employed. (The spectral radiance of a 300°K black body at 10 microns is about 10 W m^{-2} sr^{-1} $micron^{-1}$, so the value 0.1 represents roughly 1% error.)

The primary quality control measure for the spectral radiometer radiance data is the comparison of measured blackbody radiance with the calculated value based on the calibration constants in use. For each half hourly set of measurements, if the blackbody radiance departs from the expected value by more than 0.25 W m^{-2} sr^{-1} $micron^{-1}$ in any filter channel the data from that observation is flagged as suspect and is not used. This powerful test detects virtually all of the known erroneous data produced by the spectral radiometer.

The manual editing procedure relied primarily on inspection of the entire data set as printed out on microfiche. However, two types of graphic displays were used. Graphical displays of data were examined for days chosen at random. Also, graphical displays of the daily calibration constants were examined for the entire data set in order to locate changes indicative of malfunctions.

As a result of the editing process, some of the data was processed in a special manner. For example, the rain detector at St. Louis failed in a way which gave a continuous indication of rain. It thus became

necessary to estimate the number of measurements genuinely lost due to rain rather than equipment malfunction. Another, more important problem occurred because the air temperature sensor used at San Antonio indicated values in error by about 2 degrees Celsius over most of the period of data acquisition. In this case the measured radiance derived from the 15 micrometer filter at a zenith angle of 80 degrees was used to infer the air temperature. This procedure appears to give values accurate to within 1 degree Celsius, and is probably better for average values.

2.d) Limitations of the Pyrgeometer Data

The pyrgeometer data is quite important for our analysis because it measures the total downward thermal flux from the atmosphere. We wish to develop here approximate methods whereby spectral fluxes can be derived from the total flux. We thus require, and will subsequently present, correlations of various spectral emissivities with the total emissivity. Unfortunately, the pyrgeometer data has a number of limitations. Some of the wintertime data is missing because the pyrgeometers were returned to the manufacturer for recalibration. Data was also lost due to battery failure and other equipment problems. Thus the number of months of data for which simultaneous pyrgeometer measurements accompany all the spectral radiometer measurements is only a fraction of the full data set (29 of 57 months).

Another difficulty lies in the fact that the 2 or 3 % errors typical of pyrgeometer data are undesirable. In a previous paper [3] we succeeded in transferring a monthly calibration from the spectral radiometer to the pyrgeometer to reduce these errors, but the process is

rather laborious. Furthermore, this process --- even when complete --- would only extend the useful data set to 29 months.

Still a third difficulty occurs because the pyrgeometer data is biased during daylight hours due to the absorption of sunlight by its silicon dome. The warmed dome transfers heat to the radiation sensing thermopile by conduction, leading to experimental error. This issue is discussed at some length in reference [3].

As a result of these experimental difficulties, we shall avoid using the pyrgeometer data whenever possible. Instead we employ a quantity called the pseudo pyrgeometer to develop correlations with the spectral data, and use a separate correlation between pyrgeometer and pseudo pyrgeometer to express final results in terms of pyrgeometer measurements.

Our discussion of the limitations of the pyrgeometer should not be interpreted as an indictment of the particular instrument used. We have no reason to believe that any currently available instrument is superior.

3. Analysis of the Experimental Measurements

3a) The Sky Radiance Equation

An empirical equation has been developed to describe the spectral sky emissivity $\varepsilon_s(\lambda,\theta)$ as a function of zenith angle θ and total sky emissivity ε_s. The spectral emissivity of the sky can be written in terms of the apparent sky transmissivity:

$$\varepsilon_s(\lambda,\theta) = 1 - \tau(\lambda,\theta) \tag{8}$$

We make the assumption that the wavelength and angular dependences can be separated, and that the angle enters in the form

$$\varepsilon_s(\lambda,\theta) = 1 - At(\lambda)e^{-b/\cos\theta} \tag{9}$$

where $1/\cos\theta$ is the air mass. The constant A can be determined by the condition that $\varepsilon_s(\lambda,\theta)$ averaged over all wavelengths and over the angles 0 to 90^0 corresponding to the sky dome must equal the total sky emissivity ε_s (Eq.7):

$$\varepsilon_s = 1 - 2A\bar{t}\int_0^1 e^{-b/\cos\theta}\cos\theta \; d\cos\theta \tag{10}$$

$$\text{where} \quad \bar{t} = \int_0^\infty d\lambda t(\lambda)\, B_a(\lambda) / \int_0^\infty d\lambda B_a(\lambda),$$

and $B_a(\lambda)$ is the Planck function corresponding to an ambient temperature T_a. The integral over $d\cos\theta$ in Equation (10) is equal to twice the third exponential integral [12], $2E_3(b)$, which can be well approximated over the range of interest ($0 <= b <= 0.6$) by the exponential function $e^{-1.7b}$. We can thus write Equation (10) as:

$$\varepsilon_s = 1 - \bar{t}\,A\,e^{-1.7b}$$

which yields an expression for A,

$$A = (1 - \varepsilon_s)\, e^{1.7b} / \bar{t}$$

Substitution in Equation (9) results in the sky radiance equation:

$$\varepsilon_s(\lambda,\theta) = 1 - (1 - \varepsilon_s)\left[t(\lambda)/\overline{t}\right] e^{b(1.7-1/\cos\theta)} \qquad (11)$$

The expressions $t(\lambda)/\overline{t}$ and b implicitly contain a dependence on the total sky emissivity ε_s, which will be determined by analysis of the experimental data.

3b) Determination of Total Sky Emissivity

The spectral radiometer used to make the sky radiation measurements was considered to be a more accurate instrument than the pyrgeometer. After each set of measurements (every half hour) the sensor was directed into a blackbody reference cavity of known temperature. Once a day the cavity was caused to pass through a fixed temperature range allowing an absolute calibration of the radiometer to be carried out. The pyrgeometer cannot be calibrated as readily, and is thus considered to be less accurate. Furthermore, the radiometer readings are not affected by the sun, whereas a correction must be applied to pyrgeometer readings due to heating of the silicon dome by shortwave solar radiation.

For these reasons, a quantity called the "pseudo pyrgeometer" was derived from the recorded data. The emissivities measured at each zenith angle with the "no filter" channel are weighted by the solid angle subtended by them in the sky dome, and by the cosine of the zenith angle to account for their projection onto a horizontal surface. The quantity thus constructed behaves like a pyrgeometer reading, if the pyrgeometer

is averaged over a sufficient interval to smooth out fluctuations due to cloud assymetry. A plot showing the pseudo pyrgeometer as a function of dewpoint temperature is presented in Figure (3). The straight line in the figure is a least square fit to the 57 monthly average pseudo pyrgeometer values:

$$\varepsilon_{ps} = 0.00831\ T_{dp} + 0.6033 \tag{12}$$

where T_{dp} is the dewpoint temperature in degrees Celsius. Each of the measured average monthly spectral sky emissivities $\varepsilon(\lambda,\theta)$ can be plotted against the pseudo pyrgeometer reading, where ε_{ps} replaces ε_s in Equation (11). The advantage of doing so is that this equation provides a good fit to the data points taken under all sky conditions, as well as under the clear sky conditions used to empirically establish the constants in the equation. However, since the pseudo pyrgeometer is not a readily available instrument, it is more desirable to express the equation in terms of the true total sky emissivity as would be measured by a properly calibrated pyrgeometer.

A relationship can be derived between the pseudo pyrgeometer (Equation 12) and the pyrgeometer reading based on the correlation developed by Berdahl and Fromberg [3], which can be expressed as

$$\varepsilon_s = 0.00614\ T_{dp} + 0.734 \tag{13}$$

This equation was originally developed by analyzing 11 months of clear sky data, and applying correction factors to account for daytime solar heating of the pyrgeometer and small calibration corrections. In applying this equation to the data based on 57 months of clear sky data

it was found necessary to adjust the relationship given in Equation (13) to read

$$\varepsilon_s = 0.00696 \; T_{dp} + 0.709. \qquad (14)$$

The reason for this adjustment is that the mean clear sky conditions for the original 11 month data set were systematically (if slightly) different from conditions for the full 57 month data set. The full data set indicates slightly low emissivities for a given dewpoint temperature. To maintain consistency in our analysis we require a relationship between ε_s and T_{dp} based on the entire 57 month data set. The adjustment of Equation 13 to produce Equation 14 was determined by evaluating the difference between the two data sets using the pseudo pyrgeometer and then using the approximate relation

$$\Delta\varepsilon_s \simeq 0.84 \; \Delta\varepsilon_{ps}$$

to determine the adjustment required. In principle Equation 14 is an improvement over Equation 13 because it is based on more data. However, the difference is small, especially at dewpoint temperatures above 0^oC, and the current derivation is somewhat indirect. The utility of Equation 14 in the present context is that it is consistent with Equation 12, especially since it is based on the same data set. Eliminating the dewpoint temperature between equations (12) and (14), one arrives at the desired expression for total sky emissivity ε_s as a function of the pseudo pyrgeometer value ε_{ps} .

$$\varepsilon_s = 0.838 \; \varepsilon_{ps} + 0.204 \qquad (15)$$

This relationship is plotted in Figure 4, along with the data points

which display measured pseudo pyrgeometer values versus the measured pyrgeometer values for clear skies. The small systematic difference between the derived line and the data is due to the effect of sunlight on the pyrgeometer. If it were possible to correct the pyrgeometer observations for this error, agreement would be better. The same relationship is presented in Figure 5, which shows the corresponding plot for all sky conditions. For the purposes of this paper the pyrgeometer values are always obtained from measured pseudo pyrgeometer values by the use of Equation 15.

3c) Determination of Parameters in the Sky Emissivity Equation

Equation (11) is of a form suggested by the physical phenomena taking place within the atmosphere. However, it is not a rigorously derived equation, and the primary purpose for introducing it at this time is to provide a concise analytical expression which adequately embodies the results of tens of thousands of individual spectral sky emissivity measurements. The nature of the transmissivity function $t(\lambda)$ has as yet been left undefined, except to state that it is related to the atmospheric spectral transmissivity (in the zenith direction). It is expected to be a function dependent on the total sky emissivity ε_s.

In order to fit the experimental data measured through seven infrared filters and five zenith angles, we consider the quantities $t(\lambda)/\bar{t}$ and b to be linear function of ε_s. In all four filter regions included in the atmospheric window (8-14 micrometers), and for the "no filter" case, the parameter b is a well defined linear function of ε_s. In the 15 micrometer channel there is only a slight dependence of either parameter on the total emissivity, since the atmosphere is optically dense at this wavelength. In other words, due to the fact that most 15 micrometer radiation reaching the detector originates within a few tens of meters from the instrument, the angular dependence described by the air mass term $(1/\cos\theta)$ is no longer of relevance. This is borne out by the fact that the average value of the parameter $t(\lambda)/\bar{t}$ approaches zero (approx 0.02), and each spectral emissivity, as well as the total emissivity approaches unity.

The other anomalous channel is the 17-22 micrometer region. Here

the clear sky data can be used to determine a least squares fit for the b-parameter, but a large amount of scatter exists. Again, as in the 15 micrometer case, the value of $t(\lambda)/\bar{t}$ is small (<= 0.2 for ε_s > 0.7) indicating a situation where all emissivities approach unity. The unique feature in this spectral region is that a secondary "window" begins to open at low values of ε_s (low dewpoint temperatures).

The results of performing least squares fits for the two parameters b and $t(\lambda)/\bar{t}$ to straight lines as a function of the total sky emissivity ε_s are presented in Table (2).

Table 2

Values of least squares fit parameters for use in Equation 11 to predict spectral sky emissivity.

	$b = A\varepsilon_s + B$		$t(\lambda)/\bar{t} = C\varepsilon_s + D$	
	A	B	C	D
"no filter"	1.4929	-0.8668	1.1243	0.5997
8-14μm	1.7915	-1.1127	1.8068	1.0340
8.8μm	1.2809	-0.7710	5.1191	-1.1922
9.6μm	1.3046	-0.7153	5.3211	-1.6090
11.0μm	1.7784	-1.1592	3.1744	0.4515
15.0μm	-5.7780	5.2576	0.0410	-0.0066
17-22μm	-0.6914	1.6528	-1.5486	1.2975

These values are substituted into the sky radiance equation (Equation 11) in order to produce the curved lines through the data points in

the graphs presented in section 4 (Figures 6-19). Clear sky data has been used to generate the parameters in Table 2, which have not been altered for presentation of the data from all sky conditions. In obtaining the values for these parameters, the b-coefficient is determined by fitting the data points at the zenith and 60° angles. Measurements at a zenith angle of 80° were judged to be of less practical importance for radiative cooling purposes due to the small projected area of a horizontal surface in that direction (cosine effect).

3d) Estimation of Total Sky Emissivity

The most straightforward way to obtain a value for the total sky emissivity ε_s is to measure it directly with a pyrgeometer. A correction to the reading allows compensation for heating of the silicon dome whenever the instrument is located in direct sunlight. Unfortunately, pyrgeometers are not common instruments, and little data from them is available on a long term basis. Even weather stations operated by the National Oceanic and Atmospheric Administration (NOAA) do not use such an instrument for routine measurements.

A correlation has been documented by Berdahl and Fromberg [3] for the total emissivity as a function of dewpoint temperature (°C). This correlation has been developed from clear sky pyrgeometer data which was subjected to the proper corrections to account for solar heating of the instrument. Berdahl and Fromberg report two linear relationships for this function [3]; one is a nighttime correlation; and the other is valid during the daytime:

$$\text{daytime} \quad \varepsilon_s = 0.0060 \; T_{dp} + 0.727 \tag{16a}$$

$$\text{nighttime } \varepsilon_s = 0.0062\ T_{dp} + 0.741 \qquad (16b)$$

A third relationship, valid for 24 hour average emissivities, can be obtained by simply averaging the coefficients of these two equations, and has been given as Equation 13.

Use of the linear fit which best describes the day/night conditions of interest in a given situation will yield total sky emissivities nearly as accurate as pyrgeometer readings if the clear sky condition is satisfied.

When clouds are present, a number of complexities are introduced into the estimation of the total sky emissivity. The temperature of the cloud base as well as its zenith angle and angular extent must properly be taken into consideration to produce accurate results. In practice this detailed an analysis is not usually feasible. One must be content with estimating the fraction of the sky vault covered by clouds, and the cloud base temperature must be roughly inferred from its altitude and the atmospheric lapse rate. The assumption is made that over a period of time the angular distribution of clouds as seen by an observer is uniform over the sky dome.

The method recommended here is that in the presence of clouds, the total sky emissivity be assigned a value [13]:

$$\varepsilon_s = \varepsilon_s^{clear} (1 - \Gamma n) + \Gamma n,$$

where ε_s^{clear} is the clear sky emissivity calculated from Equation 13 or 16, n is the estimated fraction of sky covered by clouds, and Γ is a parameter which depends on the cloud height and type. Values for

Γ range over 0.16 for cirrus clouds (height 12.2 km), 0.66 for altocumulus clouds (height 3.7 km), and 0.88 for stratocumulus clouds (height 1.2 km). Measurements in Atlanta, GA [14] and San Antonio, TX [15] indicate that a value of $\Gamma = 0.55$ to 0.6 can be used as an average for opaque clouds at these locations. Further information is available in the Mongraphs by Sellers [16] and Kondratyer [17].

Once the total sky emissivity has been determined by the above means, it can be used directly in the sky radiance equation, or one can use it to find the desired spectral emissivity from one of the graphs presented in section 4.

4. Discussion of Results

A total of 84 graphs are used to plot the spectral sky emissivities as a function of the total sky emissivity ϵ_s. Half of these graphs are used to plot monthly averaged emissivities over clear sky conditions only, and the other half plot the same quantities using data from all sky conditions. Each set of 42 graphs represents measurements made through seven infrared filters and six zenith angles (actually five angles and one composite channel referred to as the "global" measurement).

The seven filter regions can be further divided into three groups: (1) the "no filter" and 8-14 micrometer region, which are of most immediate applicability in the determination of radiative cooling rates from blackbody emitters and from selective radiators which emit throughout the atmospheric window; (2) the three narrow-band filters (see figure 2) which have been used to explore details of the emissivity within the window region; and (3) the 15 and 17-22 micrometer regions, which lie on the long wavelength side of the window, and do not contribute in an important way to cooling under warm ambient conditions.

4.1 "No filter" and 8-14 micrometer filter results (Figures 6 through 9)

Both the clear sky conditions and all sky conditions are well described by equation (11) using the parameters provided in Table (2). At a zenith angle of 80^o (10^o above the horizon) the equation consistently predicts larger emissivity values than are observed. In all cases it will be noted that the angular-weighted pseudo pyrgeometer measurement closely approximates the emissivity at a zenith angle of

50^{o}. For smaller zenith angles the sky emissivity varies only slightly achieving its lowest value in the overhead direction. As one approaches within 30^{o} of the horizon all the measured emissivities increase rapidly, confirming the known fact that a cooling surface should be in radiative contact with the upper portion of the sky dome. However, little is to be gained by focusing a radiator sharply toward the zenith, since the emissivity values do not begin to increase rapidly until within 30^{o} of the horizon.

The potential advantage of using a selective radiator which is highly emissive only within the 8-14 micrometer region is shown by an examination of the 8-14 micrometer global results (Figure 8a). The maximum temperature depression (below air temperature) which can be produced by a non-selective (blackbody) radiator is roughly proportional to $(1 - \varepsilon_s)$, the deviation of the total sky emissivity from unity. The maximum temperature depression which can be produced by an 8-14 micrometer selective radiator is proportional to the deviation of the corresponding emissivity from 1, with approximately the same constant of proportionality. Since the slope of the curve in Figure 8a is greater than 2, the maximum temperature depression achievable with an 8-14 micrometer selective surface is more than twice the value achievable with an ordinary blackbody radiator. This can be particularly beneficial under overheated conditions where the dewpoint temperature, and hence the total sky emissivity ε_s, is relatively high.

4.2 <u>8.8-9.6 -11.0 micrometer filters (Figures 10 through 15)</u>

The transmissivity functions of these three filters are all rela-

tively narrow banded, as can be seen in Figure 2. They sample the sky emissivity in the spectral region where the clear atmosphere is most highly transparent. Consequently, the radiation impinging on the detector originates largely from high altitudes and corresponds to the lower temperatures found at those altitudes. The ozone emission peak centered at 9.6 micrometers originates almost entirely in the ozone layer, typically (10-30 km) above the earth's surface.

A characteristic of measurements made through these filters is that the presence of cloud cover (as observed in the graphs where all sky conditions are plotted) causes greater scatter in the spectral emissivities than was observed in the broad banded filters discussed in section 4.1. Note that the presence of cloud cover always causes the spectral emissivity to increase above clear sky values at zenith angles less than 60^{o}, and to decrease at 80^{o}. This behavior is due to the fact that the emissivity of cloud skies is more nearly isotropic than the emissivity of clear skies. Another characteristic of these channels is that the spectral emissivities are uniformly lower than in the other regions measured, which is expected from the behavior shown in Figure 1.

4.3 15 micrometer and 17-22 micrometer filters (Figures 16 through 19)

The results obtained from measuring the peak 15 micrometer emissivities are exactly as anticipated, if somewhat uninteresting. It is well known that at this wavelength the atmosphere is highly opaque, and that radiation incident on the detector should have the characteristics of blackbody emission from near the instrument. The measurement indicates that, indeed, through all angular positions and sky cover condi-

tions only radiation produced at ambient air temperature is being sampled (the spectral emissivity always equals 1 to within experimental accuracy). This channel was included in the instrument package to provide an independent check on its functioning and calibration.

A close exmamination of the 15 micrometer emissivities shows that they are aboutt 0.01 larger at a zenith angle of 80^{o} compared with the zenith direction. This behavior is caused by the lapse rate (decrease of temperature with height) near the ground. The 17-22 micrometer channel, exhibits an interesting feature, even though it has no impact on the radiative cooling rate under normal warm ambient conditions. The spectral emissivity remains equal to unity under all clear sky total emissivity values in excess of approximately $\varepsilon_s = 0.75$. This corresponds to dewpoint temperatures above approximately $6^{o}C$, as was seen in section 3d. However, at cooler temperatures or under extremely arid or high altitude conditions a secondary atmospheric window is observed to open in the wavelength region.

5. Conclusions

The purpose of the extensive measurements of the thermal spectral radiance of the sky reported here has been to determine the resource for radiative cooling by systems which have spectral and/or angular selectivity. Direct estimates of the sky radiance can now be made for the six sites at which measurements were made. More significant, however, is the fact that new correlations have been developed which permit estimation of the spectral and angular components of thermal sky radiance based on pyrgeometer measurements of total sky emissivity or upon conventional meteorological measurements.

The method for estimating the detailed spectral and angular sky emissivity $\varepsilon_s(\lambda,\theta)$ makes use of the total sky emissivity ε_s. Thus the empirical sky radiance Equation (11) allows the disaggregation of into its spectral and angular components. This procedure is analogous to the well-known Liu and Jordan procedure which estimates the distribution of sunlight over the sky dome when only the global solar radiation value is known. In a given application, once $\varepsilon_s(\lambda,\theta)$ and the air temperature are known, Equation (3) can be used to compute the full sky radiance function $R_s(\lambda,\theta)$ necessary for the calculation of the cooling rates of various radiator systems. The first such application of the sky radiance equation has already been completed [18].

If the total sky emissivity is not known, it can be estimated based on meteorological data. For clear skies, the dewpoint temperature can be used to determine this quantity. For cloudy skies, cloud amount and cloudbase heights are additionally required to estimate ε_s. Our recommendations for performing these estimates are given in Section 3d. Once

ε_s is known, further calculations are to be performed as though it had been measured.

The sky radiance data has been collected in the southern United States with the primary emphasis on summertime conditions. Therefore, the resulting correlations should be most reliable for conditions where the dewpoint temperatures lies in the range $-10 < T_{dp} < 25^{o}C$. A phenomenological equation describes the data from all six locations.

6. References

1. P. Berdahl and M. Martin, "The resource for radiative cooling." Proc. of the Third National Passive Solar Conference, Vol. 2, p. 684, Philadelphia (1978).

2. W.L. Wolfe and G.J. Zissis (Eds), The Infrared Handbook Prepared by The Infrared Information and Analysis Center of the Environmental Research Institute of Michigan, Chap. 5 (1978).

3. P. Berdahl and R. Fromberg, "The Thermal Radiance of Clear Skies," to be published in Solar Energy, 1982.

4. R.E. Roberts, J.E. Selby and L.M. Biberman, "Infrared continuum absorption by atmospheric water vapor in the 8-12 micron window." Appl. Optics 15, 2085 (1976).

5. M. Martin and P. Berdahl, "Description of a Spectral Atmospheric Radiation Monitoring Network," in Proc. of the Third Conference on Atmospheric Radiation, Davis, California (June, 1978).

6. P. Berdahl and M. Martin, "Spectral Measurements of Infrared Sky Radiance," in Proc. of the Third National Passive Solar Conference; San Jose, California (January, 1979).

7. P. Berdahl, "Routine Spectral Measurements of Infrared Radiation from the Atmosphere," in Proc. of the Second International Conference on Infrared Physics, Zurich (March, 1979).

8. P. Berdahl and M. Martin, "Infrared Radiative Cooling," in Proc. of the International Solar Energy Society, Atlanta, Georgia (May, 1979).

9. P. Berdahl and M. Martin, "Spectral radiance of the clear midlatitude-summer atmosphere," in volume of extended abstracts for the 1980 International Radiation Symp., 167, Fort Collins, Colorado (1980). Available as Lawrence Berkeley Laboratory report LBL-10935 (May, 1980).

10. E. Clark and P. Berdahl, "Radiative Cooling: Resource and Applications," in the Passive Cooling Workbook issued at the Fifth National Passive Solar Conference, Amherst, Mass. (October 1980). Also Lawrence Berkeley Laboratory PUB-375.

11. P. Berdahl and M. Martin, "Thermal Radiance of Skies with Low Clouds," in Proc. of the International Passive and Hybrid Cooling Conference, 266, Miami Beach, Florida (November, 1981).

12. M. Abramowitz and I. Stegun, eds., Handbook of Mathematical Functions, National Bureau of Standards Applied Mathematics Series, published by the U.S. Gov't. Printing Office, p.228, formula 5.1.4 (1964).

13. P. Berdahl and R. Fromberg, "An Empirical Method for Estimating the Thermal Radiance of Clear Skies," Lawrence Berkeley Laboratory Report LBL-12720, (May 1981). This report is a sightly more comprehensive version of Ref.3.

14. K.G. Picha and J. Villanueva, "Noctunal radiation measurements," Atlanta, Georgia, Solar Energy 6, 151 (1962).

15. G. Clark and C.P. Allen, "The estimation of atmospheric radiation for clear and cloudy skies," Proceedings Second National Passive Solar Conference, Vol. 2, p.676, Philadelphia (1978).

16. W. Sellers, Physical Climatology, p.58, Univ. of Chicago Press, Chicago (1965).

17. K. Kondratyev, Radiation in the Atmosphere p.576, Academic Press, New York (1969).

18. P. Berdahl, M. Martin, and F. Sakkal, "Thermal Performance of Radiative Cooling Panels," Lawrence Berkeley Laboratory Report LBL-14409 (June, 1982).

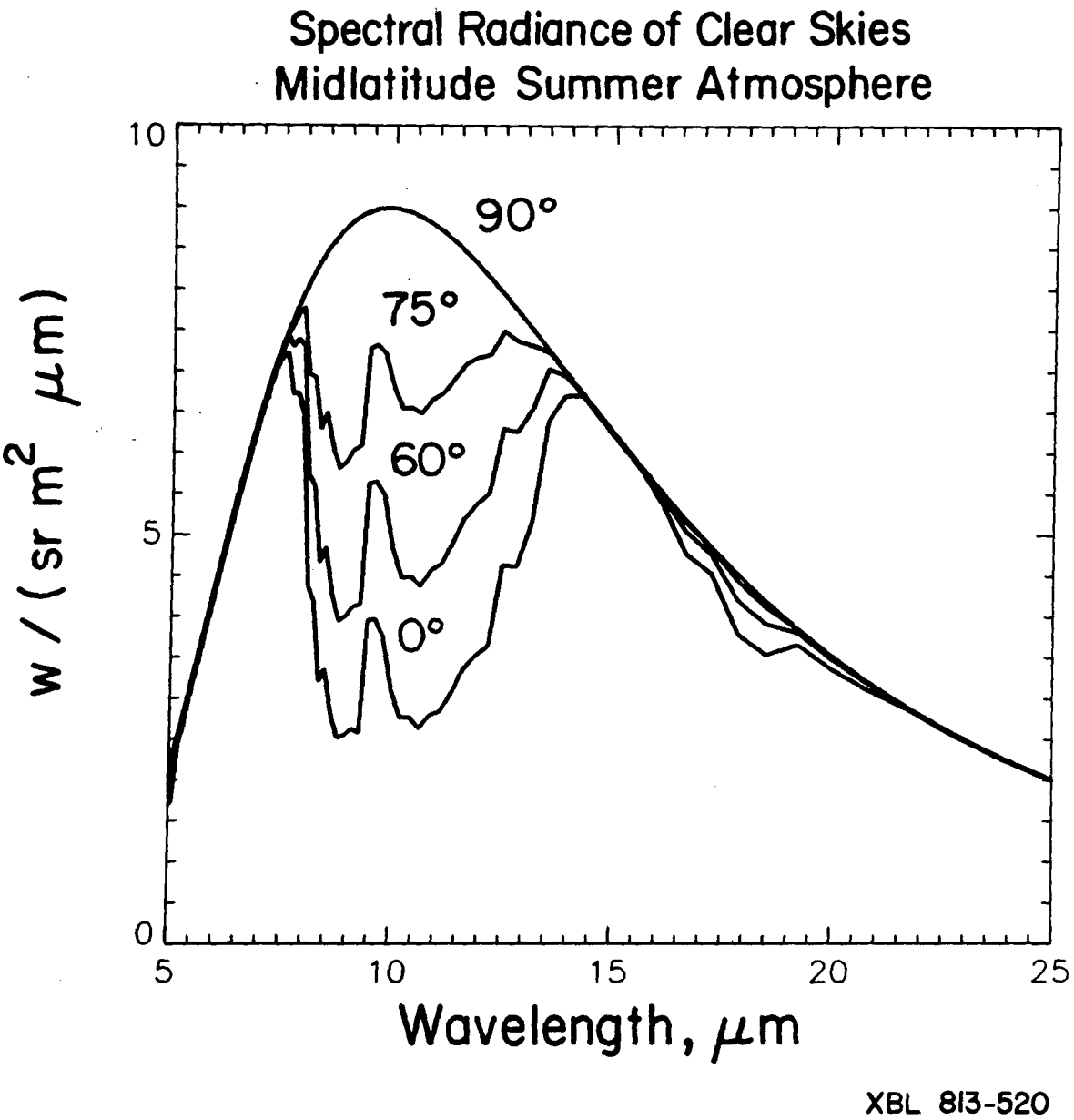

XBL 813-520

FIGURE 1

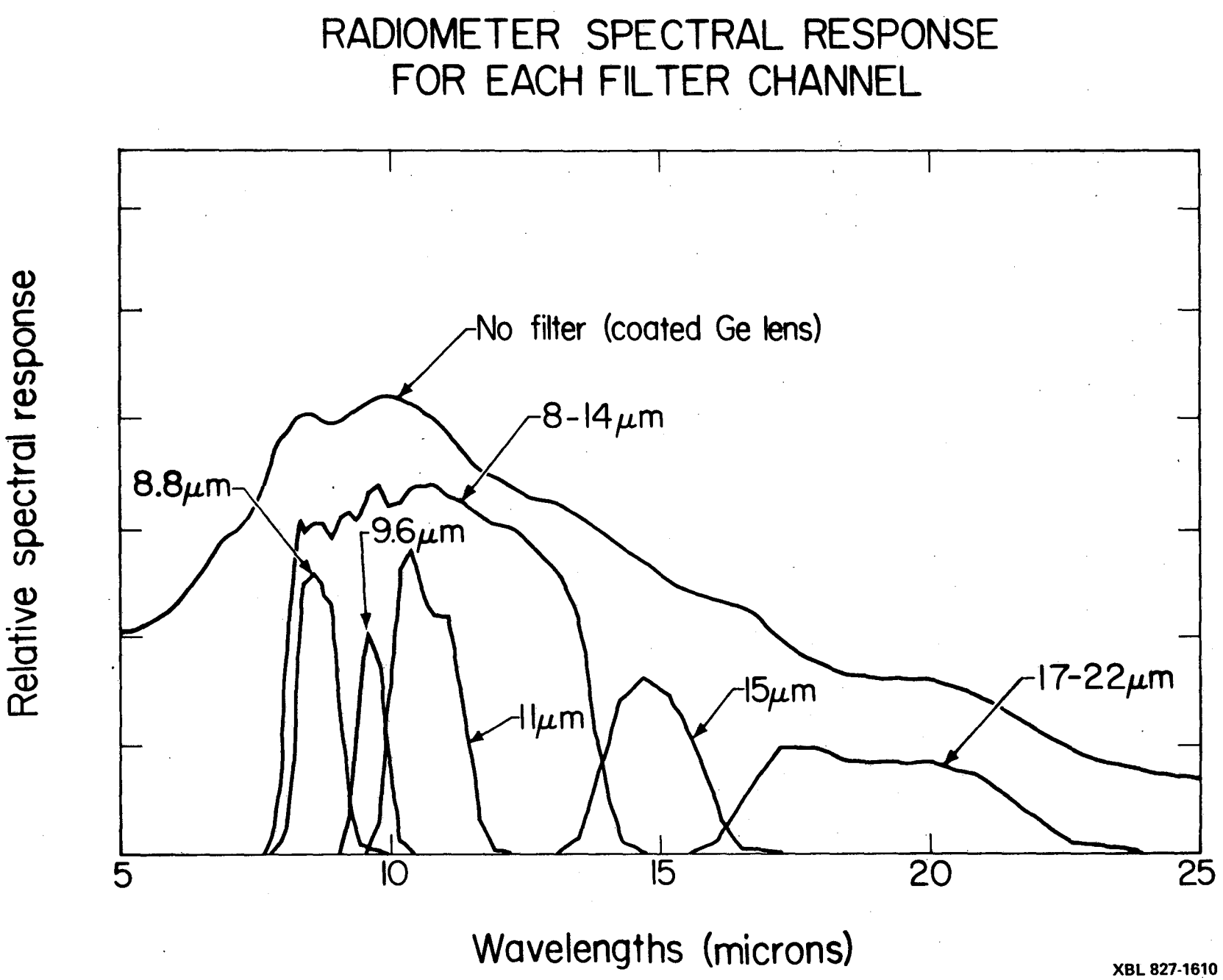
RADIOMETER SPECTRAL RESPONSE
FOR EACH FILTER CHANNEL
Relative spectral response
No filter (coated Ge lens)
8-14μm
8.8μm
9.6μm
11μm
15μm
17-22μm
5
10
15
20
25
Wavelengths (microns)
XBL 827-1610

FIGURE 2

NOTATION: In all the subsequent graphs each letter symbol represents a full month of averaged data from one of the six U.S. cities at which radiometer measurements were taken. The key to interpreting these symbols is:

A = San Antonio, TX

B = Boulder City, NV

G = Gaithersburg, MD

L = St. Louis, MO

T = Tucson, AZ

W = West Palm Beach, FL

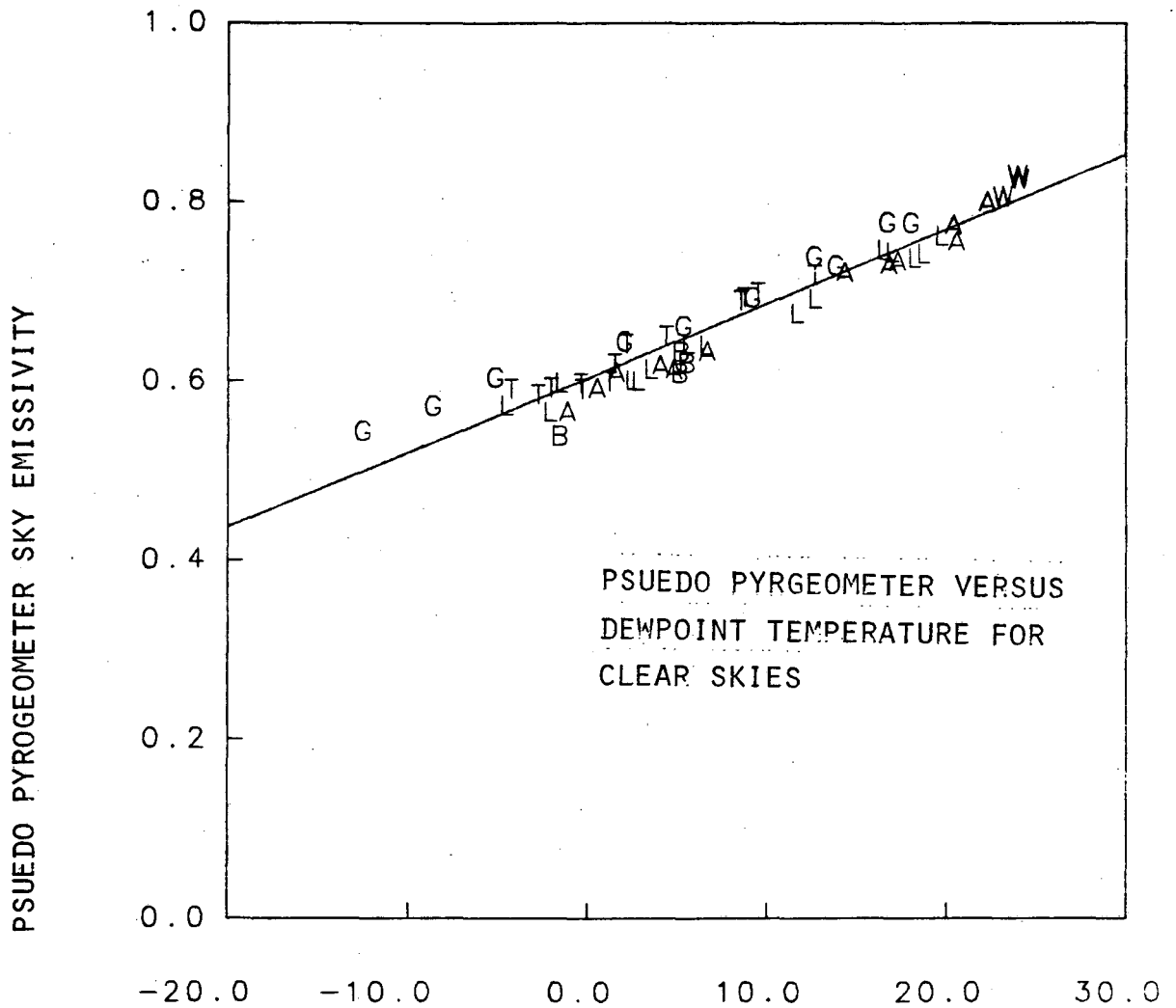
1.0
0.8
0.6
0.4
0.2
0.0
PSUEDO PYROGEOMETER SKY EMISSIVITY
PSUEDO PYRGEOMETER VERSUS
DEWPOINT TEMPERATURE FOR
CLEAR SKIES
-20.0
-10.0
0.0
10.0
20.0
30.0
DEWPOINT TEMEPRATURE

FIGURE 3

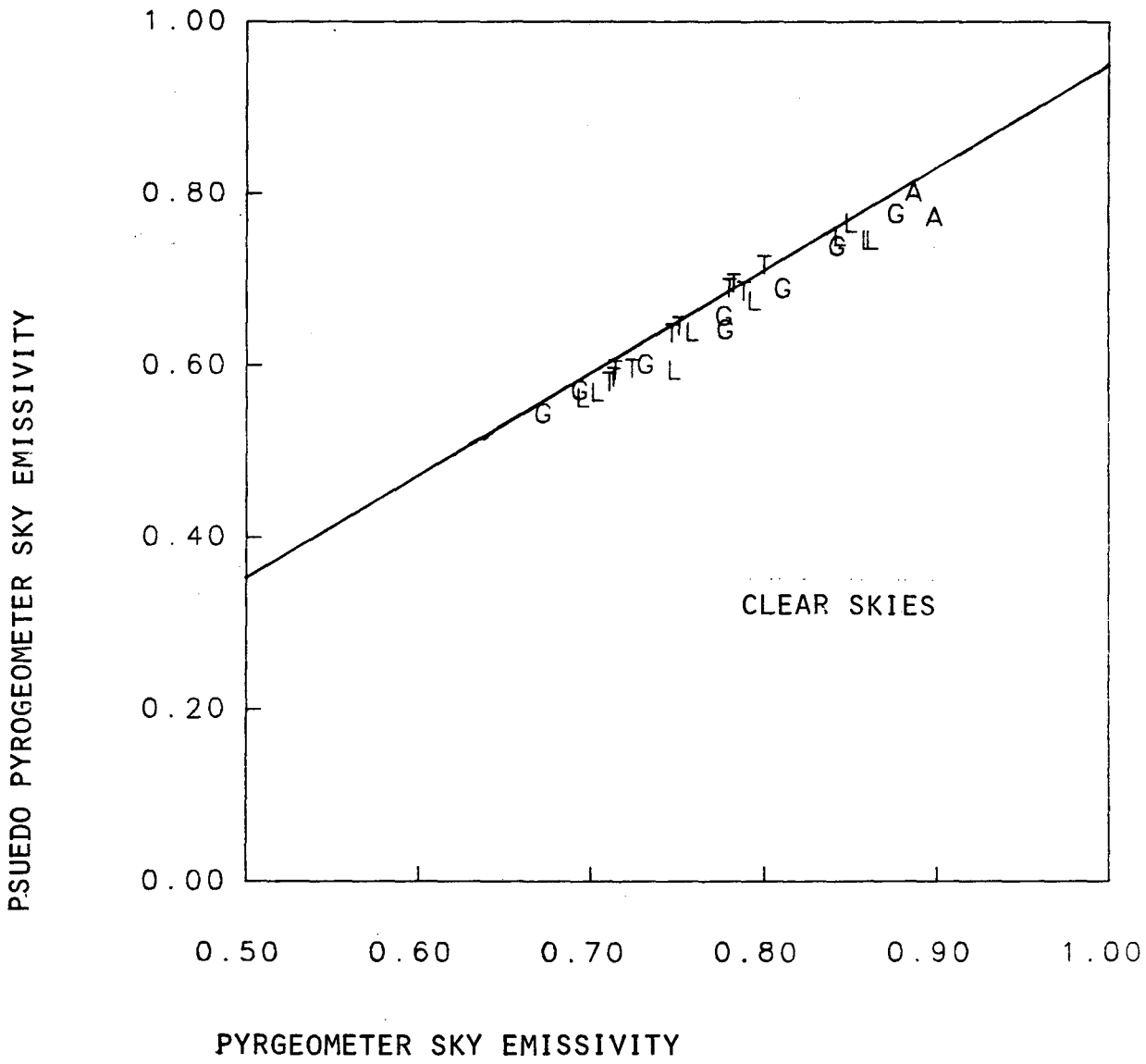
1.00
0.80
0.60
0.40
0.20
0.00
0.50
0.60
0.70
0.80
0.90
1.00
PSUEDO PYROGEOMETER SKY EMISSIVITY
PYRGEOMETER SKY EMISSIVITY
CLEAR SKIES

FIGURE 4

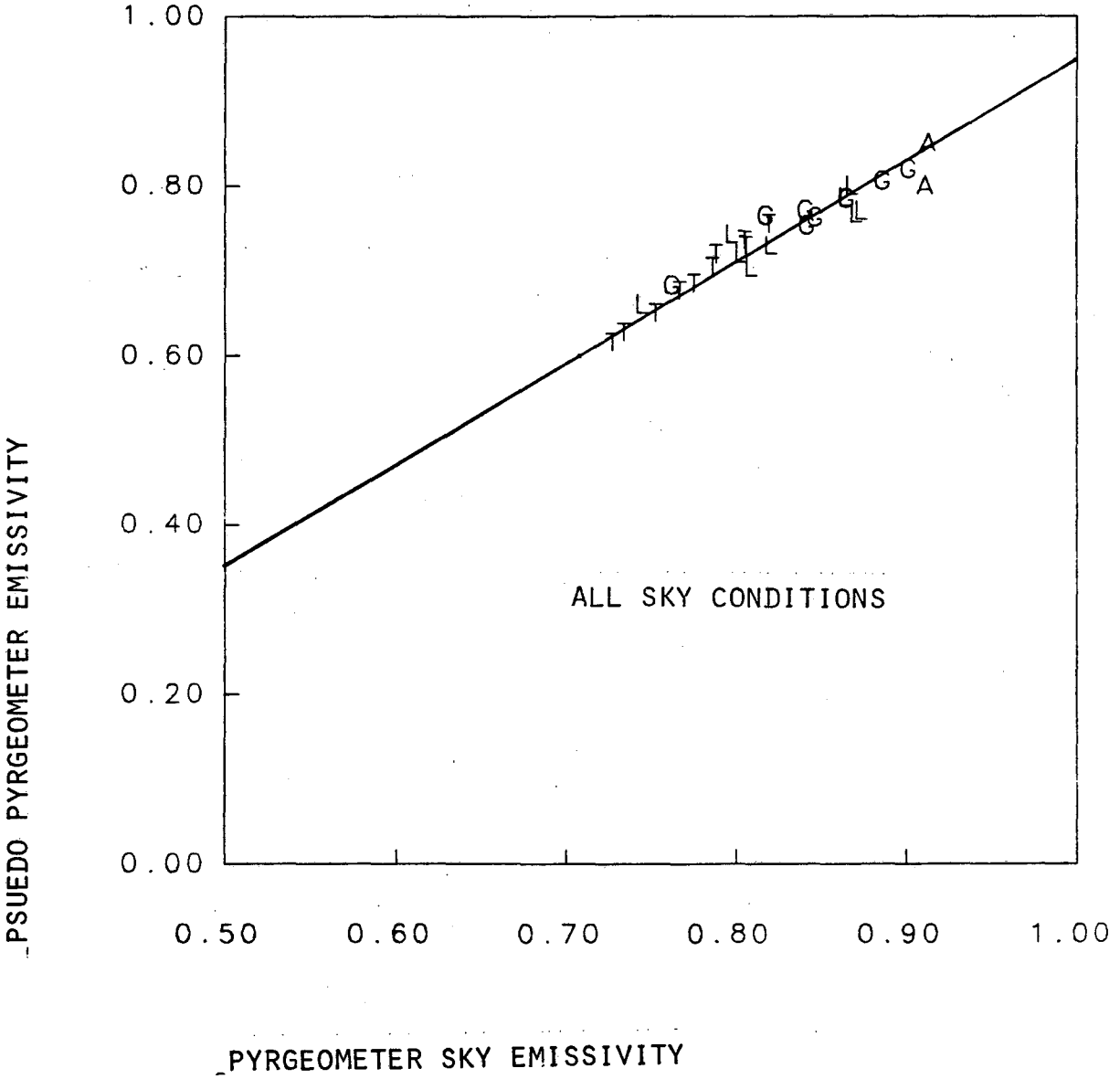
1.00
0.80
0.60
0.40
0.20
0.00
0.50
0.60
0.70
0.80
0.90
1.00
ALL SKY CONDITIONS
PSUEDO PYRGEOMETER EMISSIVITY
PYRGEOMETER SKY EMISSIVITY

FIGURE 5

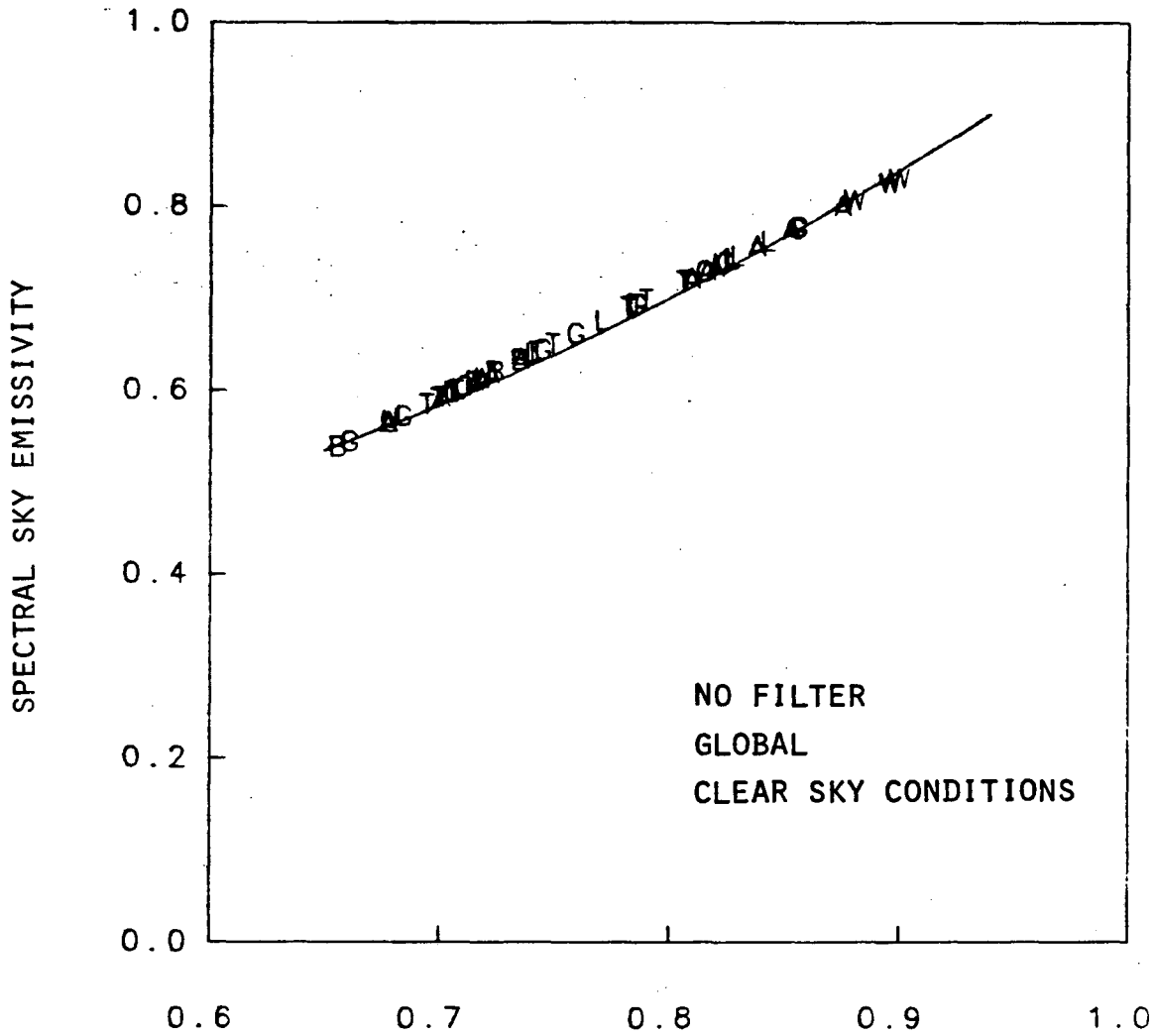
1.0
0.8
0.6
0.4
0.2
0.0
SPECTRAL SKY EMISSIVITY
NO FILTER
GLOBAL
CLEAR SKY CONDITIONS
0.6
0.7
0.8
0.9
1.0
TOTAL SKY EMISSIVITY

FIGURE 6A

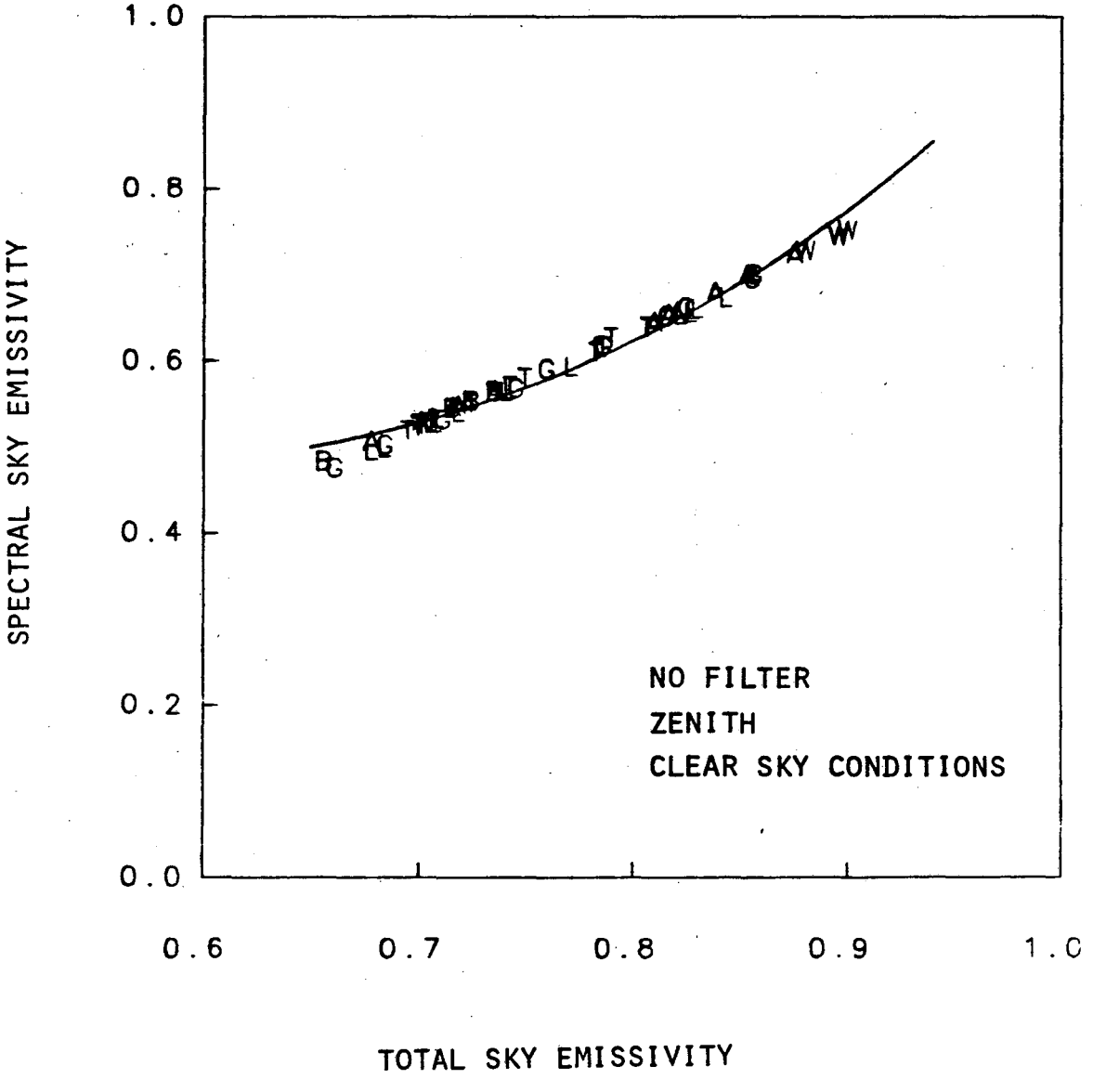
1.0
0.8
0.6
0.4
0.2
0.0
SPECTRAL SKY EMISSIVITY
NO FILTER
ZENITH
CLEAR SKY CONDITIONS
0.6
0.7
0.8
0.9
1.0
TOTAL SKY EMISSIVITY

FIGURE 6B

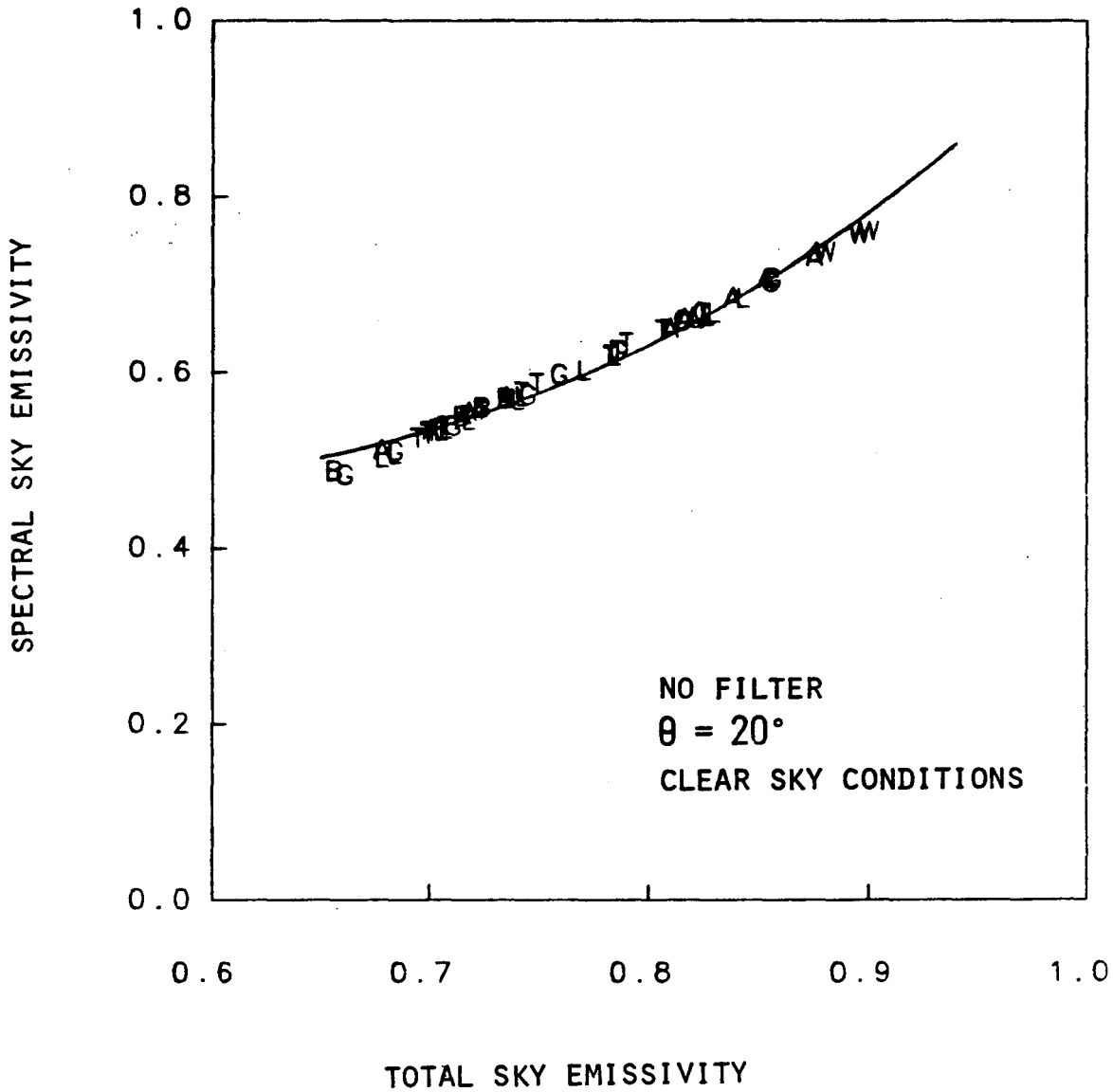
1.0
0.8
0.6
0.4
0.2
0.0
SPECTRAL SKY EMISSIVITY
NO FILTER
θ = 20°
CLEAR SKY CONDITIONS
0.6
0.7
0.8
0.9
1.0
TOTAL SKY EMISSIVITY

FIGURE 6c

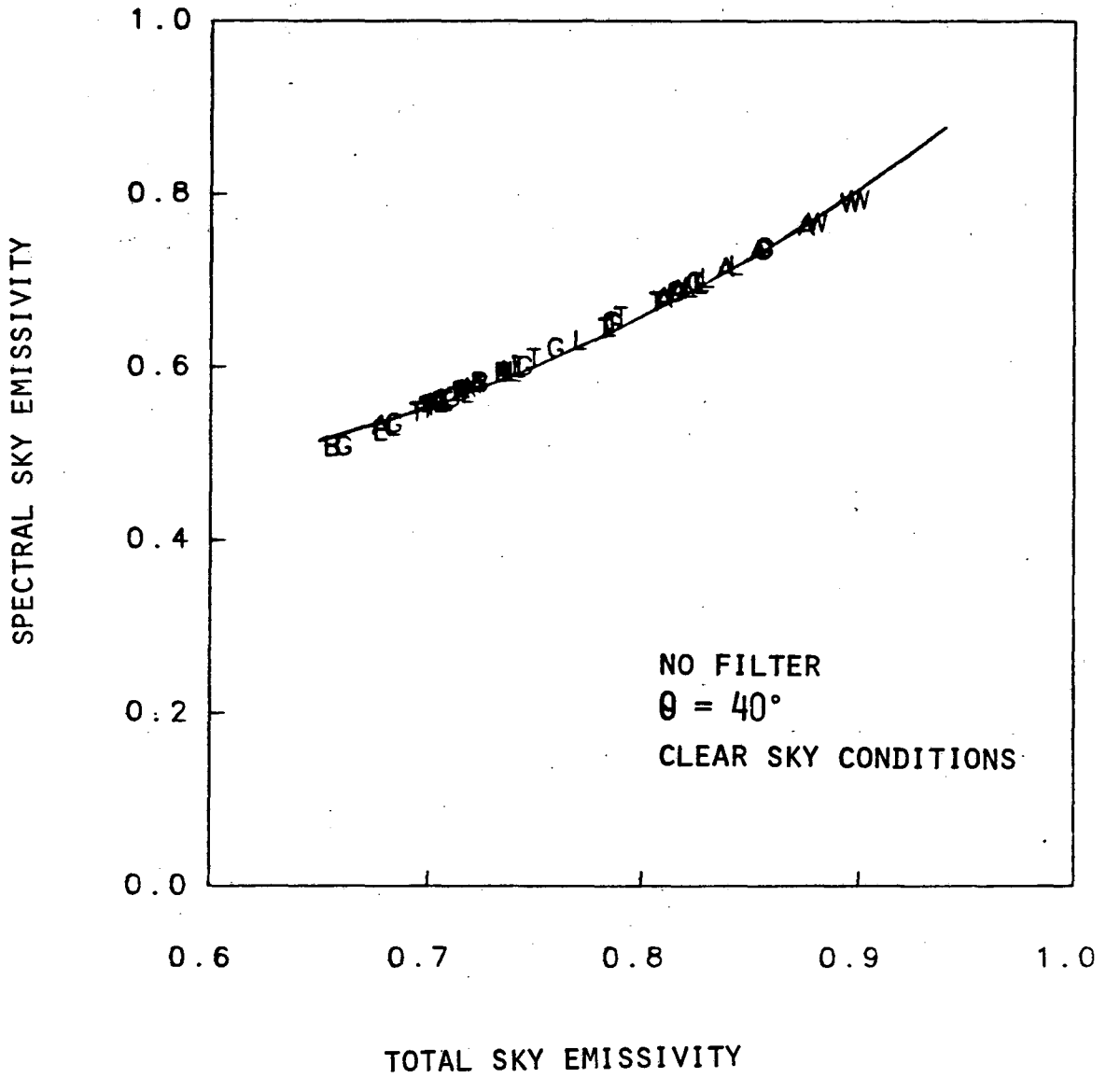
1.0
0.8
0.6
0.4
0.2
0.0
SPECTRAL SKY EMISSIVITY
NO FILTER
θ = 40°
CLEAR SKY CONDITIONS
0.6
0.7
0.8
0.9
1.0
TOTAL SKY EMISSIVITY

FIGURE 6D

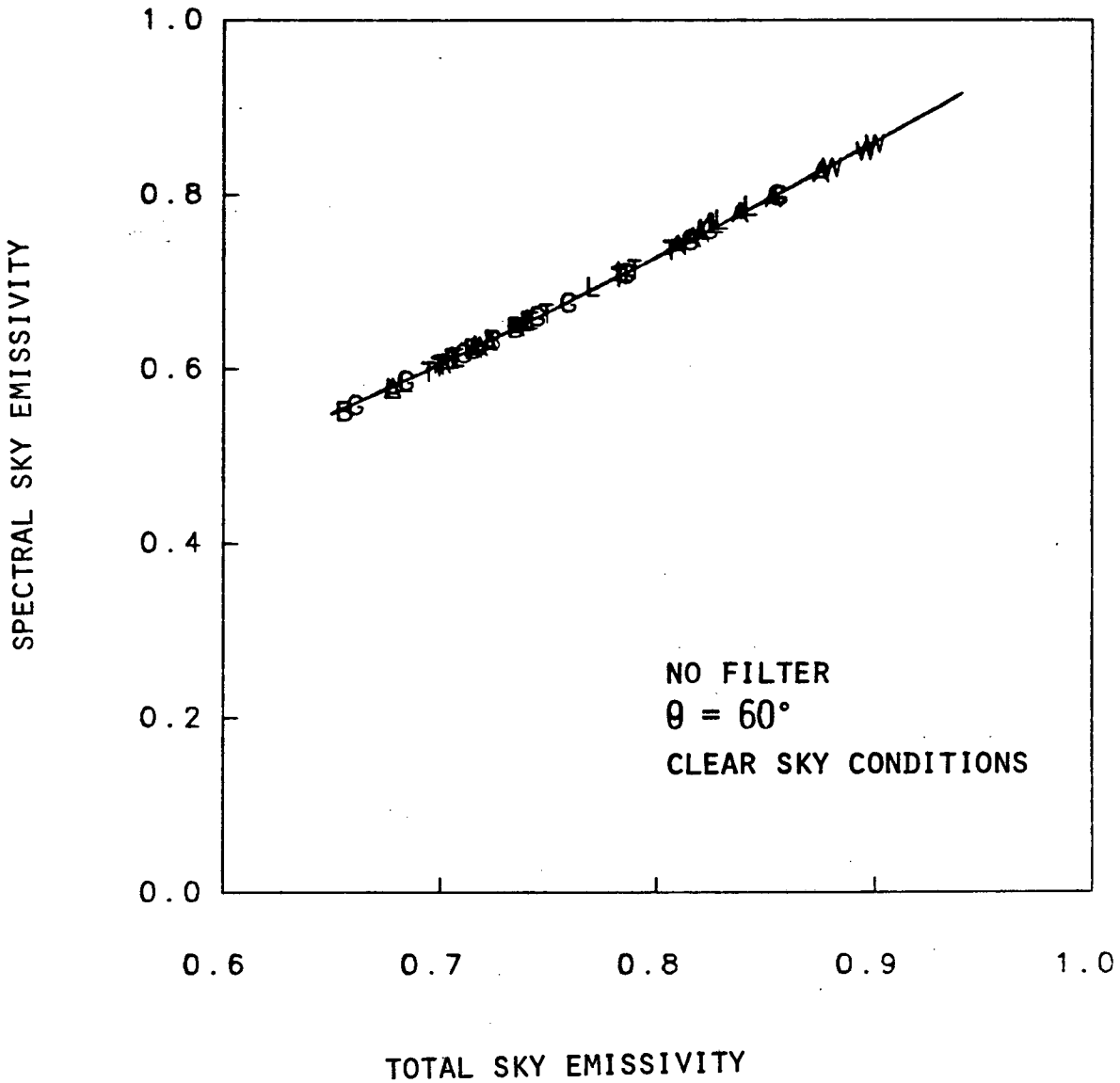
1.0
0.8
0.6
0.4
0.2
0.0
SPECTRAL SKY EMISSIVITY
NO FILTER
θ = 60°
CLEAR SKY CONDITIONS
0.6
0.7
0.8
0.9
1.0
TOTAL SKY EMISSIVITY

FIGURE 6E

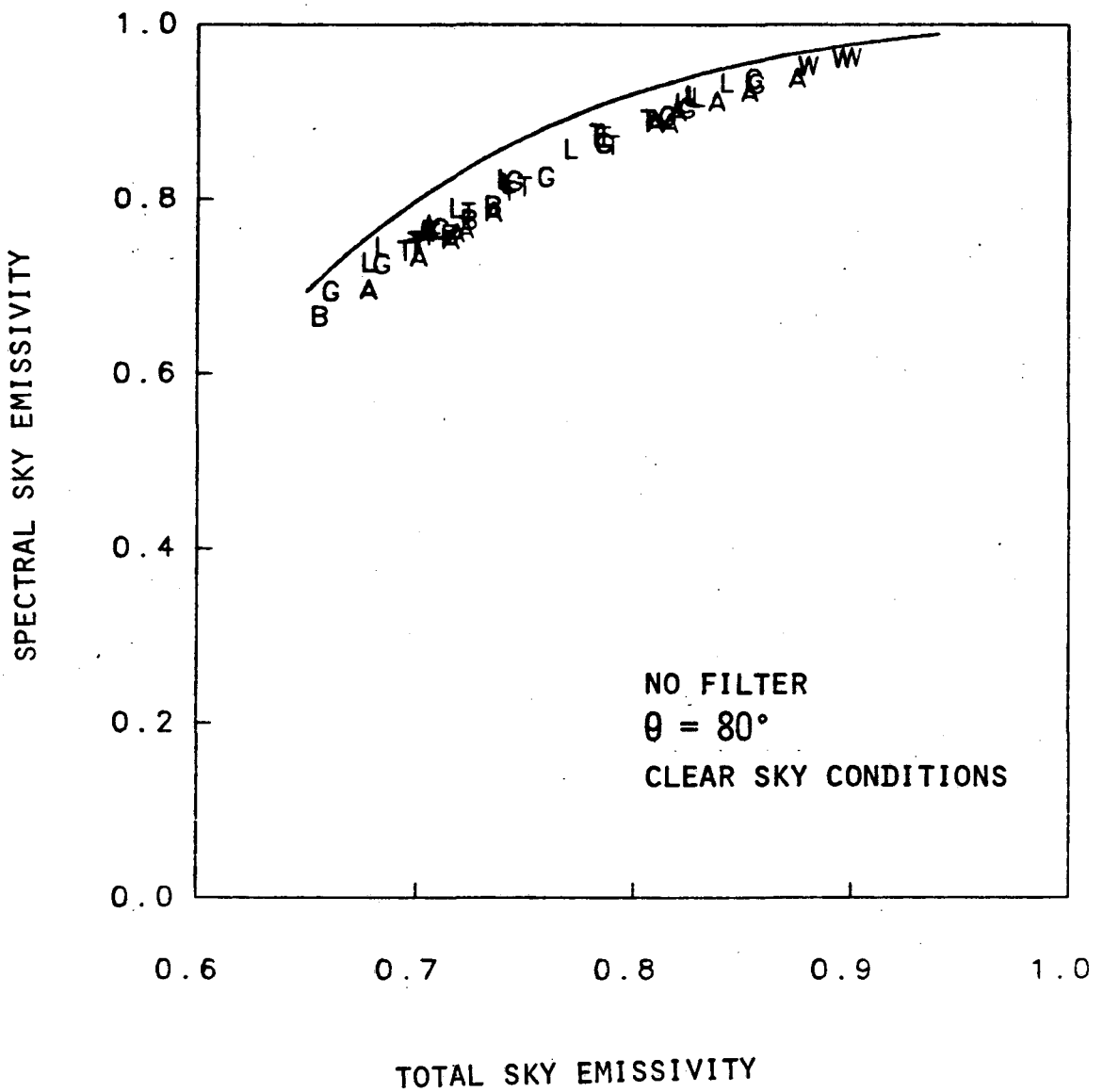
1.0
0.8
0.6
0.4
0.2
0.0
SPECTRAL SKY EMISSIVITY
NO FILTER
θ = 80°
CLEAR SKY CONDITIONS
0.6
0.7
0.8
0.9
1.0
TOTAL SKY EMISSIVITY

FIGURE 6F

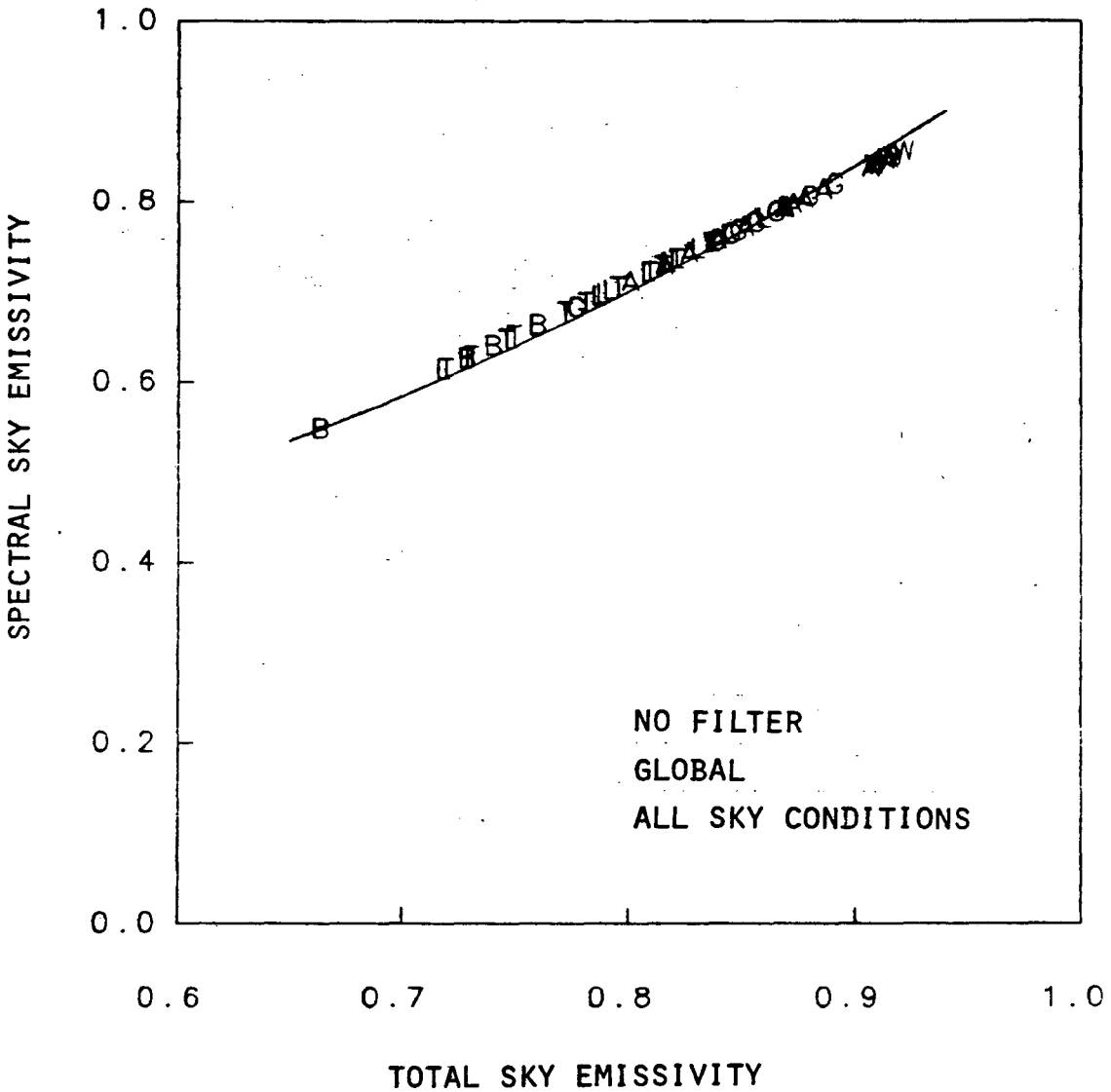
1.0
0.8
0.6
0.4
0.2
0.0
SPECTRAL SKY EMISSIVITY
NO FILTER
GLOBAL
ALL SKY CONDITIONS
0.6
0.7
0.8
0.9
1.0
TOTAL SKY EMISSIVITY

FIGURE 7A

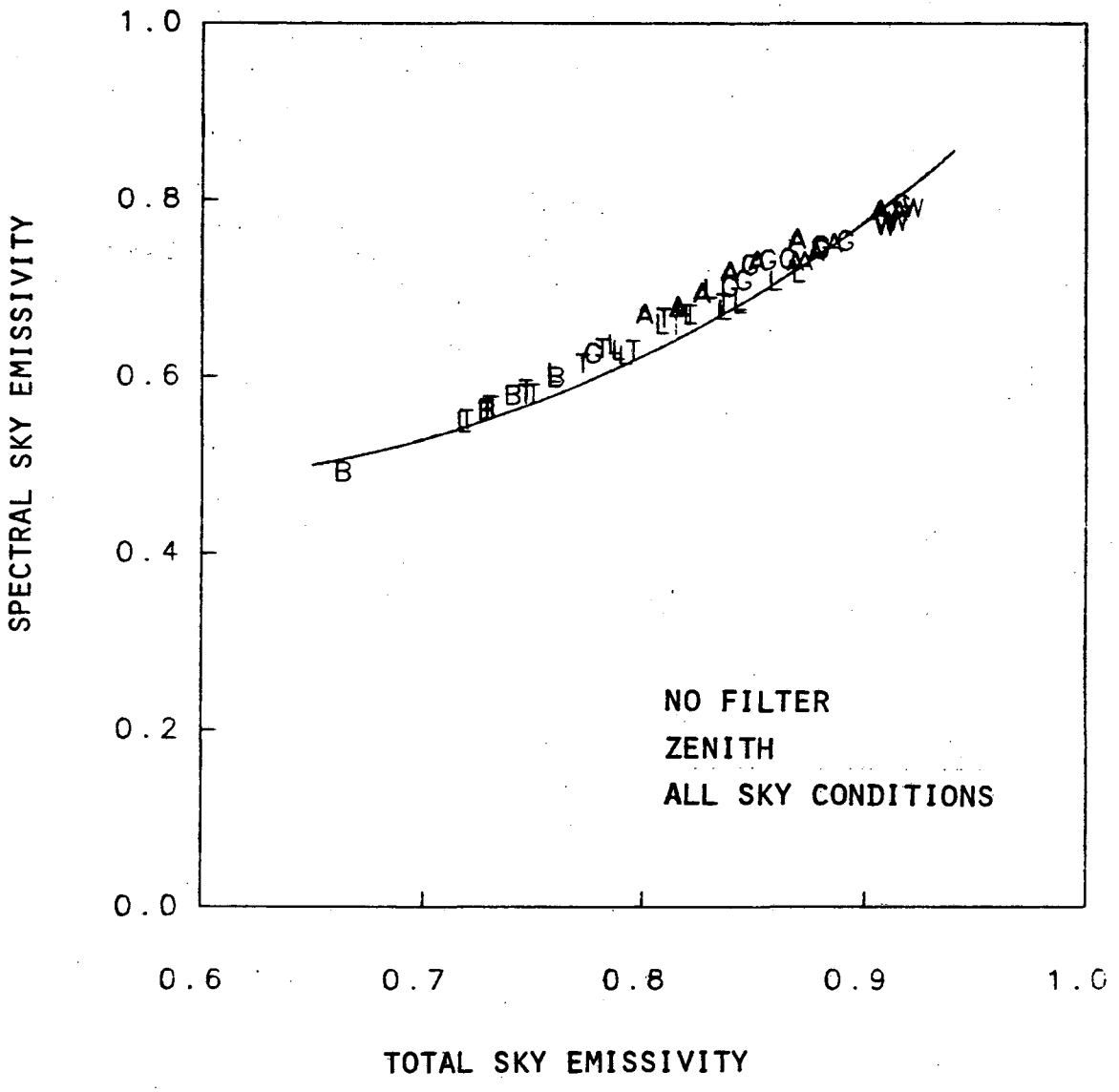
1.0
0.8
0.6
0.4
0.2
0.0
SPECTRAL SKY EMISSIVITY
NO FILTER
ZENITH
ALL SKY CONDITIONS
0.6
0.7
0.8
0.9
1.0
TOTAL SKY EMISSIVITY

FIGURE 7B

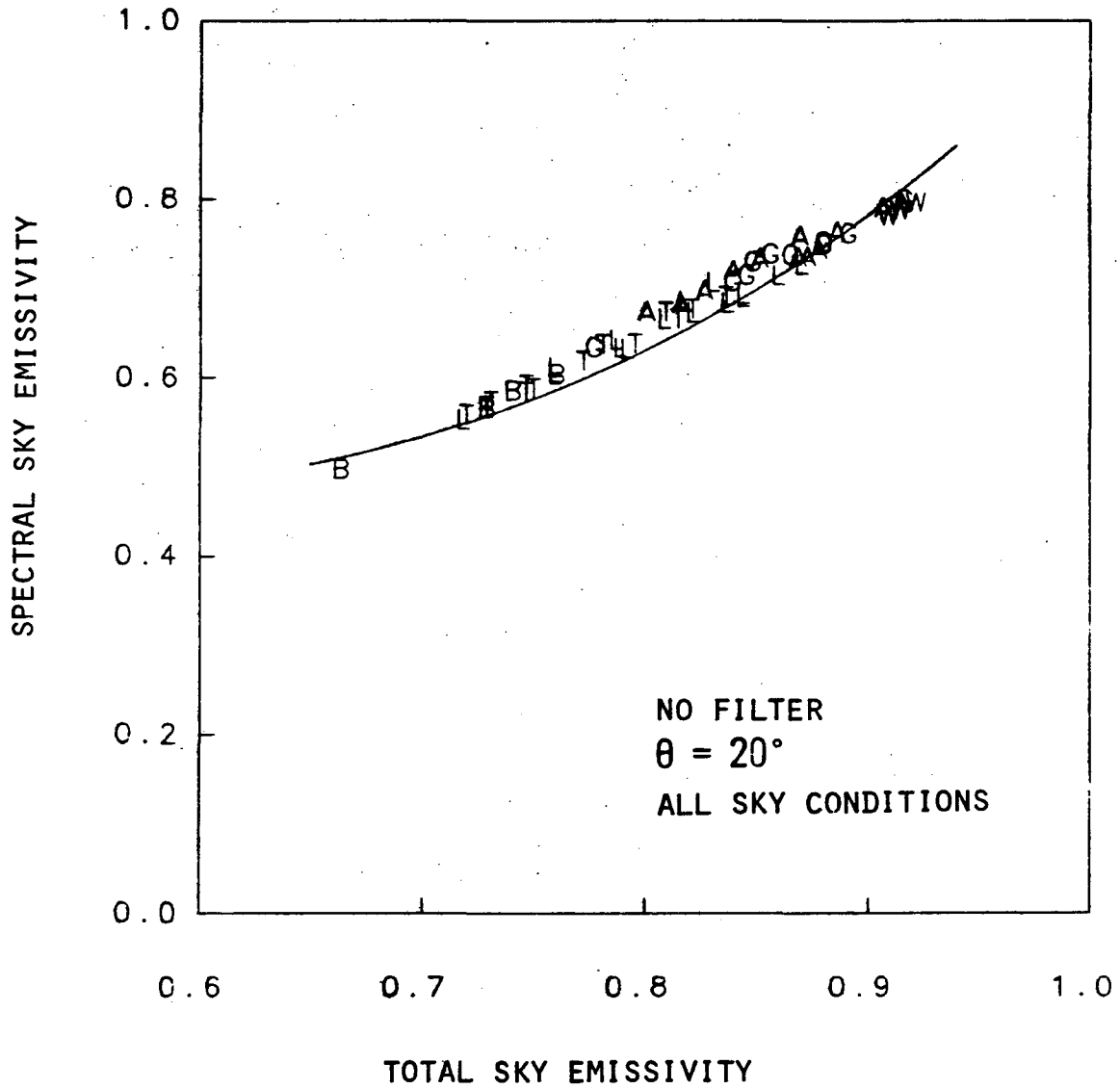
1.0
0.8
0.6
0.4
0.2
0.0
SPECTRAL SKY EMISSIVITY
NO FILTER
θ = 20°
ALL SKY CONDITIONS
0.6
0.7
0.8
0.9
1.0
TOTAL SKY EMISSIVITY

FIGURE 7C

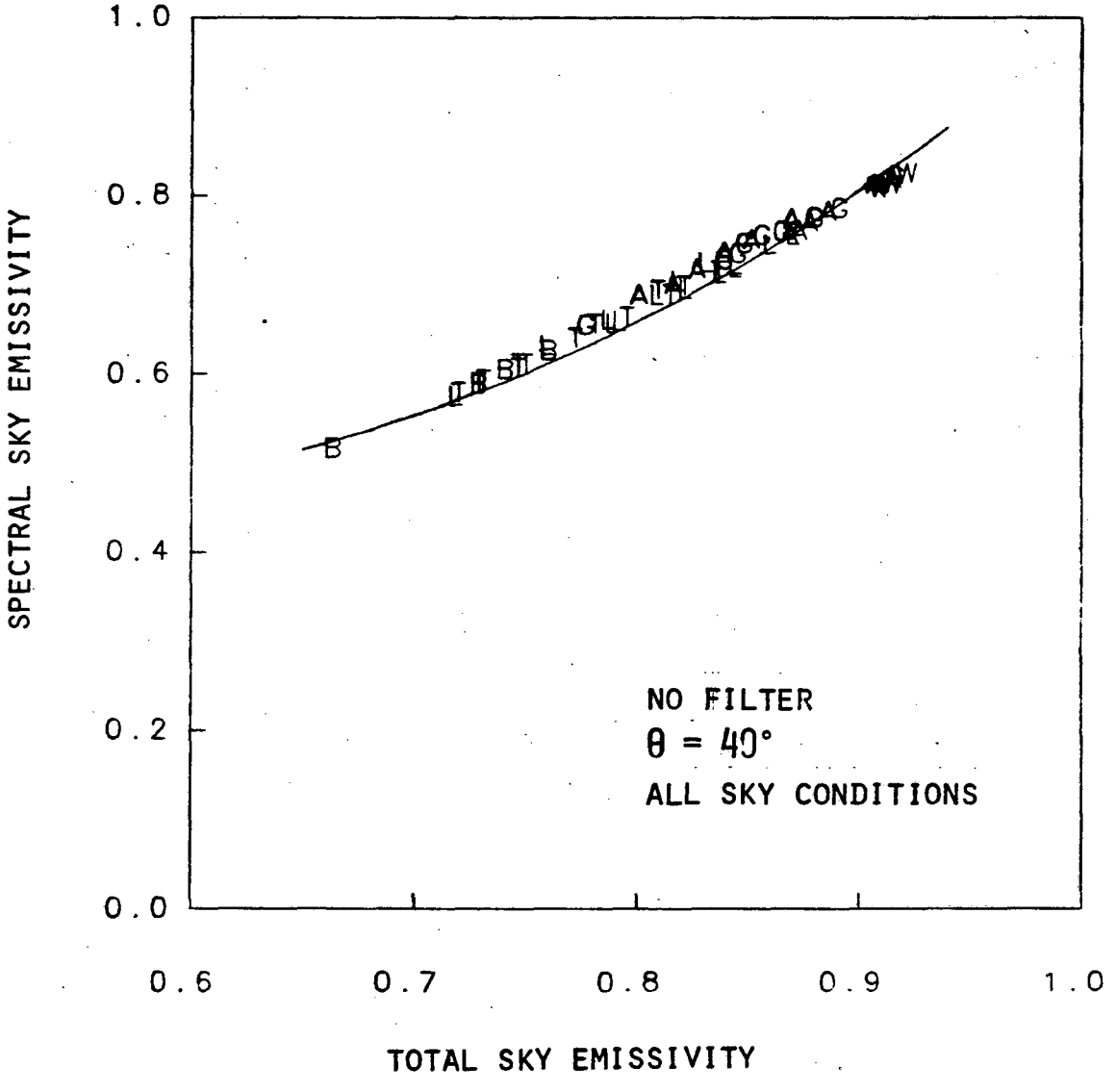
1.0
0.8
0.6
0.4
0.2
0.0
SPECTRAL SKY EMISSIVITY
NO FILTER
θ = 40°
ALL SKY CONDITIONS
0.6
0.7
0.8
0.9
1.0
TOTAL SKY EMISSIVITY

FIGURE 7D

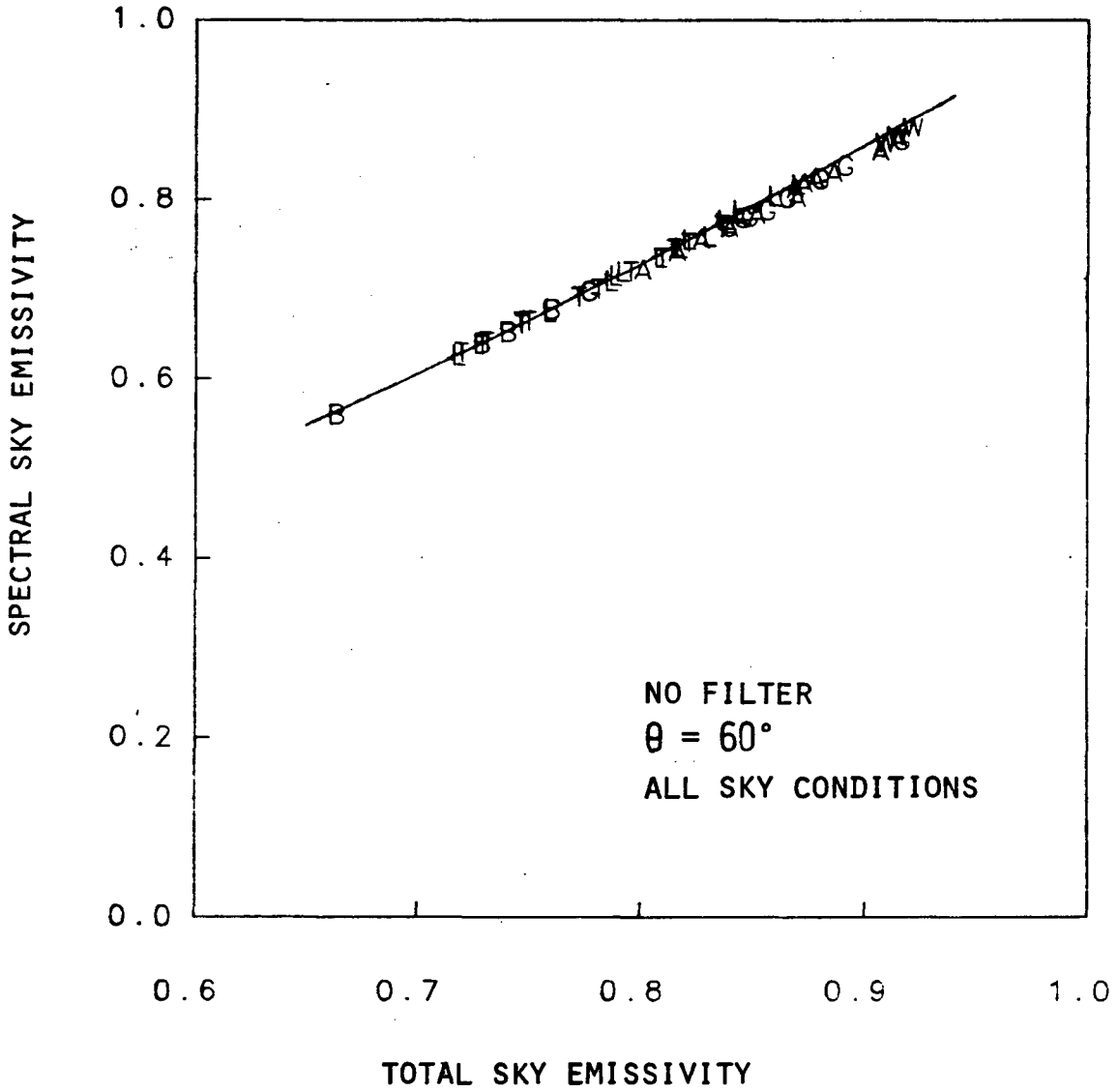
1.0
0.8
0.6
0.4
0.2
0.0
SPECTRAL SKY EMISSIVITY
NO FILTER
θ = 60°
ALL SKY CONDITIONS
0.6
0.7
0.8
0.9
1.0
TOTAL SKY EMISSIVITY

FIGURE 7E

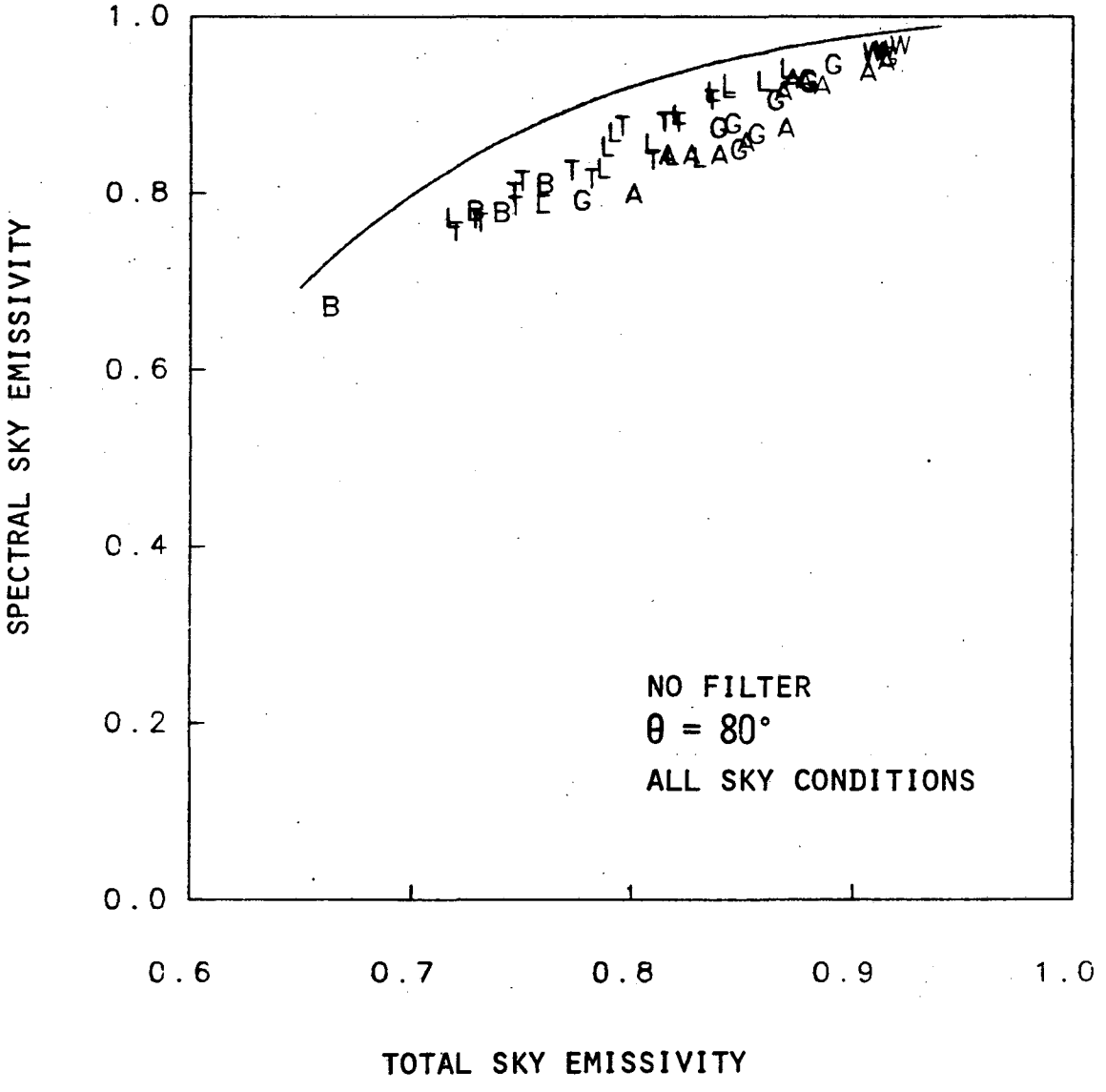
1.0
0.8
0.6
0.4
0.2
0.0
SPECTRAL SKY EMISSIVITY
0.6
0.7
0.8
0.9
1.0
TOTAL SKY EMISSIVITY
NO FILTER
θ = 80°
ALL SKY CONDITIONS

FIGURE 7F

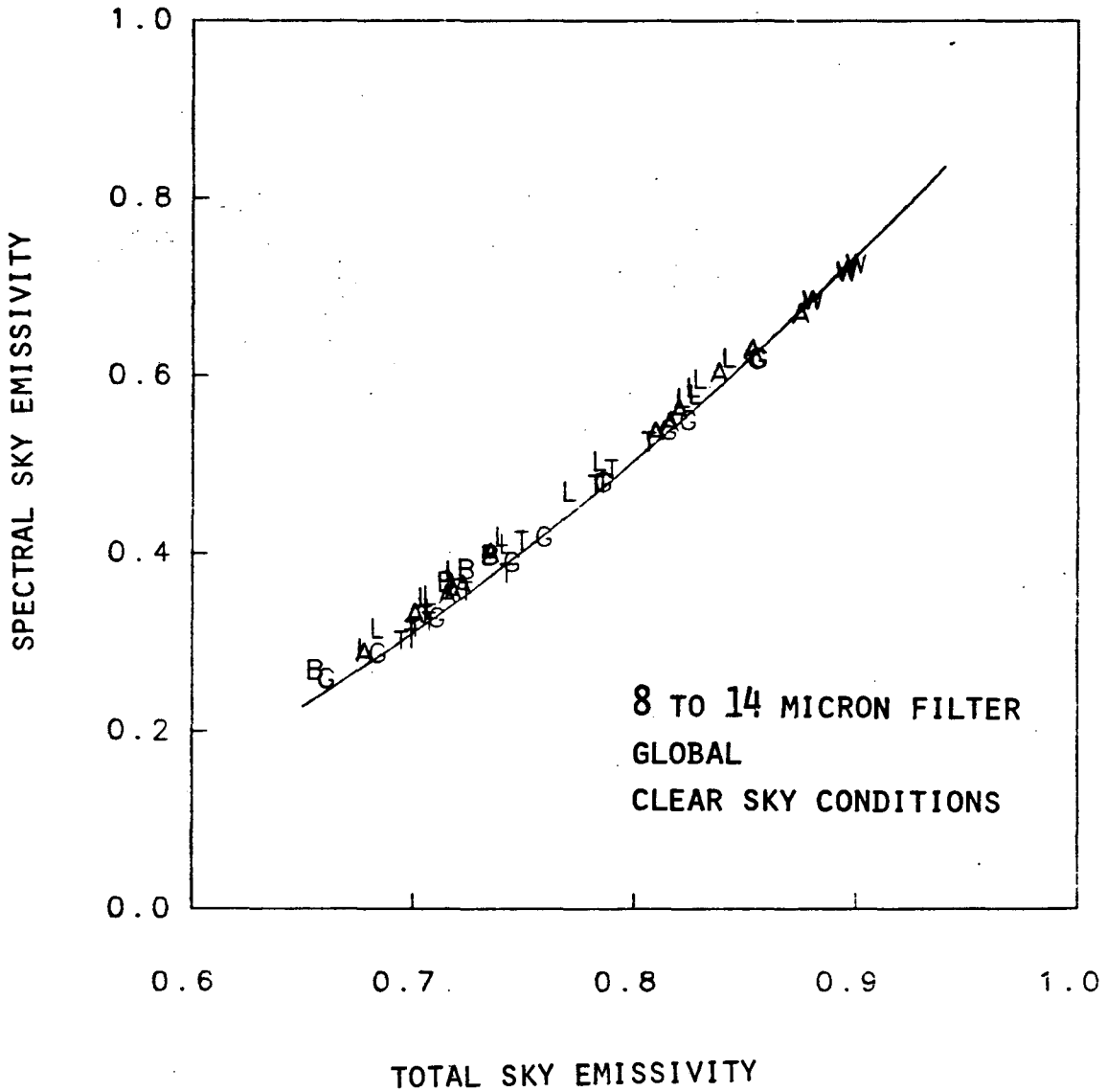
1.0
0.8
0.6
0.4
0.2
0.0
SPECTRAL SKY EMISSIVITY
0.6
0.7
0.8
0.9
1.0
TOTAL SKY EMISSIVITY
8 TO 14 MICRON FILTER
GLOBAL
CLEAR SKY CONDITIONS

FIGURE 8A

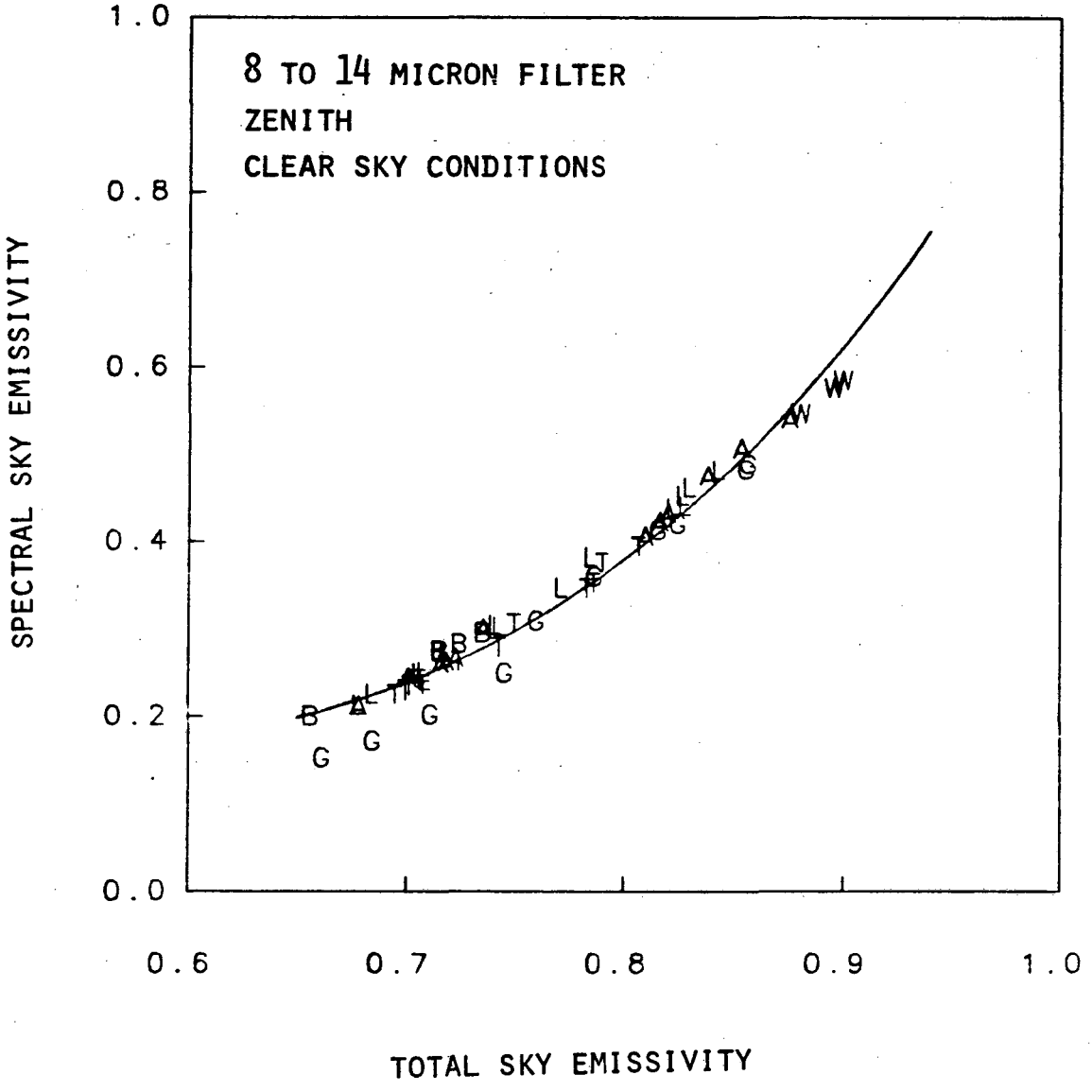
8 TO 14 MICRON FILTER
ZENITH
CLEAR SKY CONDITIONS
SPECTRAL SKY EMISSIVITY
TOTAL SKY EMISSIVITY
1.0
0.8
0.6
0.4
0.2
0.0
0.6
0.7
0.8
0.9
1.0

FIGURE 8B

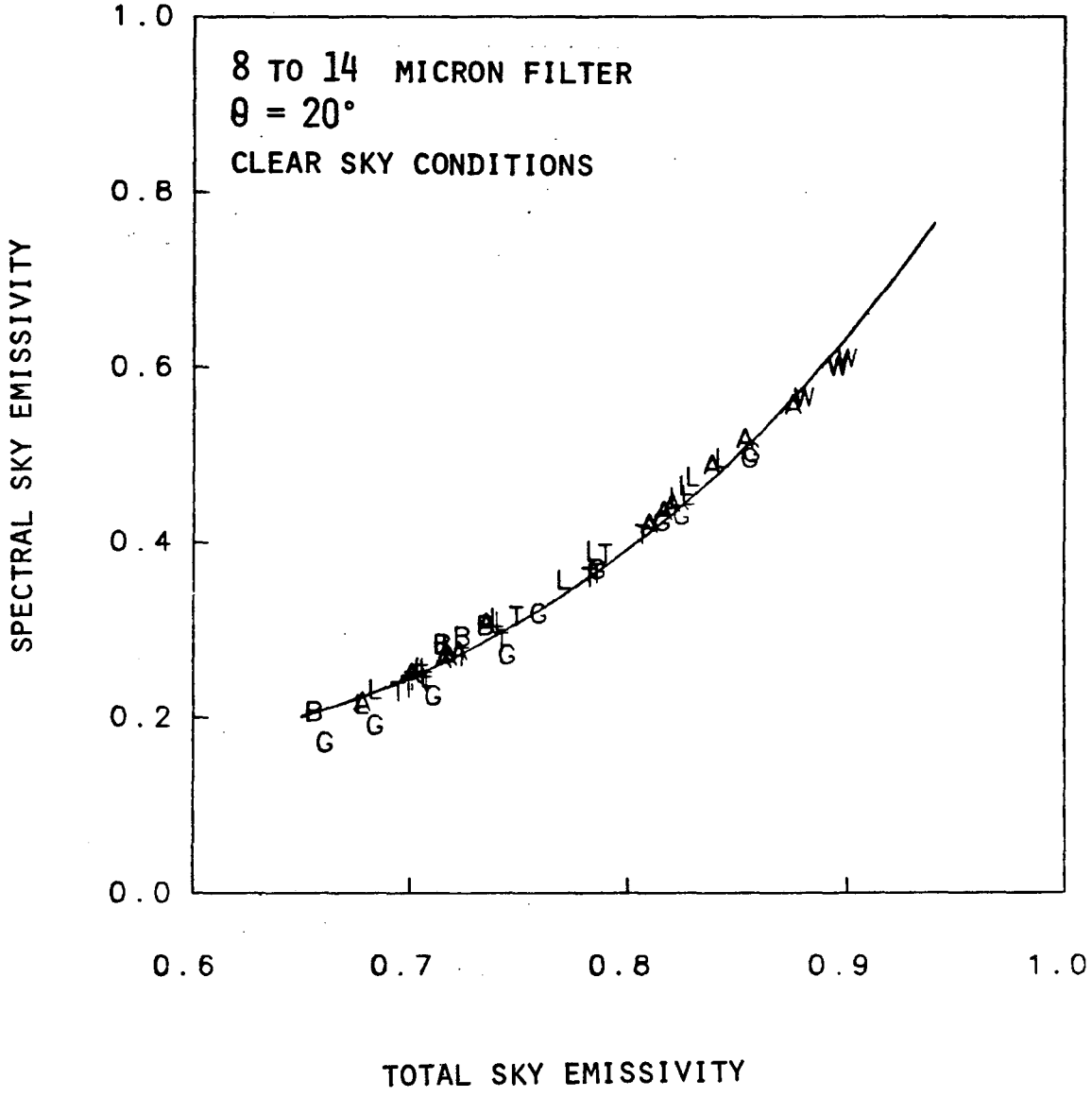
8 TO 14 MICRON FILTER
θ = 20°
CLEAR SKY CONDITIONS
SPECTRAL SKY EMISSIVITY
TOTAL SKY EMISSIVITY
1.0
0.8
0.6
0.4
0.2
0.0
0.6
0.7
0.8
0.9
1.0

FIGURE 8C

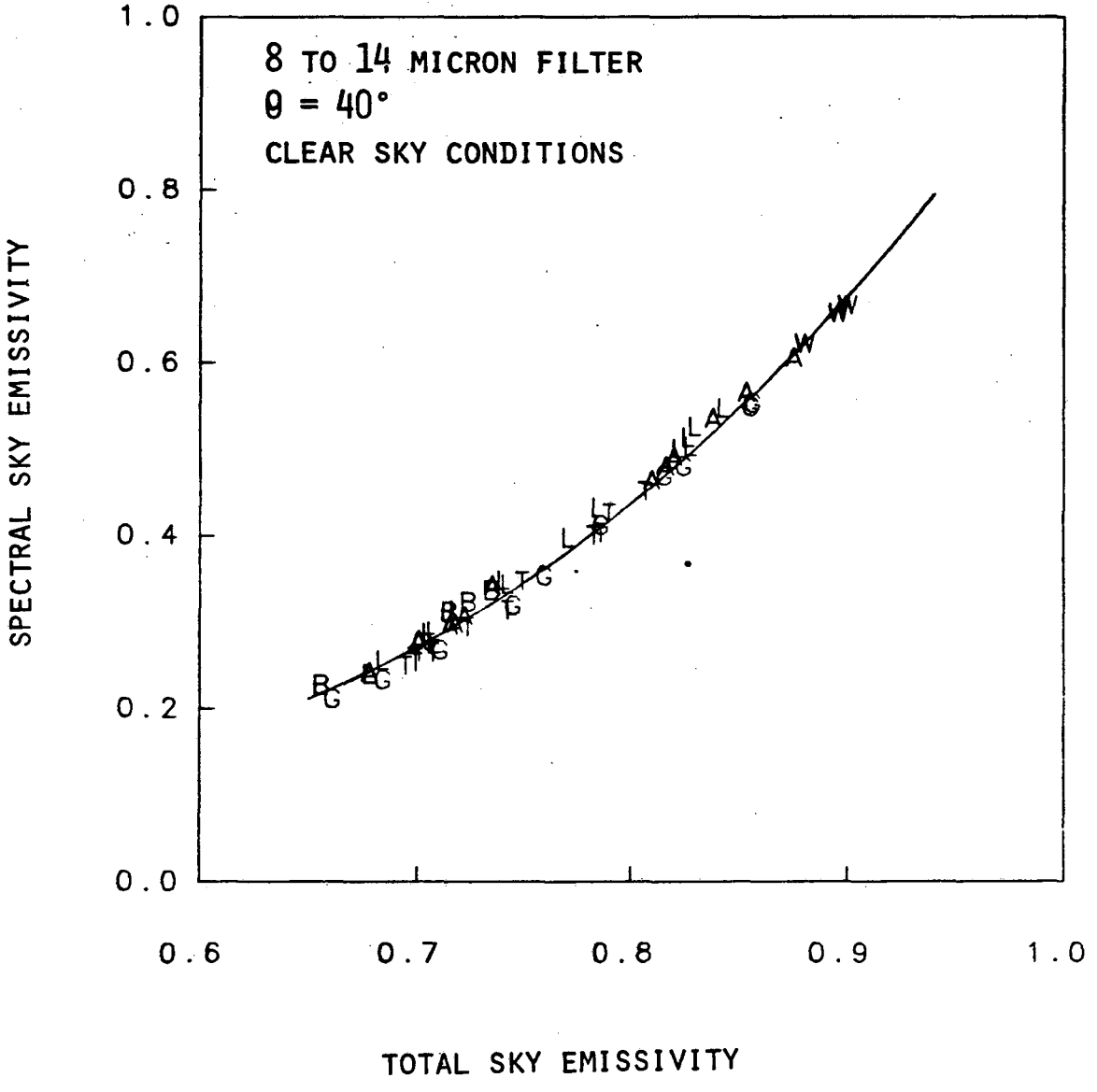
8 TO 14 MICRON FILTER
θ = 40°
CLEAR SKY CONDITIONS
SPECTRAL SKY EMISSIVITY
TOTAL SKY EMISSIVITY
1.0
0.8
0.6
0.4
0.2
0.0
0.6
0.7
0.8
0.9
1.0

FIGURE 8D

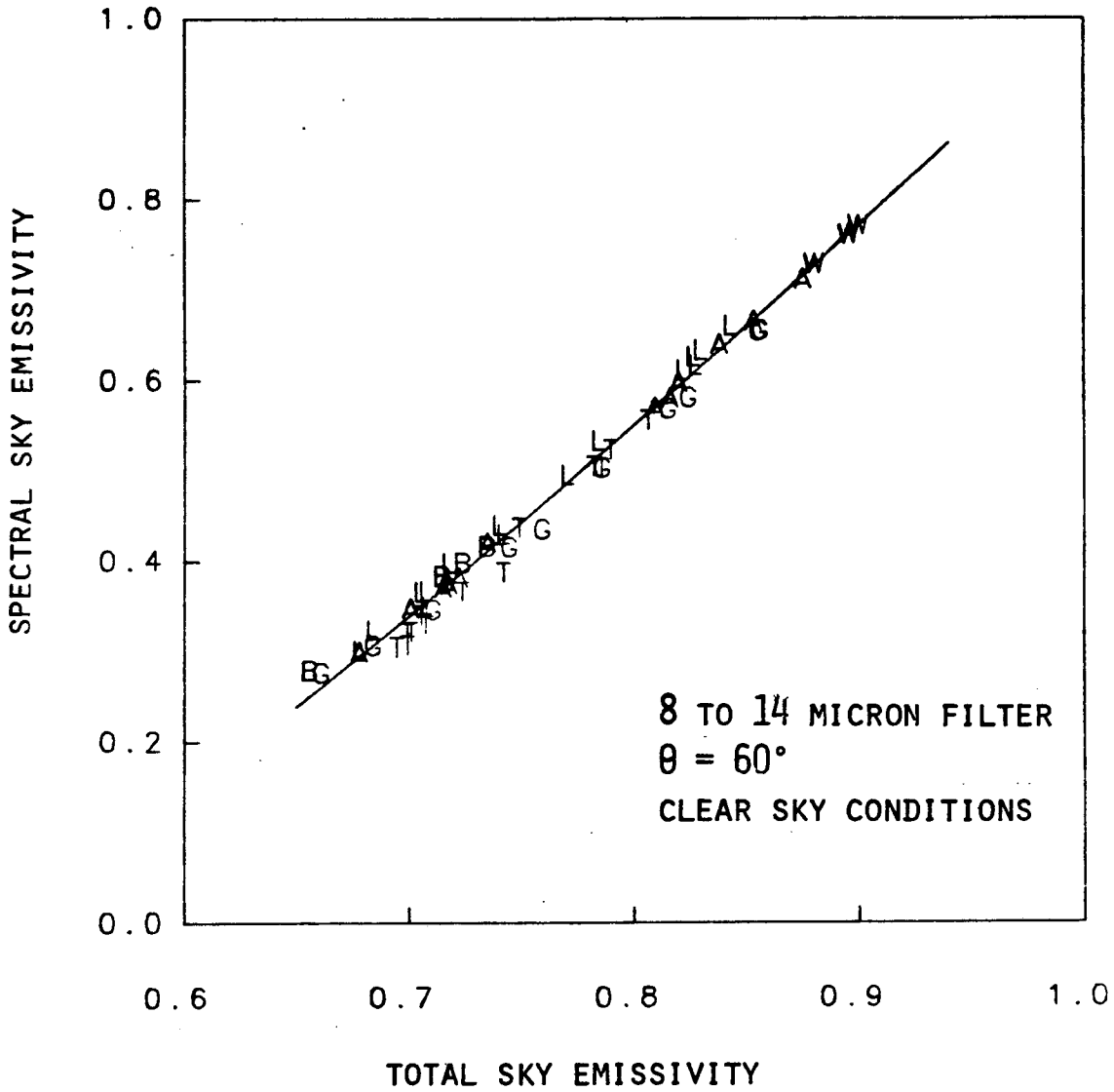
1.0
0.8
0.6
0.4
0.2
0.0
SPECTRAL SKY EMISSIVITY
0.6
0.7
0.8
0.9
1.0
TOTAL SKY EMISSIVITY
8 TO 14 MICRON FILTER
θ = 60°
CLEAR SKY CONDITIONS

FIGURE 8E

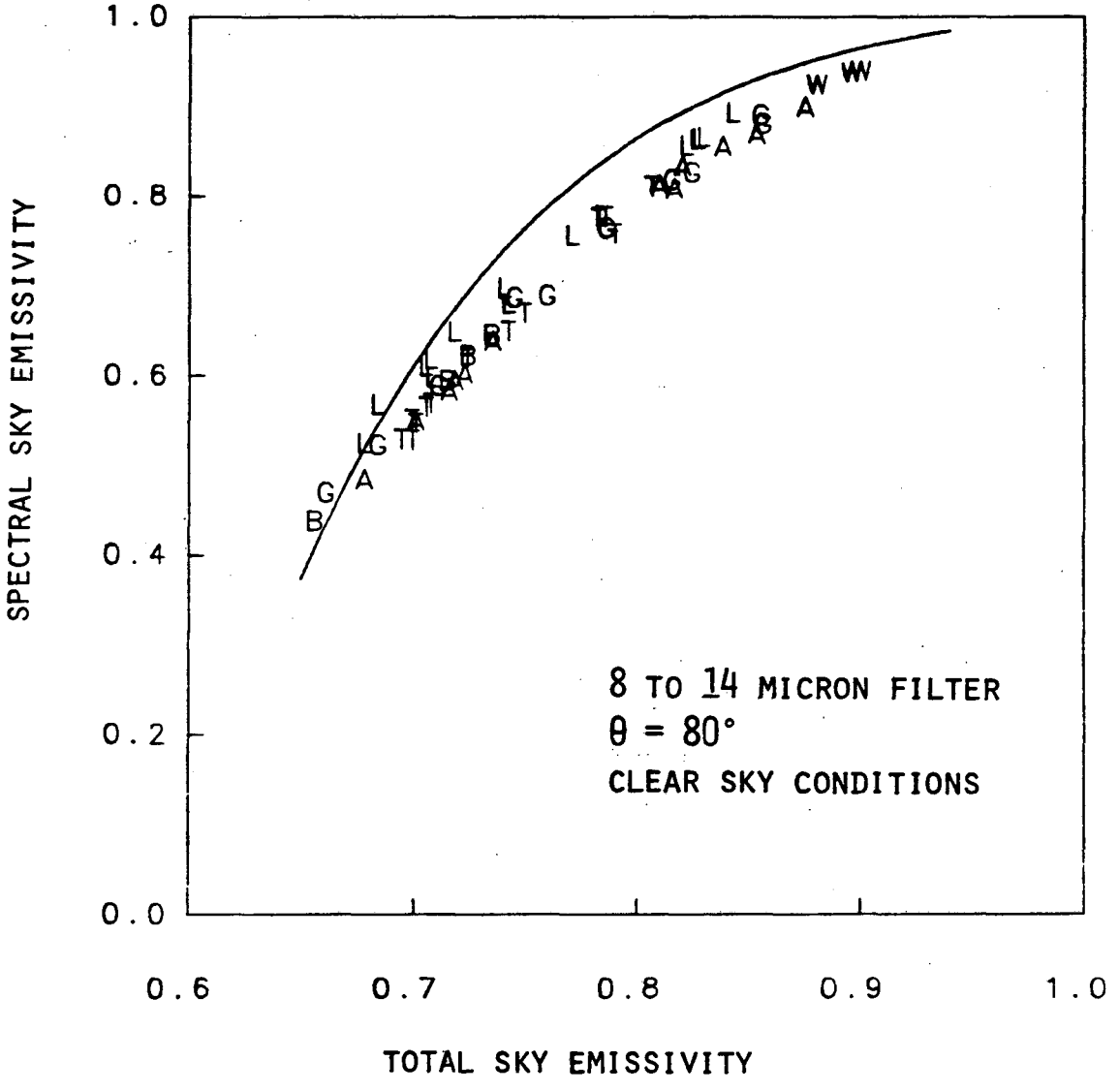
1.0
0.8
0.6
0.4
0.2
0.0
SPECTRAL SKY EMISSIVITY
0.6
0.7
0.8
0.9
1.0
TOTAL SKY EMISSIVITY
8 TO 14 MICRON FILTER
θ = 80°
CLEAR SKY CONDITIONS

FIGURE 8F

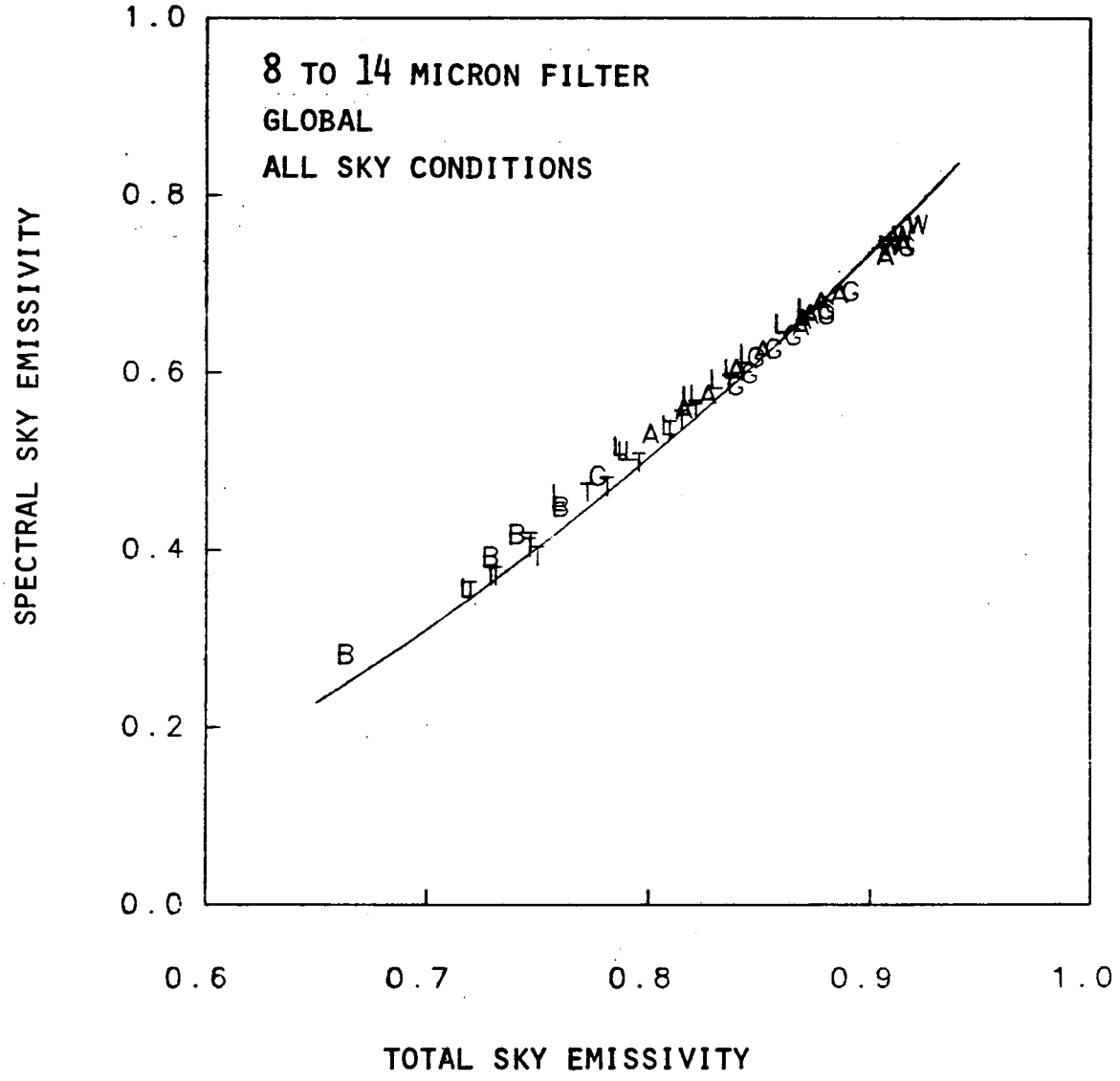
8 TO 14 MICRON FILTER
GLOBAL
ALL SKY CONDITIONS
SPECTRAL SKY EMISSIVITY
TOTAL SKY EMISSIVITY
1.0
0.8
0.6
0.4
0.2
0.0
0.6
0.7
0.8
0.9
1.0

FIGURE 9A

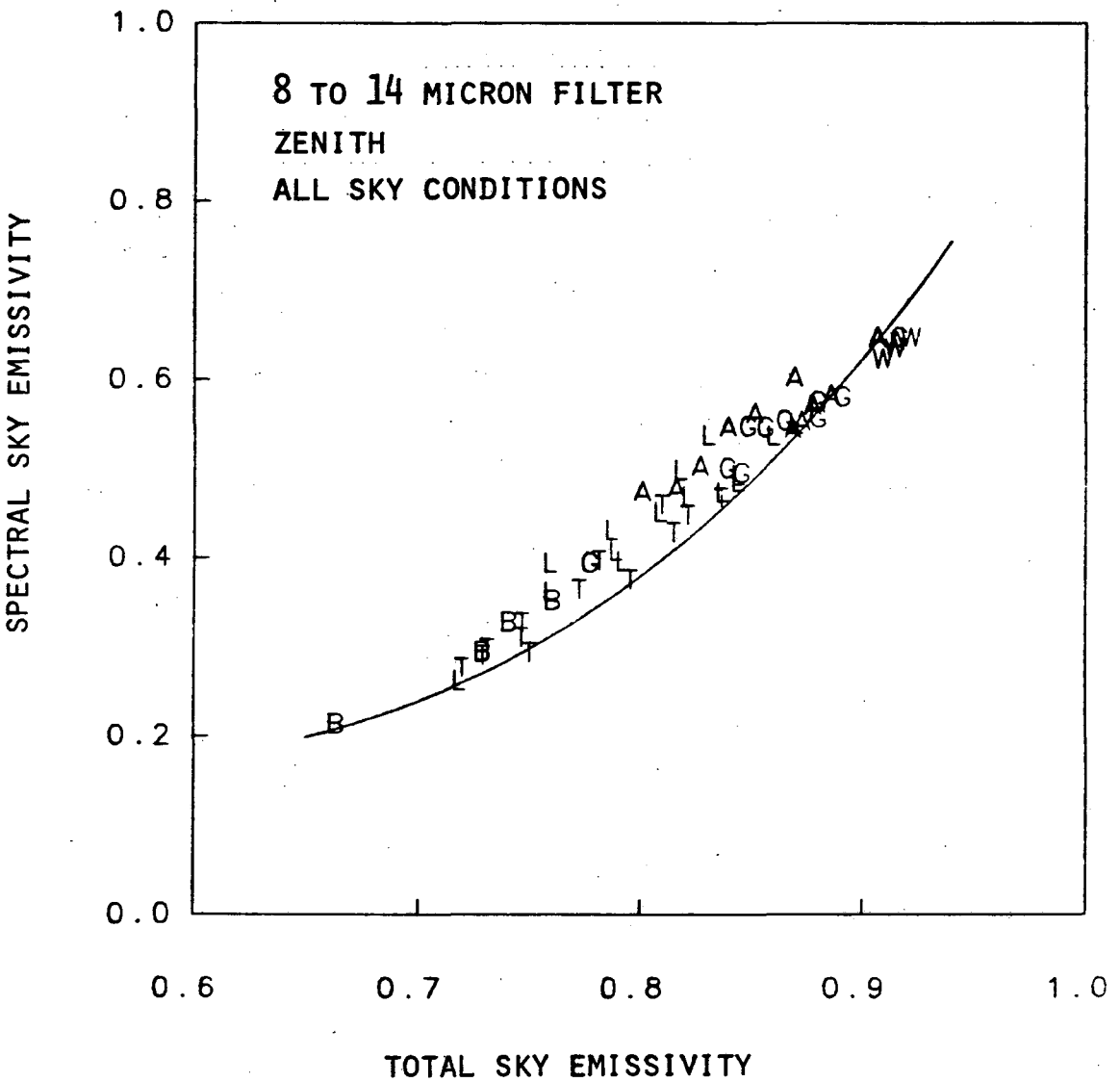
8 TO 14 MICRON FILTER
ZENITH
ALL SKY CONDITIONS
SPECTRAL SKY EMISSIVITY
TOTAL SKY EMISSIVITY
1.0
0.8
0.6
0.4
0.2
0.0
0.6
0.7
0.8
0.9
1.0

FIGURE 9B

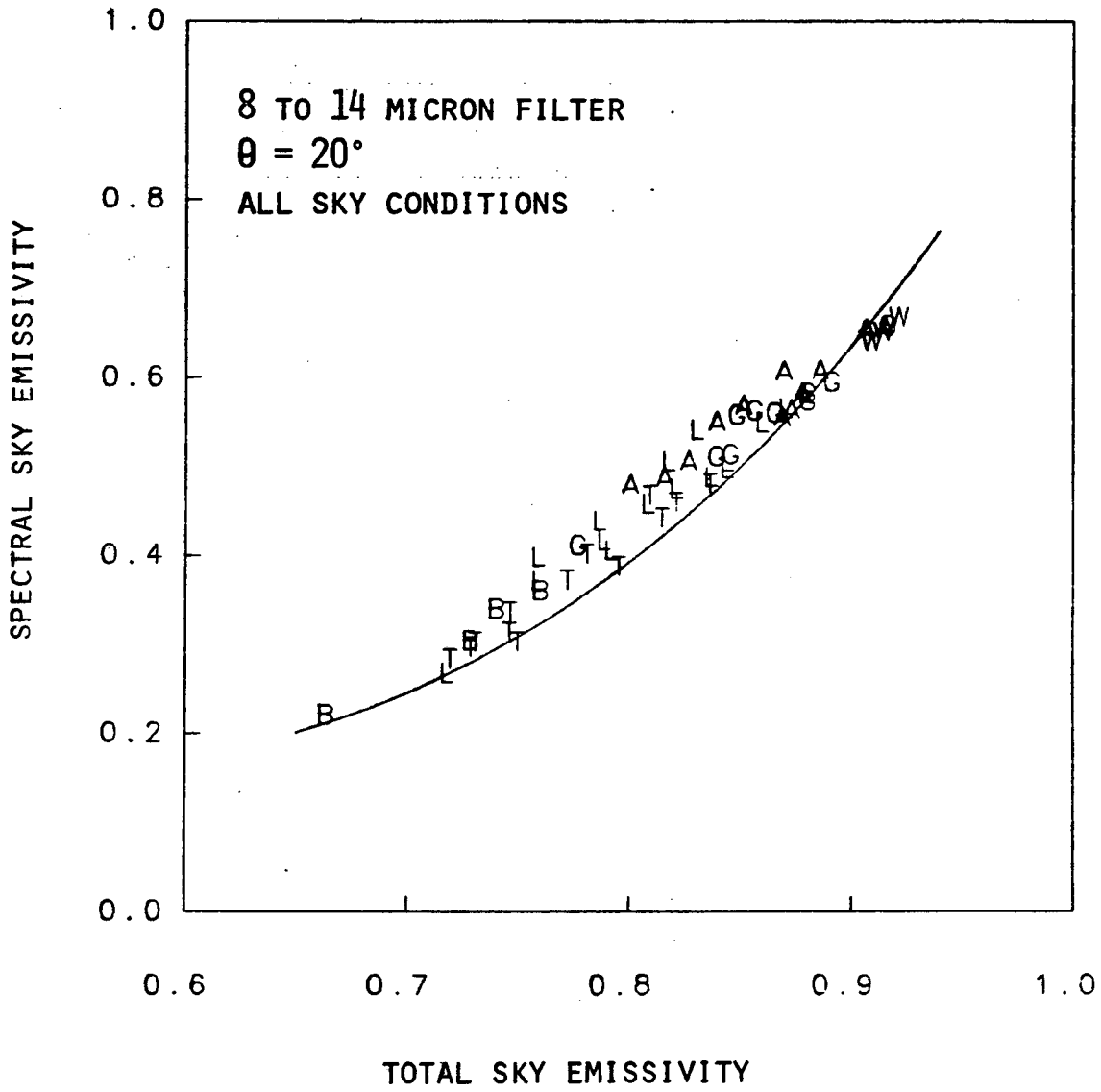
8 TO 14 MICRON FILTER
θ = 20°
ALL SKY CONDITIONS
SPECTRAL SKY EMISSIVITY
TOTAL SKY EMISSIVITY
1.0
0.8
0.6
0.4
0.2
0.0
0.6
0.7
0.8
0.9
1.0

FIGURE 9c

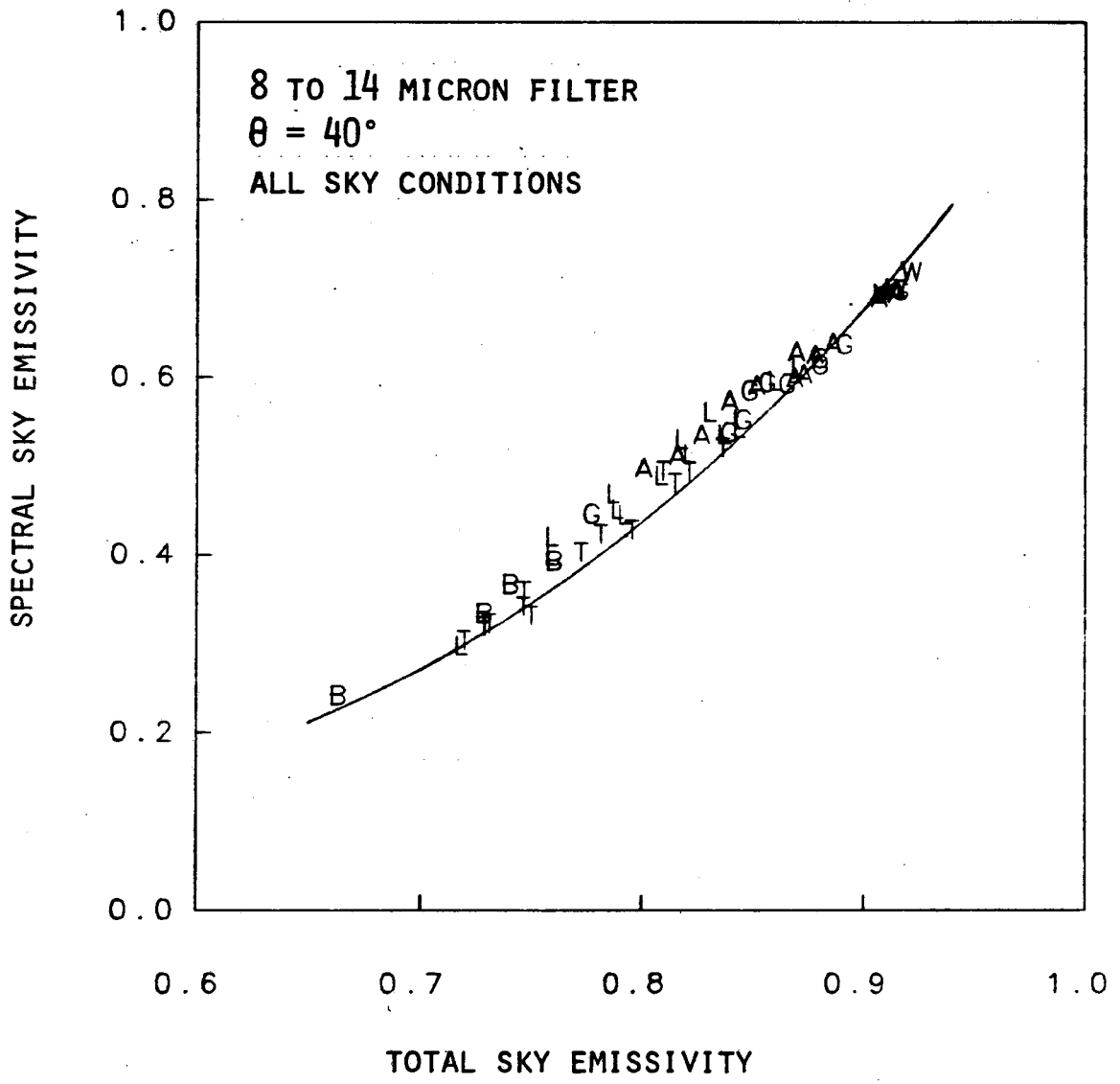
8 TO 14 MICRON FILTER
θ = 40°
ALL SKY CONDITIONS
SPECTRAL SKY EMISSIVITY
TOTAL SKY EMISSIVITY
1.0
0.8
0.6
0.4
0.2
0.0
0.6
0.7
0.8
0.9
1.0

FIGURE 9D

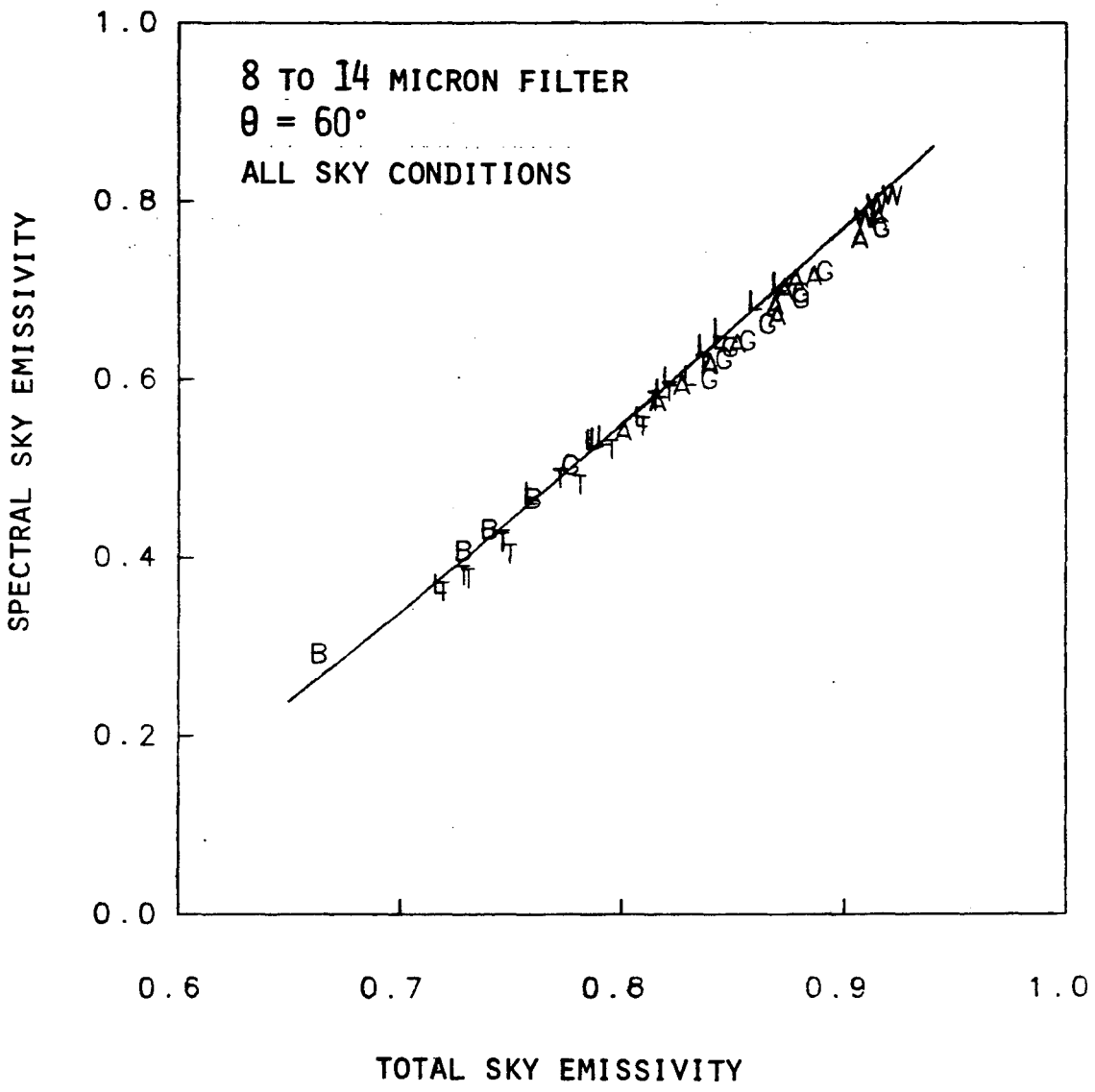
8 TO 14 MICRON FILTER
θ = 60°
ALL SKY CONDITIONS
SPECTRAL SKY EMISSIVITY
TOTAL SKY EMISSIVITY
1.0
0.8
0.6
0.4
0.2
0.0
0.6
0.7
0.8
0.9
1.0

FIGURE 9E

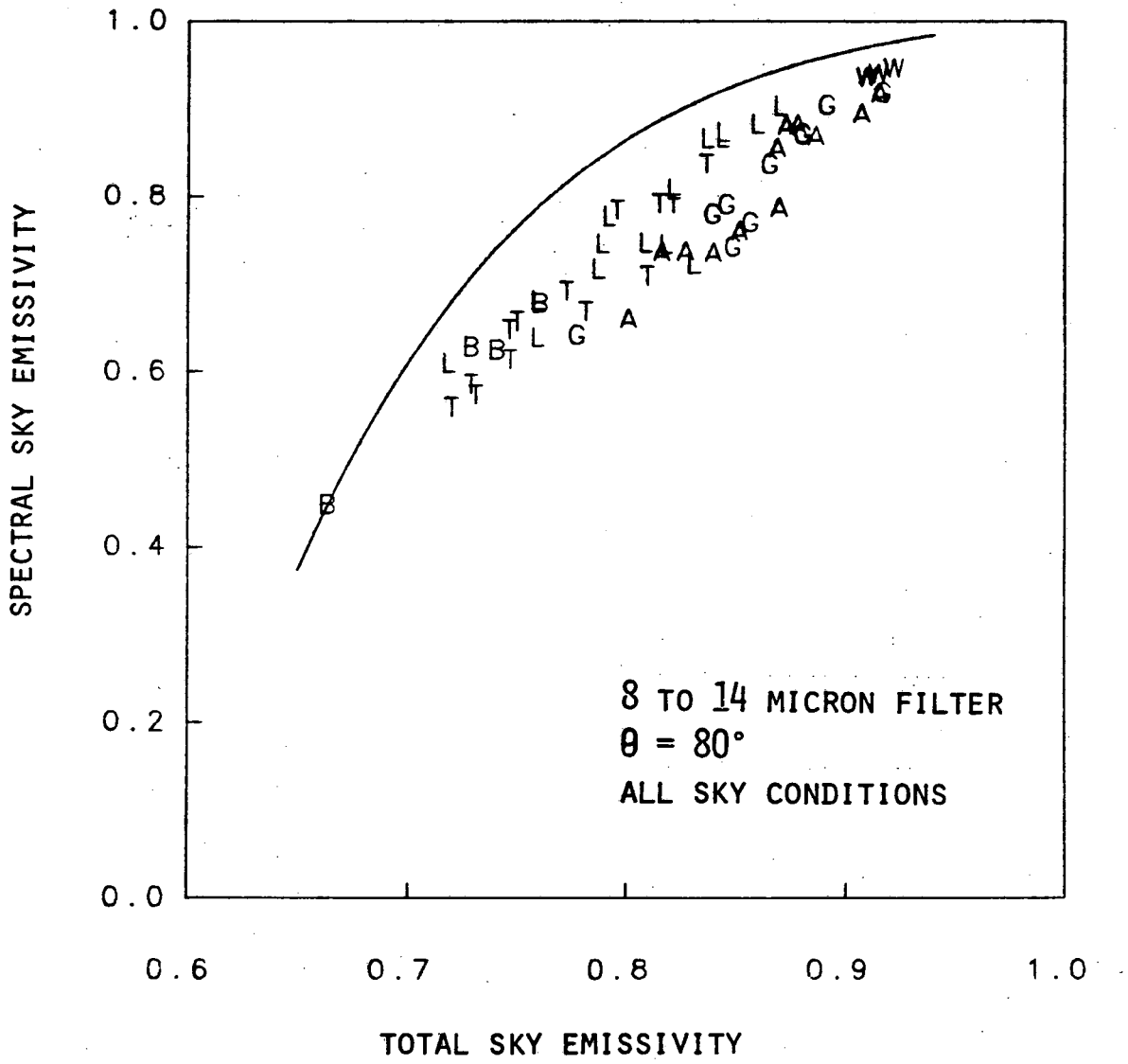
1.0
0.8
0.6
0.4
0.2
0.0
SPECTRAL SKY EMISSIVITY
0.6
0.7
0.8
0.9
1.0
TOTAL SKY EMISSIVITY
8 TO 14 MICRON FILTER
θ = 80°
ALL SKY CONDITIONS

FIGURE 9F

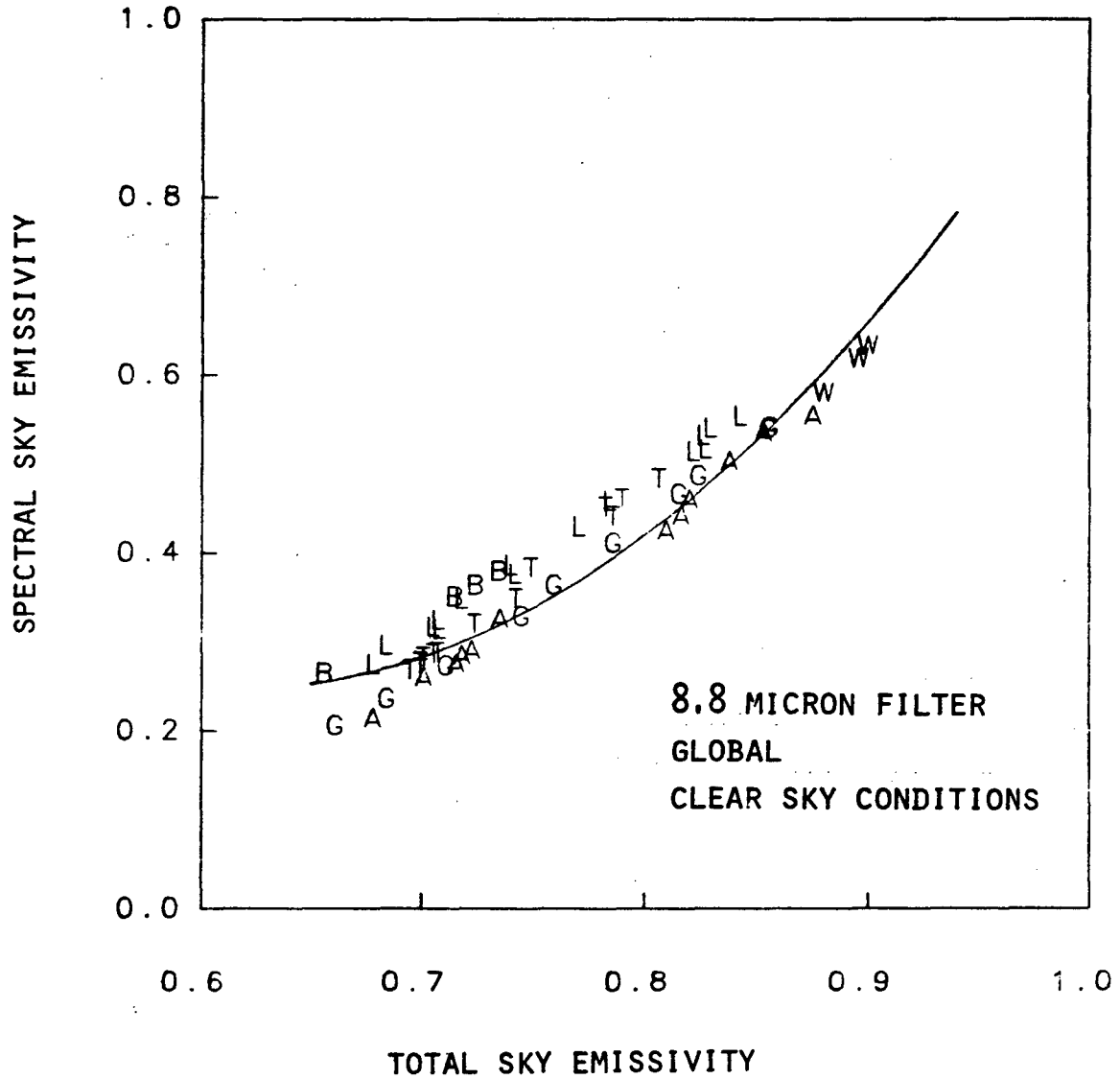
1.0
0.8
0.6
0.4
0.2
0.0
SPECTRAL SKY EMISSIVITY
0.6
0.7
0.8
0.9
1.0
TOTAL SKY EMISSIVITY
8.8 MICRON FILTER
GLOBAL
CLEAR SKY CONDITIONS

FIGURE 10A

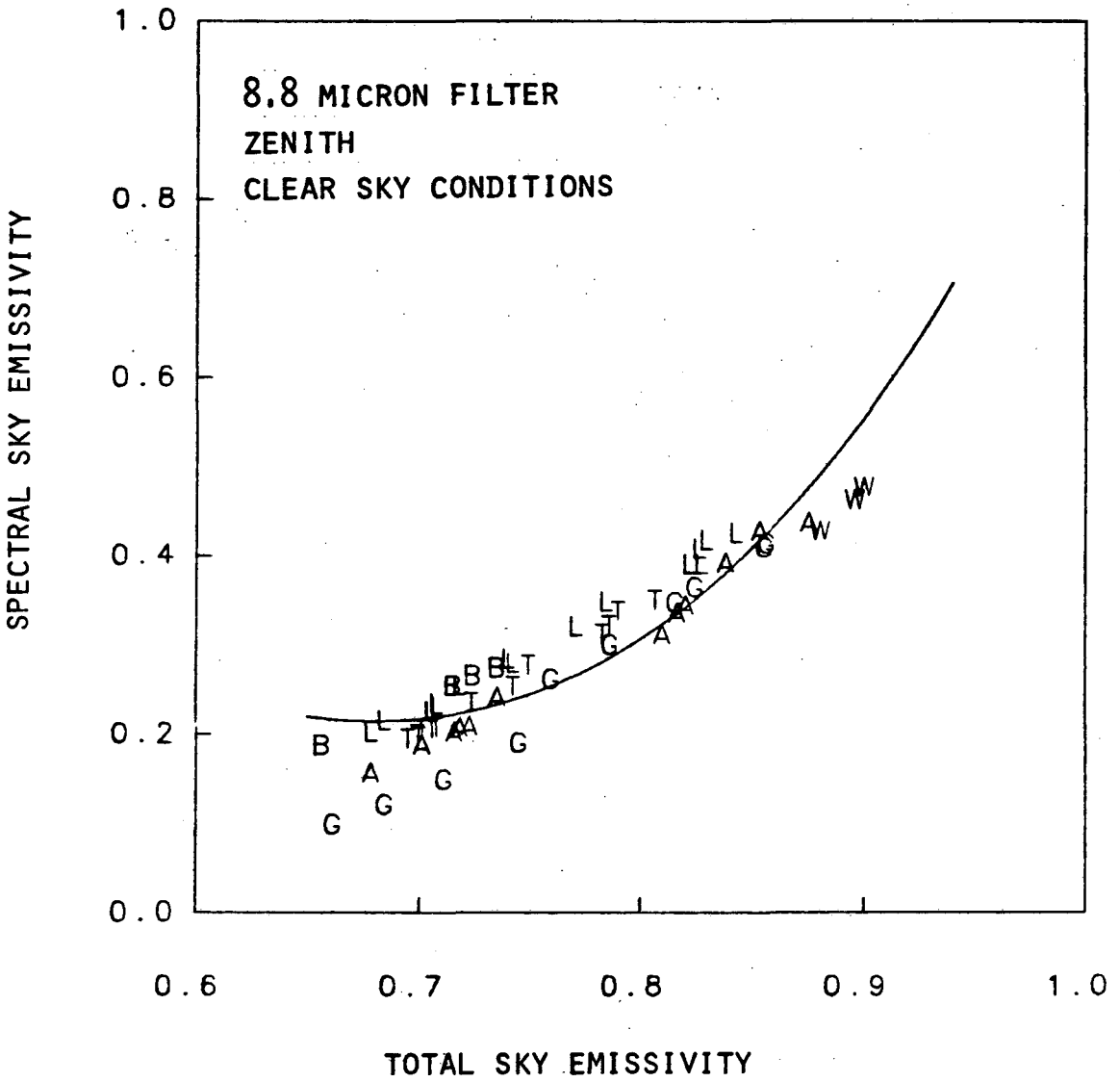
8.8 MICRON FILTER
ZENITH
CLEAR SKY CONDITIONS
SPECTRAL SKY EMISSIVITY
TOTAL SKY EMISSIVITY
1.0
0.8
0.6
0.4
0.2
0.0
0.6
0.7
0.8
0.9
1.0

FIGURE 10B

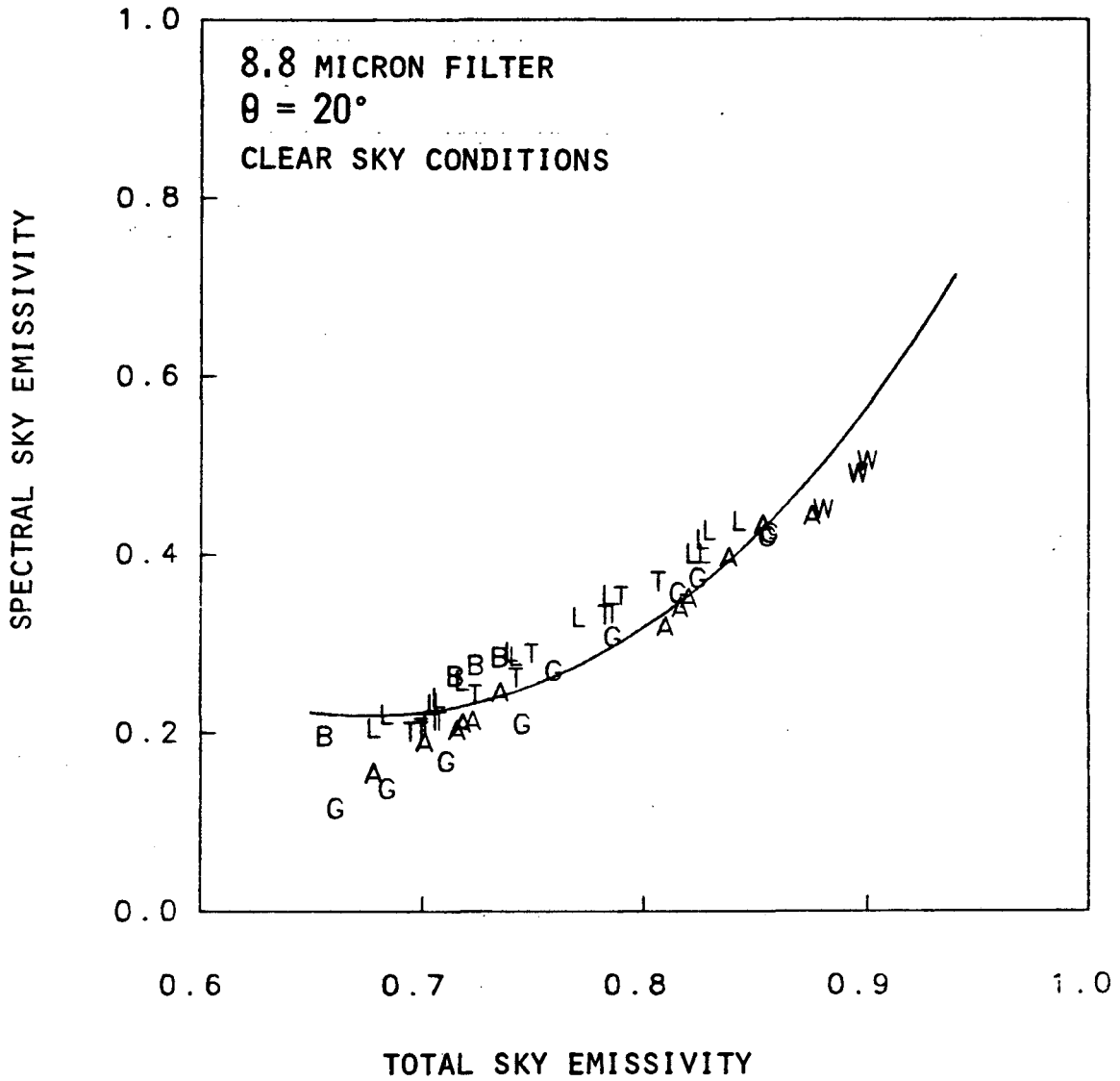
8.8 MICRON FILTER
θ = 20°
CLEAR SKY CONDITIONS
SPECTRAL SKY EMISSIVITY
TOTAL SKY EMISSIVITY
1.0
0.8
0.6
0.4
0.2
0.0
0.6
0.7
0.8
0.9
1.0

FIGURE 10c

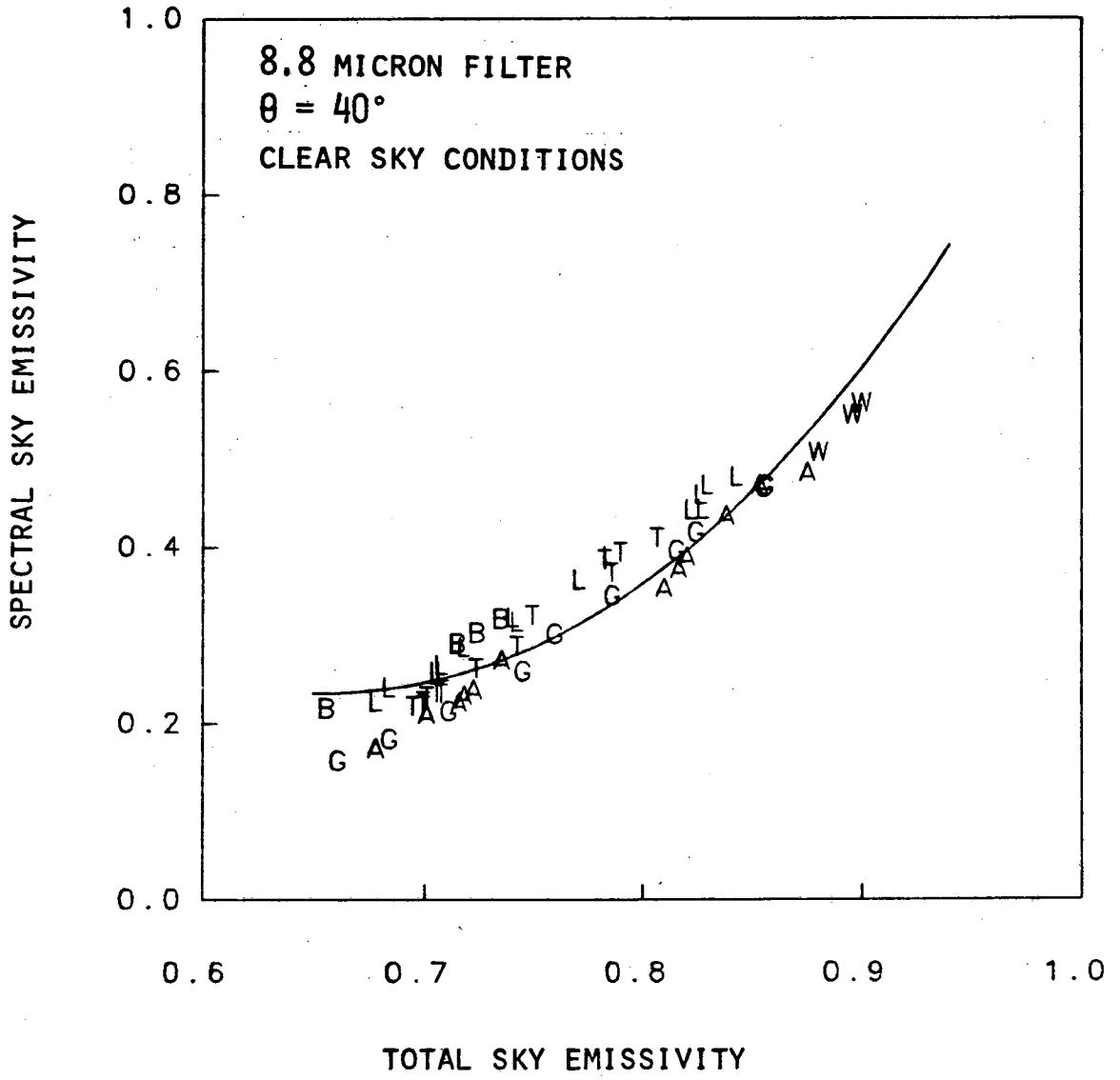
8.8 MICRON FILTER
θ = 40°
CLEAR SKY CONDITIONS
SPECTRAL SKY EMISSIVITY
TOTAL SKY EMISSIVITY
1.0
0.8
0.6
0.4
0.2
0.0
0.6
0.7
0.8
0.9
1.0

FIGURE 10D

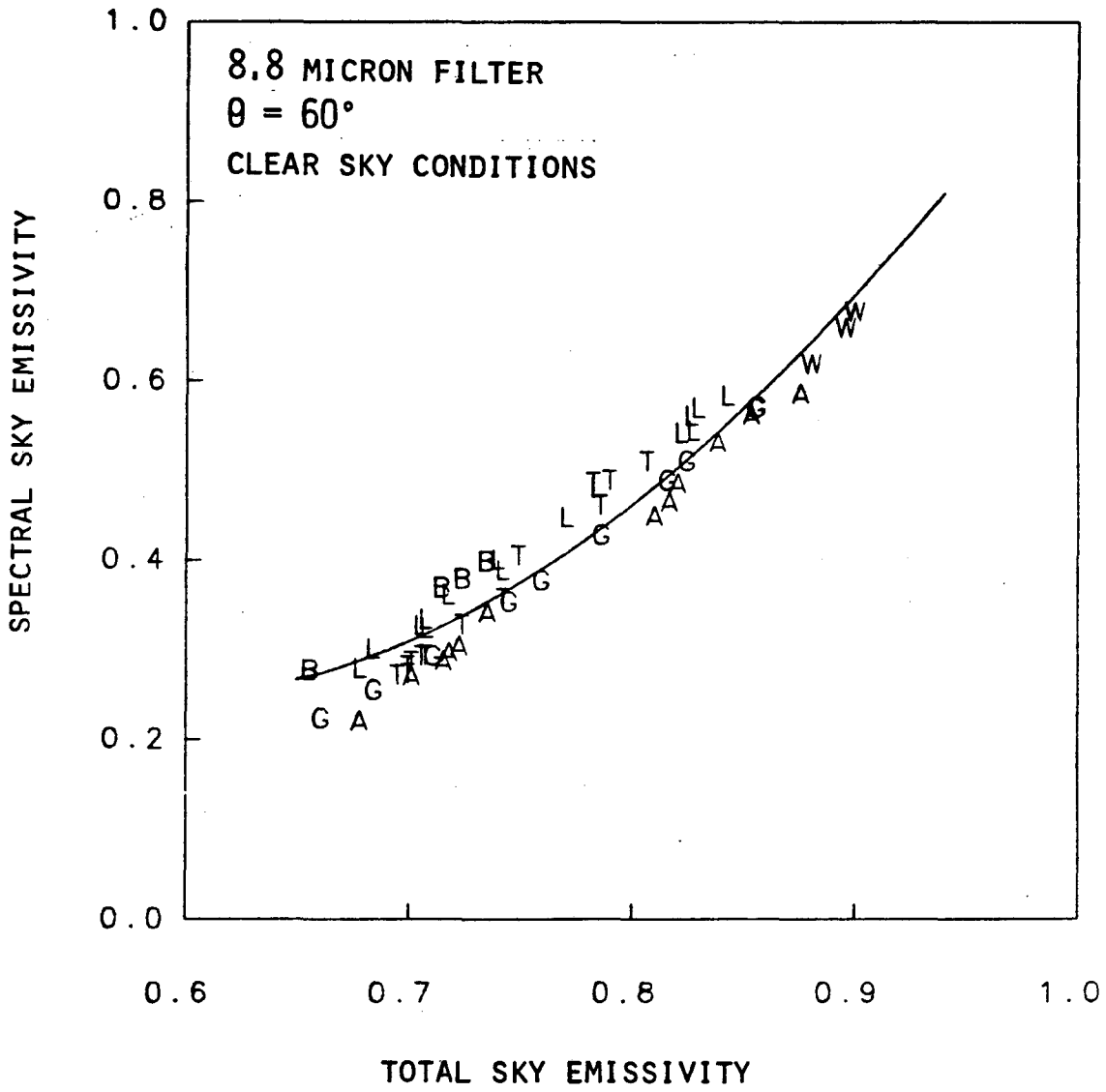
8.8 MICRON FILTER
θ = 60°
CLEAR SKY CONDITIONS
SPECTRAL SKY EMISSIVITY
TOTAL SKY EMISSIVITY
1.0
0.8
0.6
0.4
0.2
0.0
0.6
0.7
0.8
0.9
1.0

FIGURE 10E

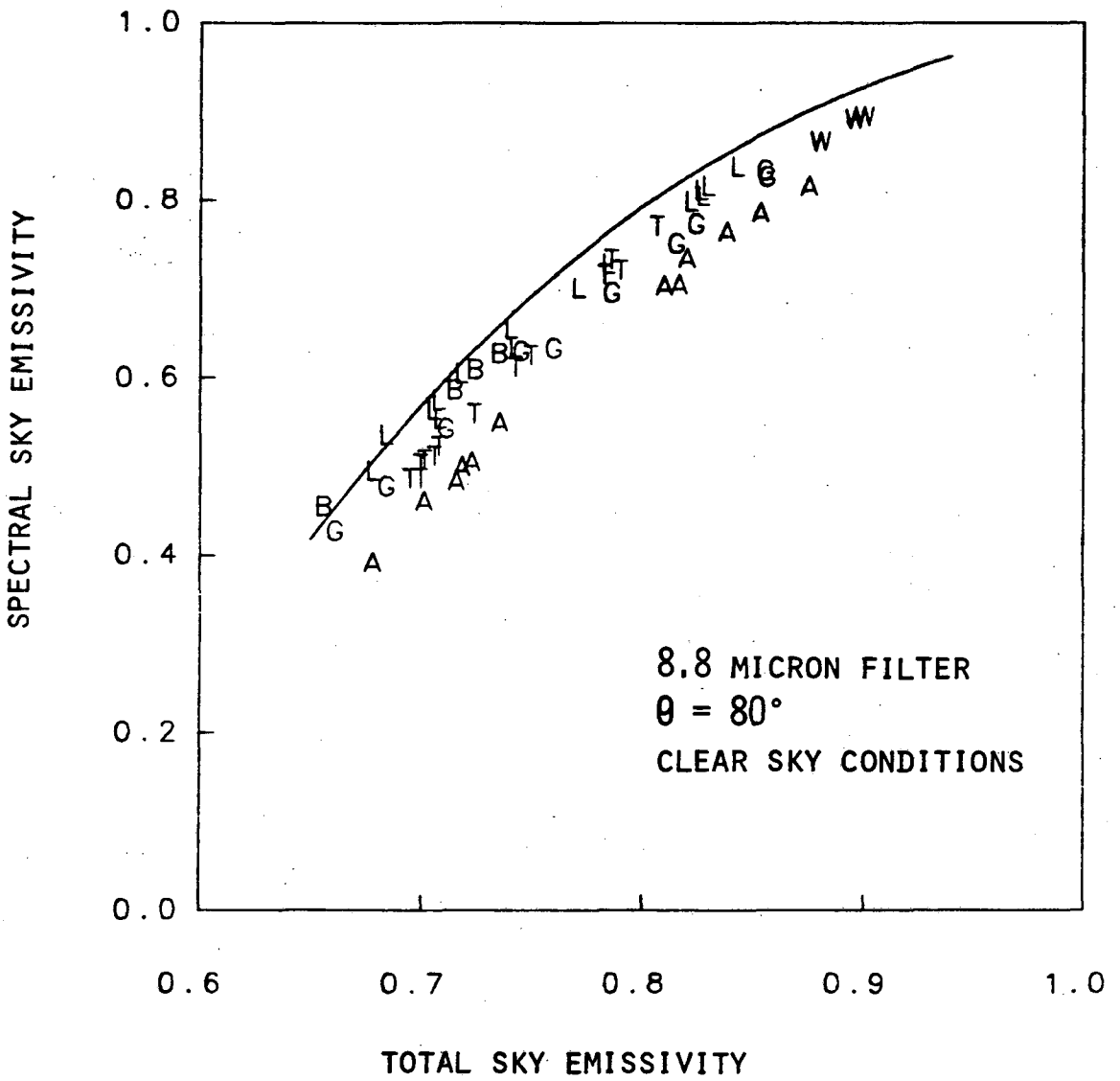
1.0
0.8
0.6
0.4
0.2
0.0
SPECTRAL SKY EMISSIVITY
0.6
0.7
0.8
0.9
1.0
TOTAL SKY EMISSIVITY
8.8 MICRON FILTER
θ = 80°
CLEAR SKY CONDITIONS

FIGURE 10F

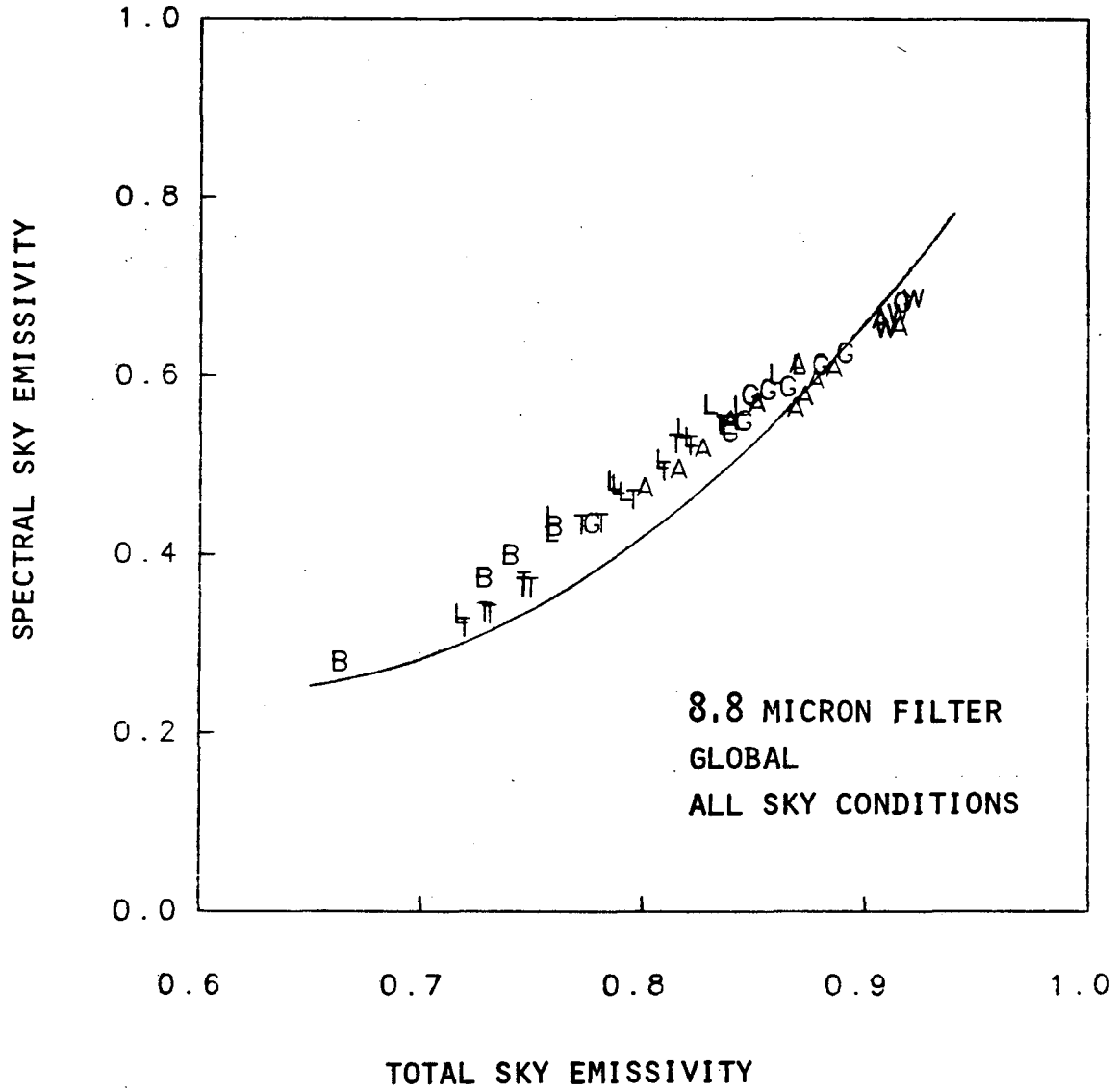
1.0
0.8
0.6
0.4
0.2
0.0
SPECTRAL SKY EMISSIVITY
0.6
0.7
0.8
0.9
1.0
TOTAL SKY EMISSIVITY
8.8 MICRON FILTER
GLOBAL
ALL SKY CONDITIONS

FIGURE 11A

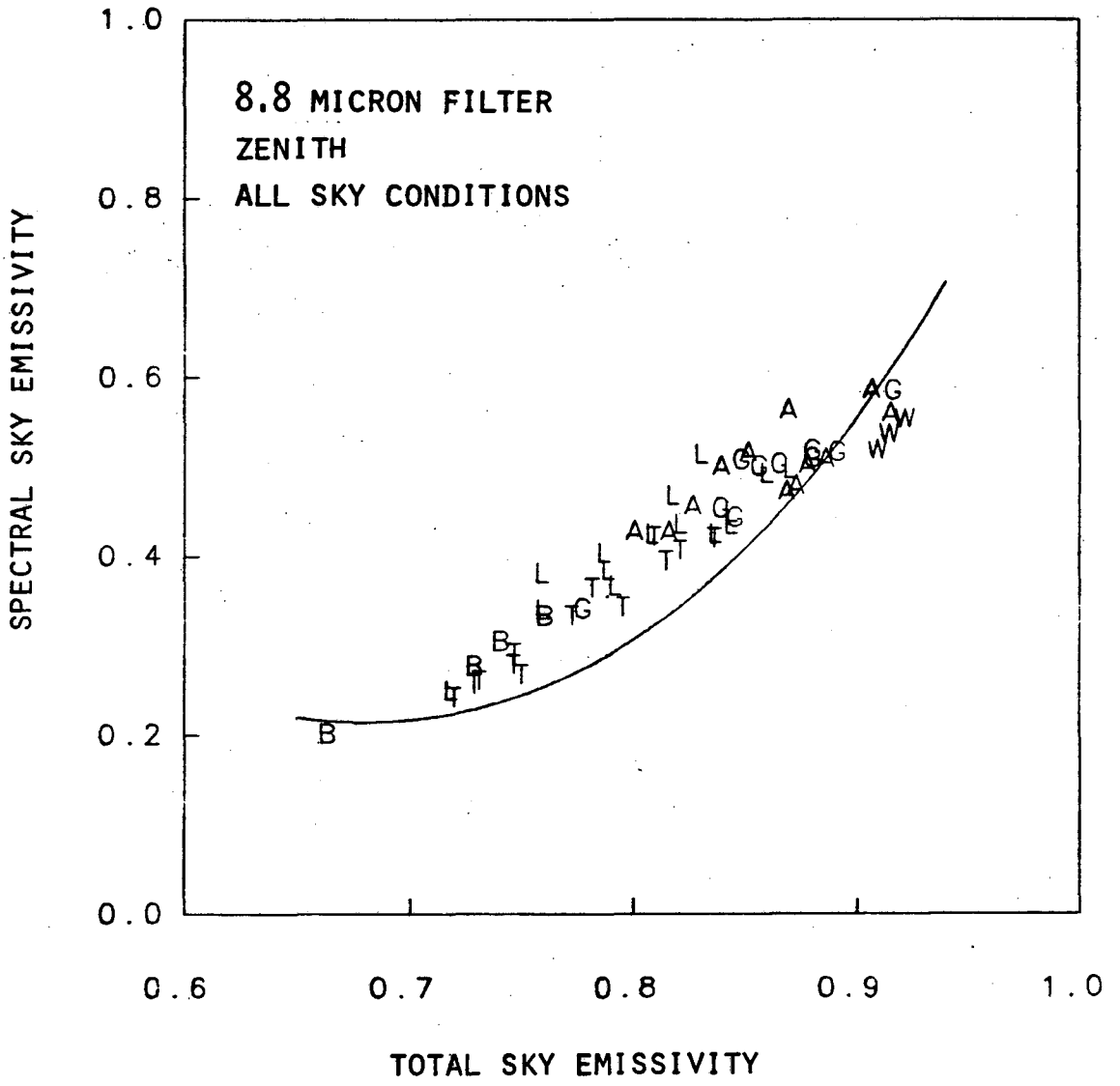
8.8 MICRON FILTER
ZENITH
ALL SKY CONDITIONS
SPECTRAL SKY EMISSIVITY
TOTAL SKY EMISSIVITY
1.0
0.8
0.6
0.4
0.2
0.0
0.6
0.7
0.8
0.9
1.0

FIGURE 11B

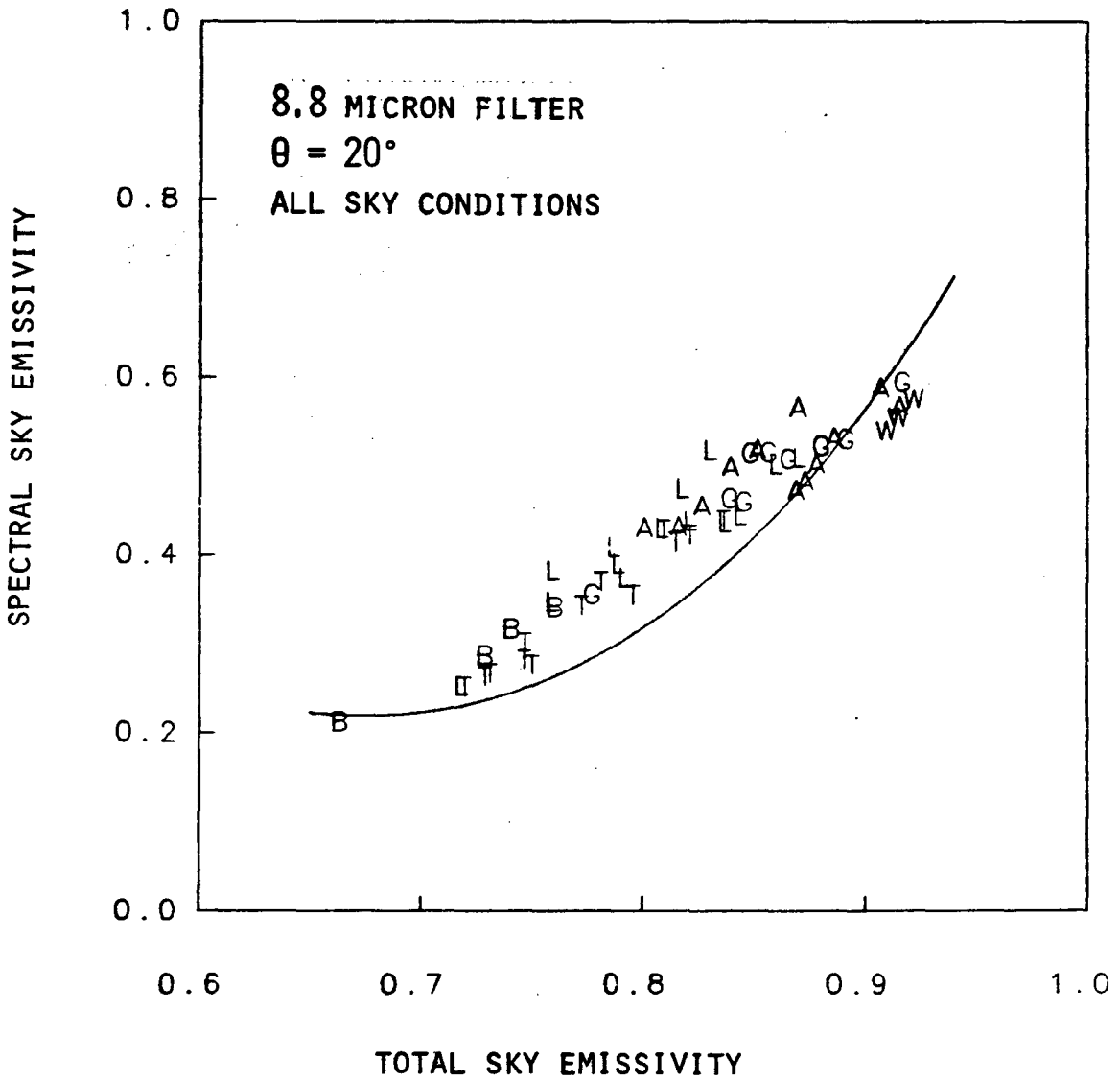
8.8 MICRON FILTER
θ = 20°
ALL SKY CONDITIONS
SPECTRAL SKY EMISSIVITY
TOTAL SKY EMISSIVITY
1.0
0.8
0.6
0.4
0.2
0.0
0.6
0.7
0.8
0.9
1.0

FIGURE 11c

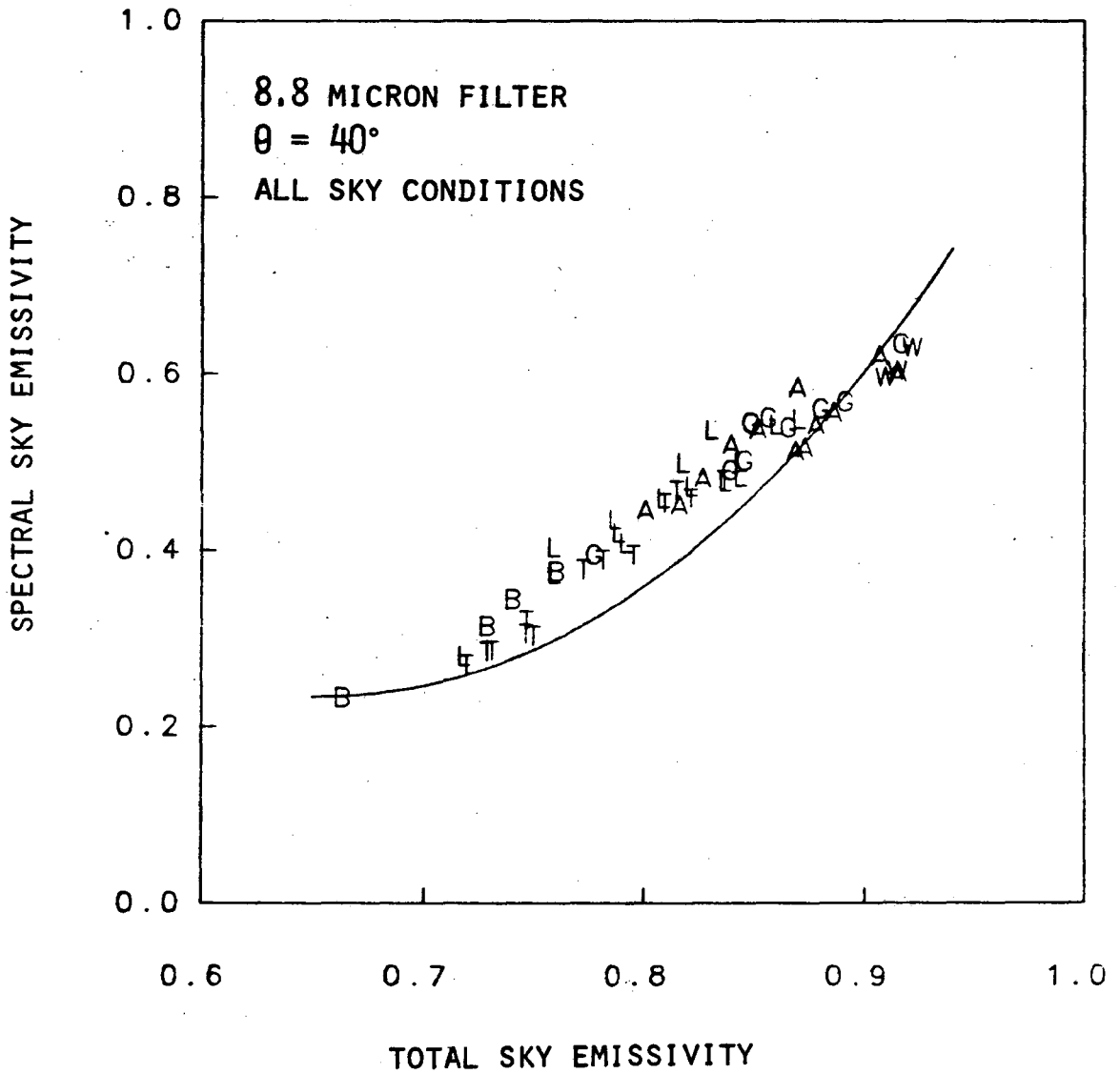
8.8 MICRON FILTER
θ = 40°
ALL SKY CONDITIONS
SPECTRAL SKY EMISSIVITY
TOTAL SKY EMISSIVITY
1.0
0.8
0.6
0.4
0.2
0.0
0.6
0.7
0.8
0.9
1.0

FIGURE 11D

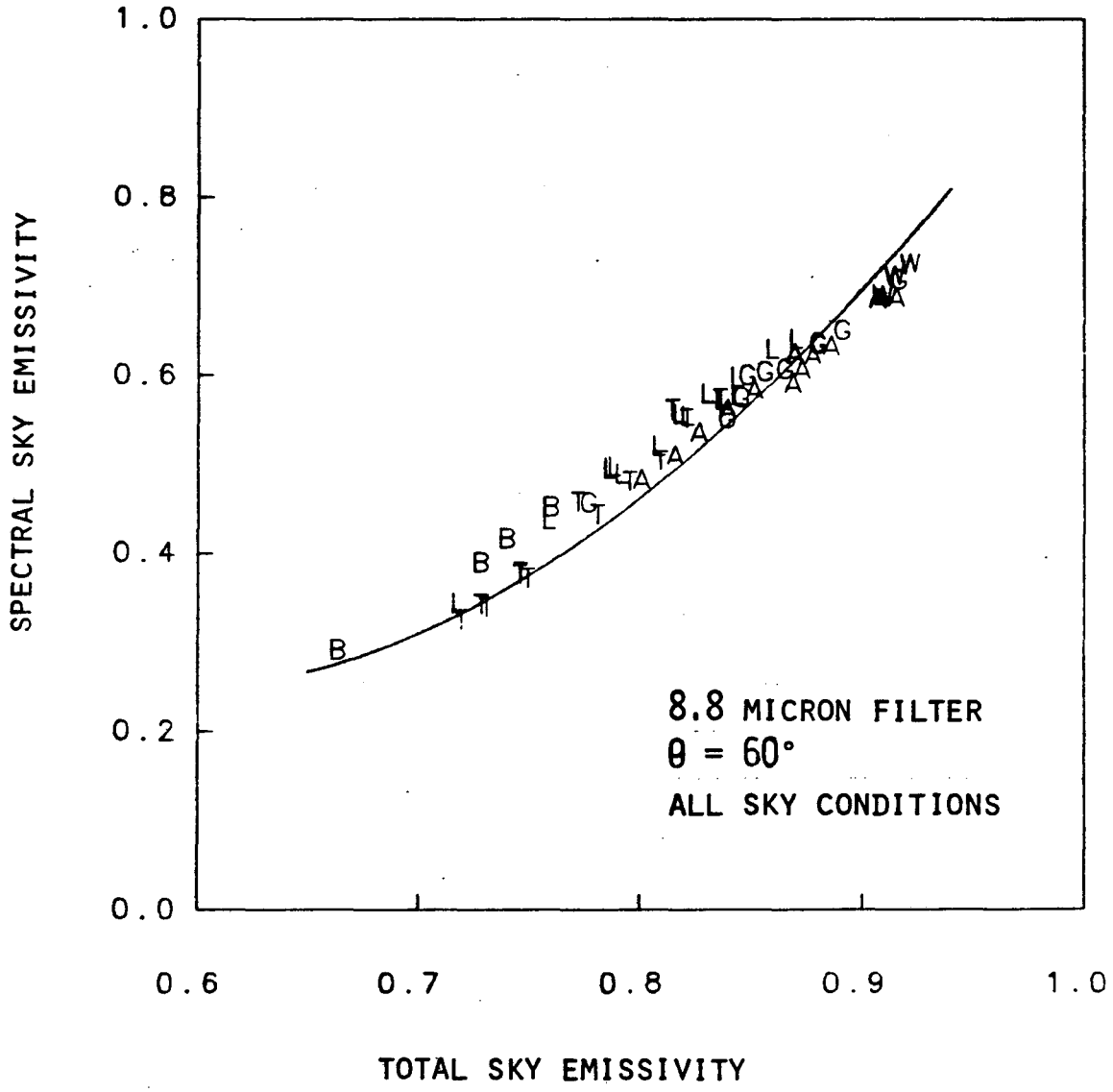
1.0
0.8
0.6
0.4
0.2
0.0
SPECTRAL SKY EMISSIVITY
0.6
0.7
0.8
0.9
1.0
TOTAL SKY EMISSIVITY
8.8 MICRON FILTER
θ = 60°
ALL SKY CONDITIONS

FIGURE 11E

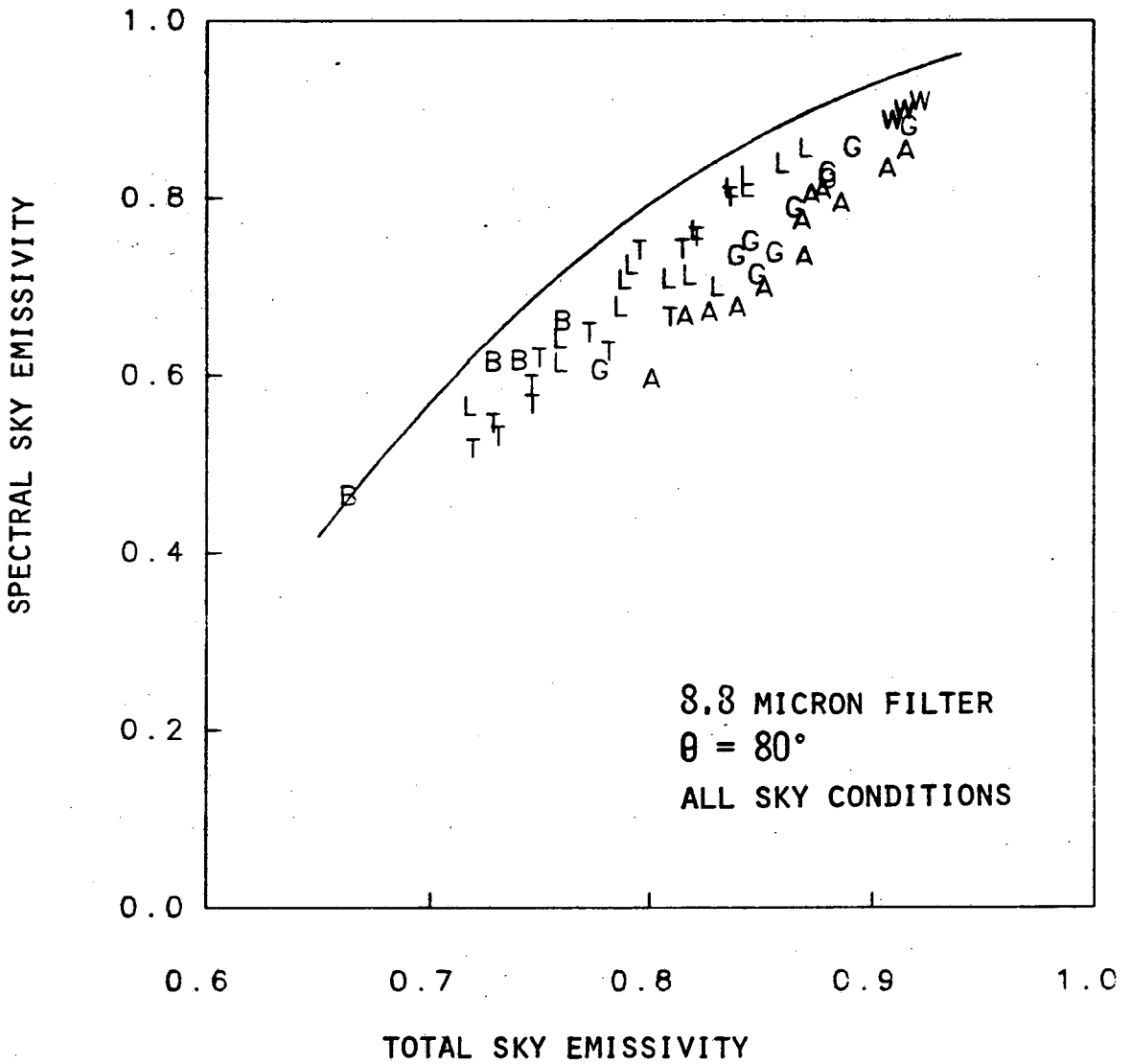
1.0
0.8
0.6
0.4
0.2
0.0
SPECTRAL SKY EMISSIVITY
0.6
0.7
0.8
0.9
1.0
TOTAL SKY EMISSIVITY
8.8 MICRON FILTER
θ = 80°
ALL SKY CONDITIONS

FIGURE 11F

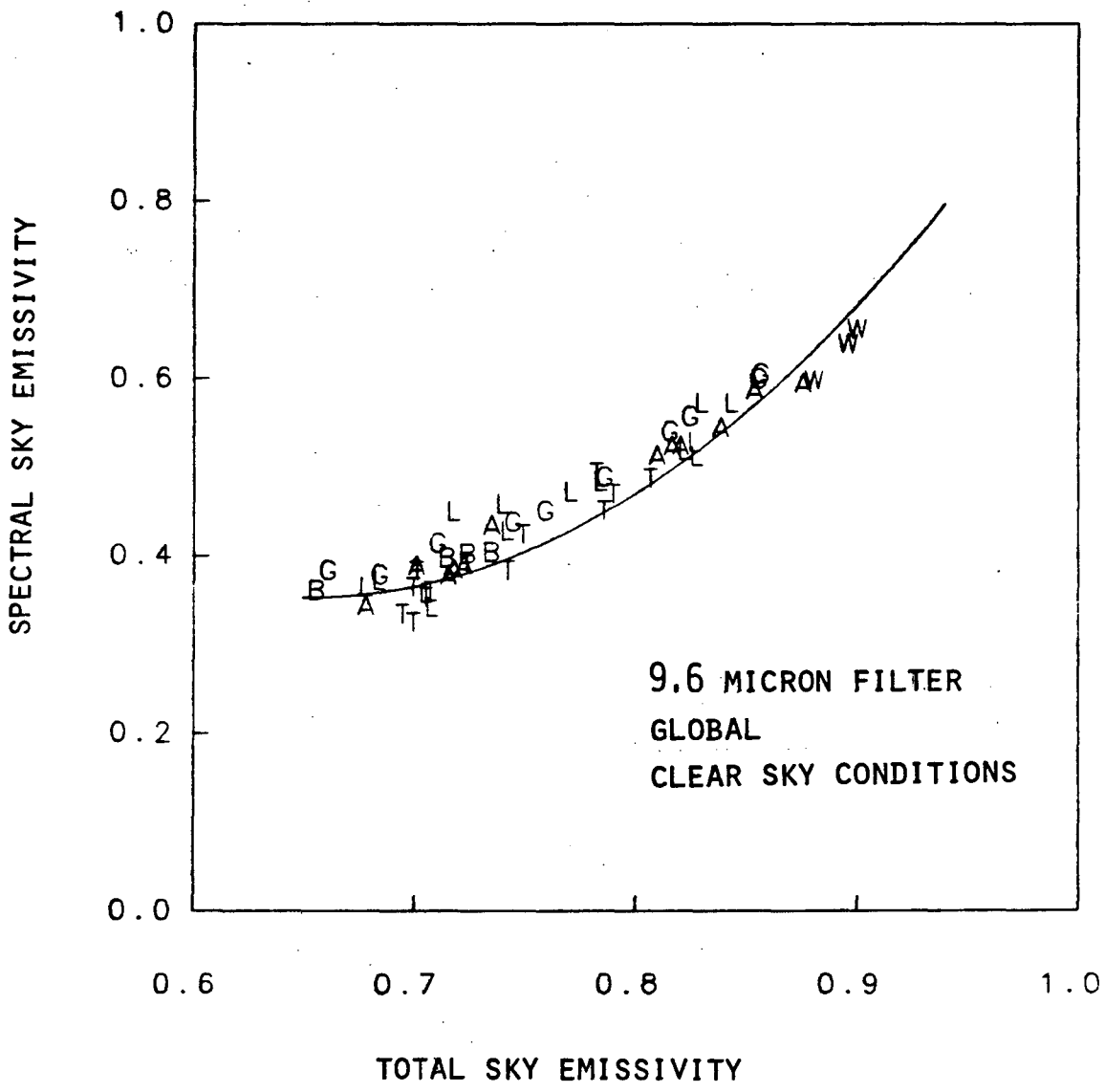
1.0
0.8
0.6
0.4
0.2
0.0
SPECTRAL SKY EMISSIVITY
0.6
0.7
0.8
0.9
1.0
TOTAL SKY EMISSIVITY
9.6 MICRON FILTER
GLOBAL
CLEAR SKY CONDITIONS

FIGURE 12A

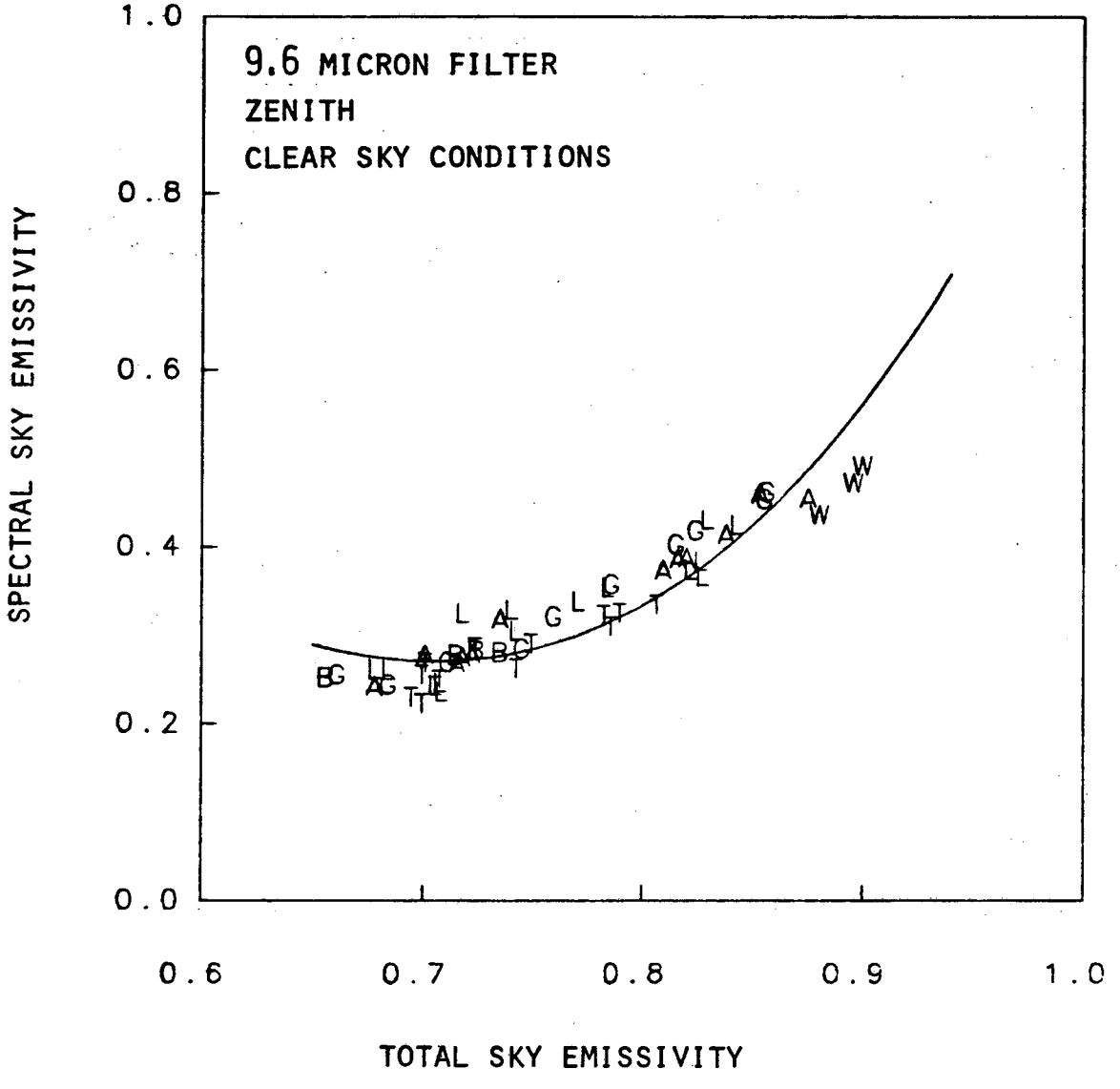
9.6 MICRON FILTER
ZENITH
CLEAR SKY CONDITIONS
SPECTRAL SKY EMISSIVITY
TOTAL SKY EMISSIVITY
1.0
0.8
0.6
0.4
0.2
0.0
0.6
0.7
0.8
0.9
1.0

FIGURE 12B

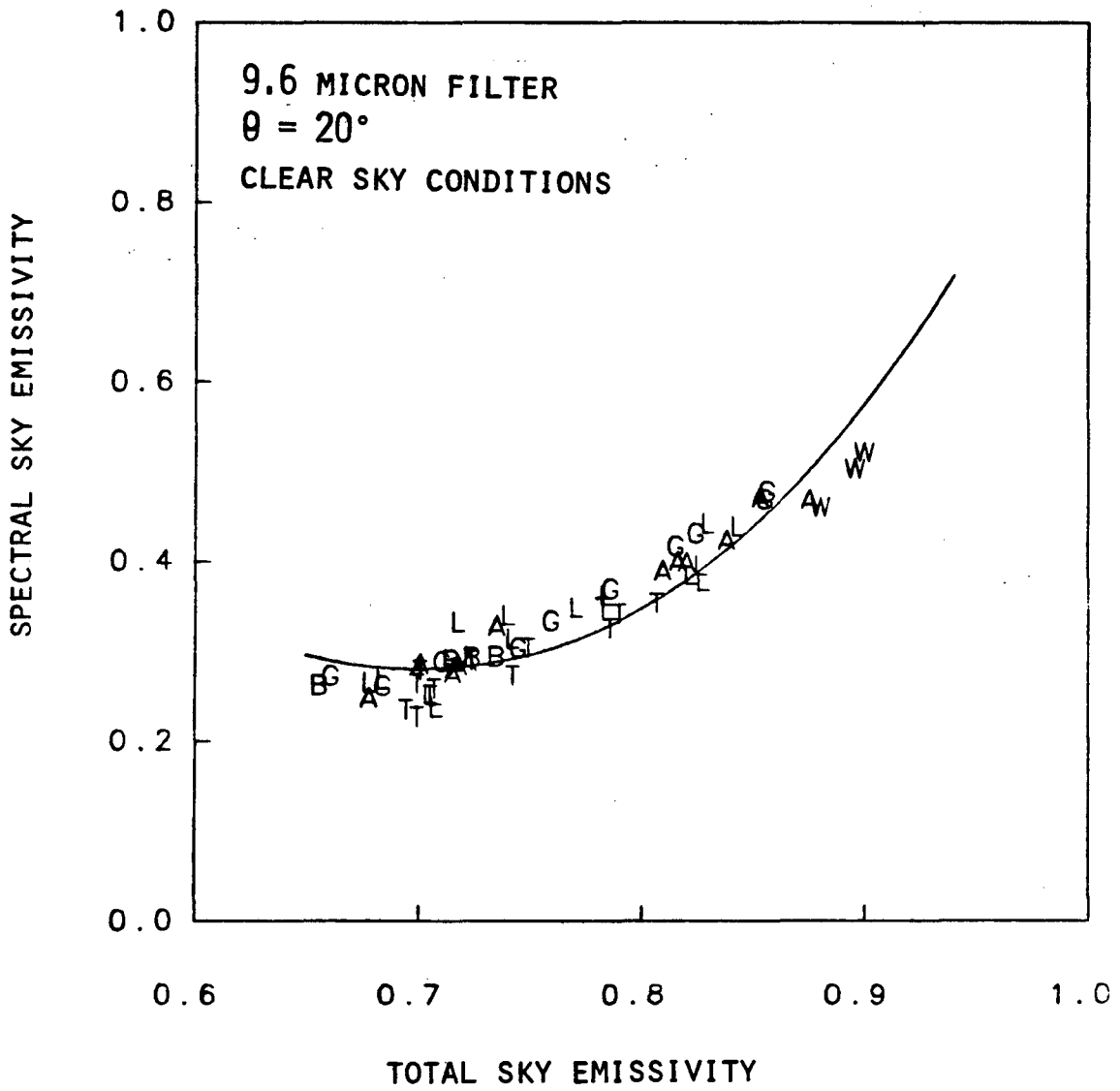
9.6 MICRON FILTER
θ = 20°
CLEAR SKY CONDITIONS
SPECTRAL SKY EMISSIVITY
TOTAL SKY EMISSIVITY
1.0
0.8
0.6
0.4
0.2
0.0
0.6
0.7
0.8
0.9
1.0

FIGURE 12c

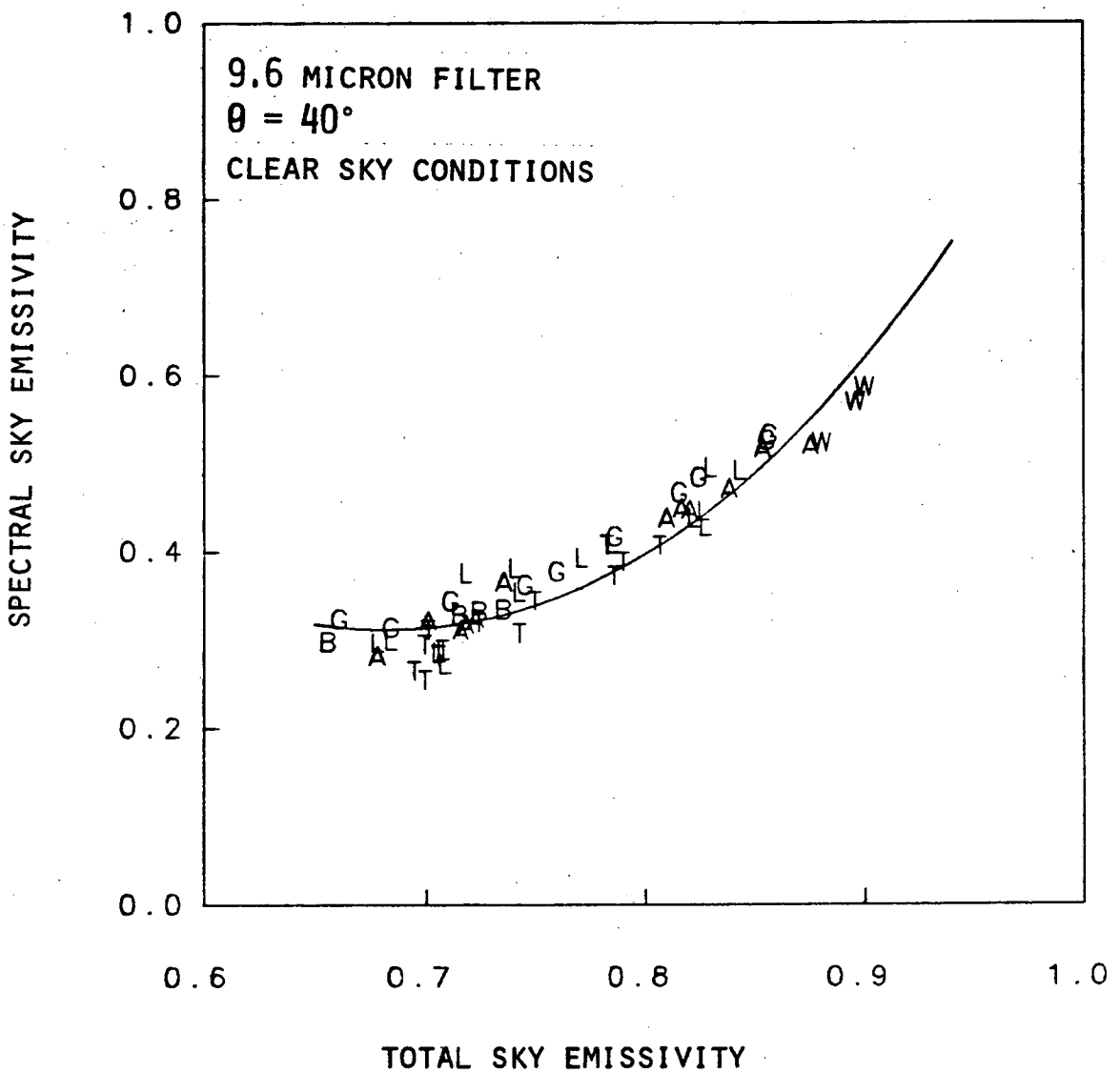
9.6 MICRON FILTER
θ = 40°
CLEAR SKY CONDITIONS
SPECTRAL SKY EMISSIVITY
TOTAL SKY EMISSIVITY
1.0
0.8
0.6
0.4
0.2
0.0
0.6
0.7
0.8
0.9
1.0

FIGURE 12D

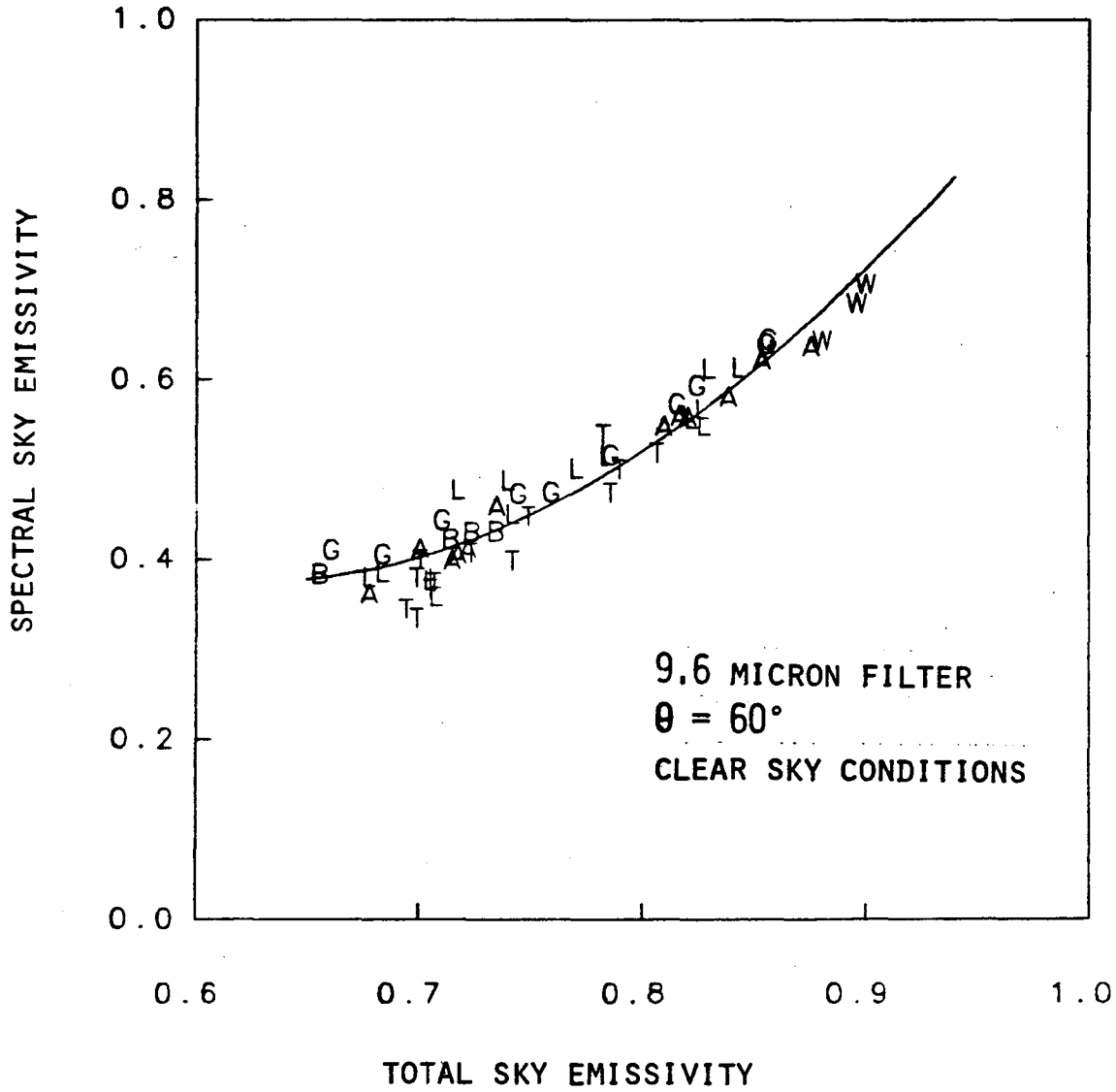
1.0
0.8
0.6
0.4
0.2
0.0
SPECTRAL SKY EMISSIVITY
0.6
0.7
0.8
0.9
1.0
TOTAL SKY EMISSIVITY
9.6 MICRON FILTER
θ = 60°
CLEAR SKY CONDITIONS

FIGURE 12E

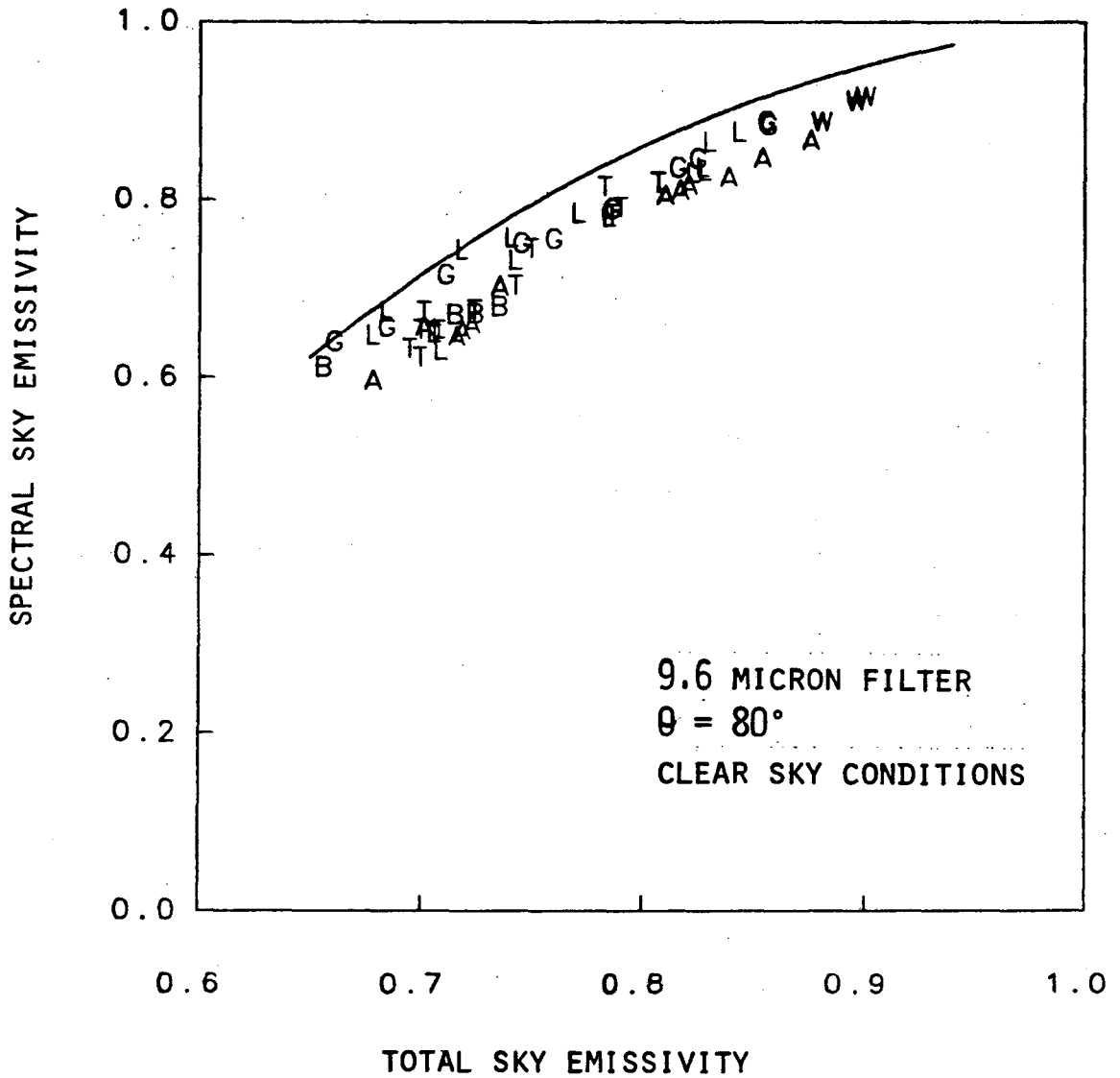
1.0
0.8
0.6
0.4
0.2
0.0
SPECTRAL SKY EMISSIVITY
0.6
0.7
0.8
0.9
1.0
TOTAL SKY EMISSIVITY
9.6 MICRON FILTER
θ = 80°
CLEAR SKY CONDITIONS

FIGURE 12F

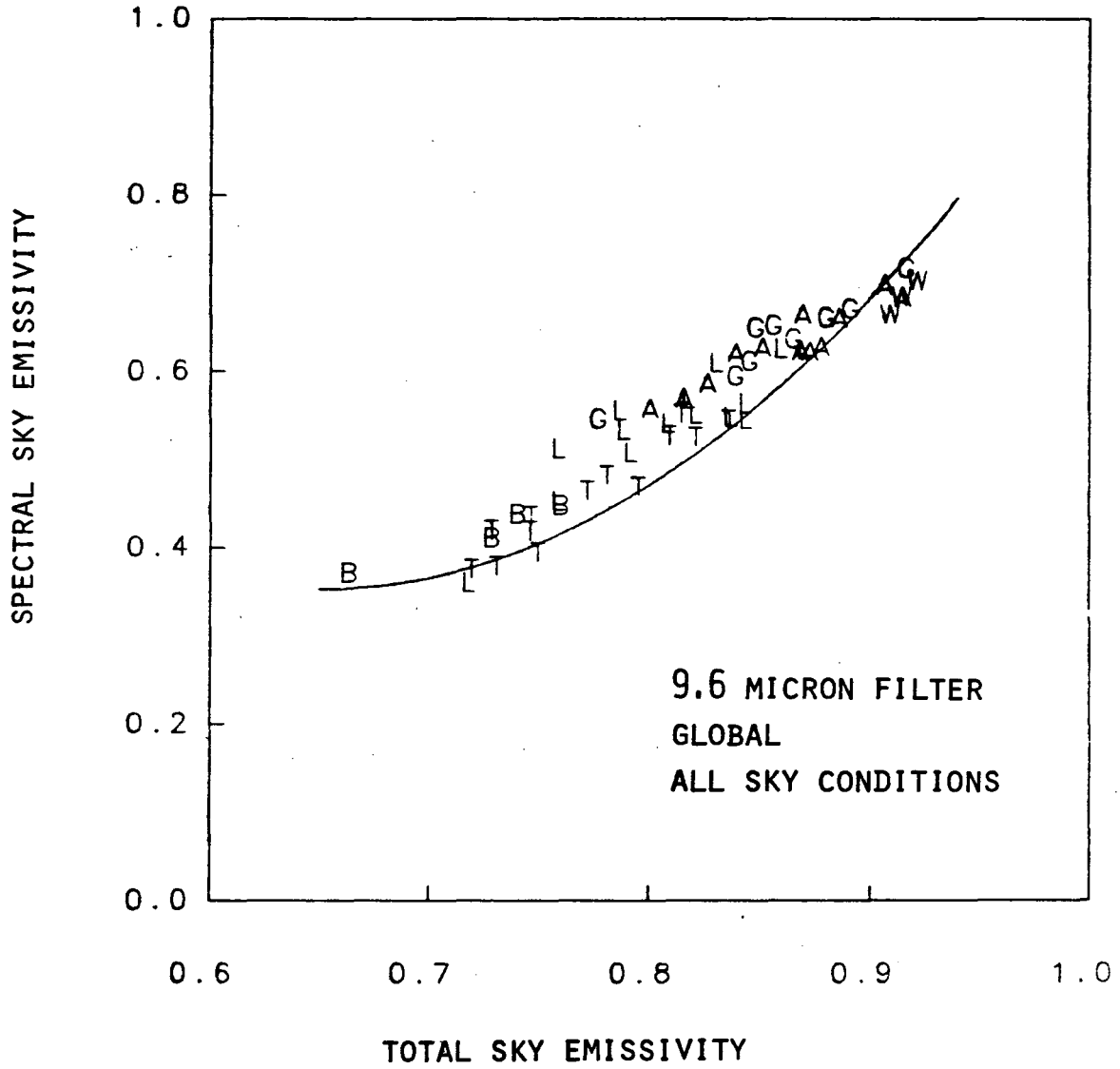
1.0
0.8
0.6
0.4
0.2
0.0
SPECTRAL SKY EMISSIVITY
0.6
0.7
0.8
0.9
1.0
TOTAL SKY EMISSIVITY
9.6 MICRON FILTER
GLOBAL
ALL SKY CONDITIONS

FIGURE 13A

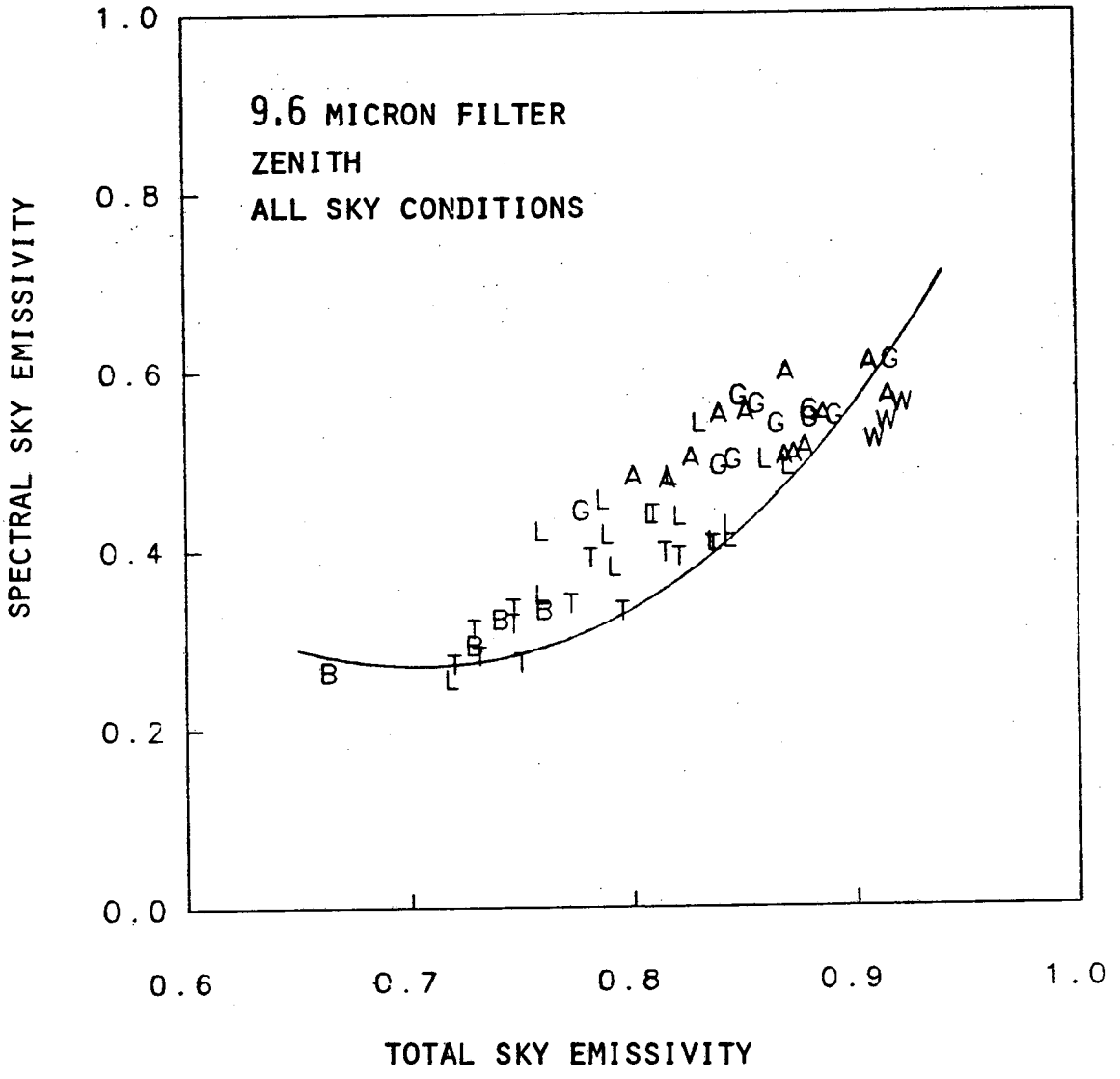
9.6 MICRON FILTER
ZENITH
ALL SKY CONDITIONS
SPECTRAL SKY EMISSIVITY
TOTAL SKY EMISSIVITY
1.0
0.8
0.6
0.4
0.2
0.0
0.6
0.7
0.8
0.9
1.0

FIGURE 13B

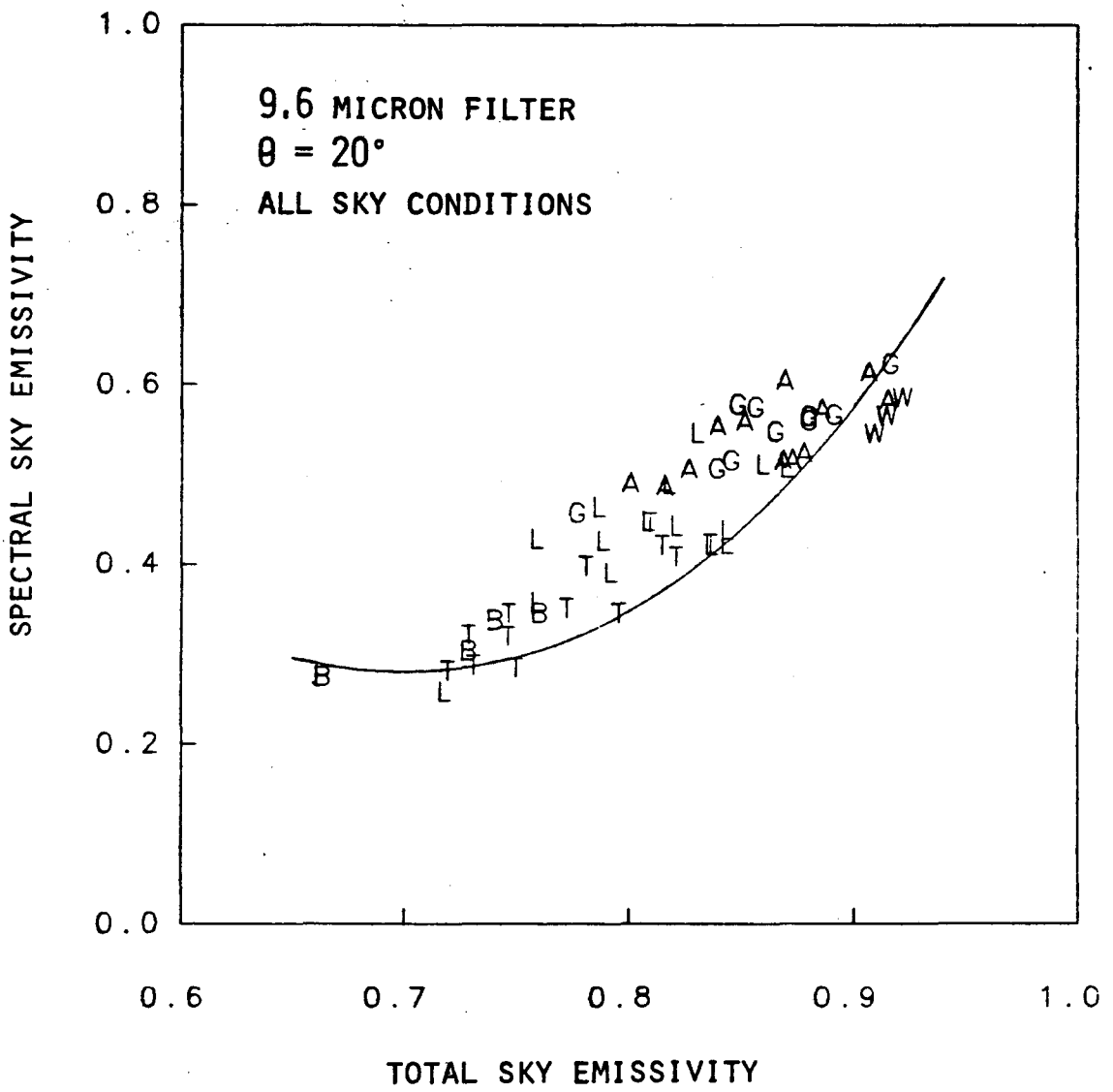
9.6 MICRON FILTER
θ = 20°
ALL SKY CONDITIONS
SPECTRAL SKY EMISSIVITY
TOTAL SKY EMISSIVITY
1.0
0.8
0.6
0.4
0.2
0.0
0.6
0.7
0.8
0.9
1.0

FIGURE 13c

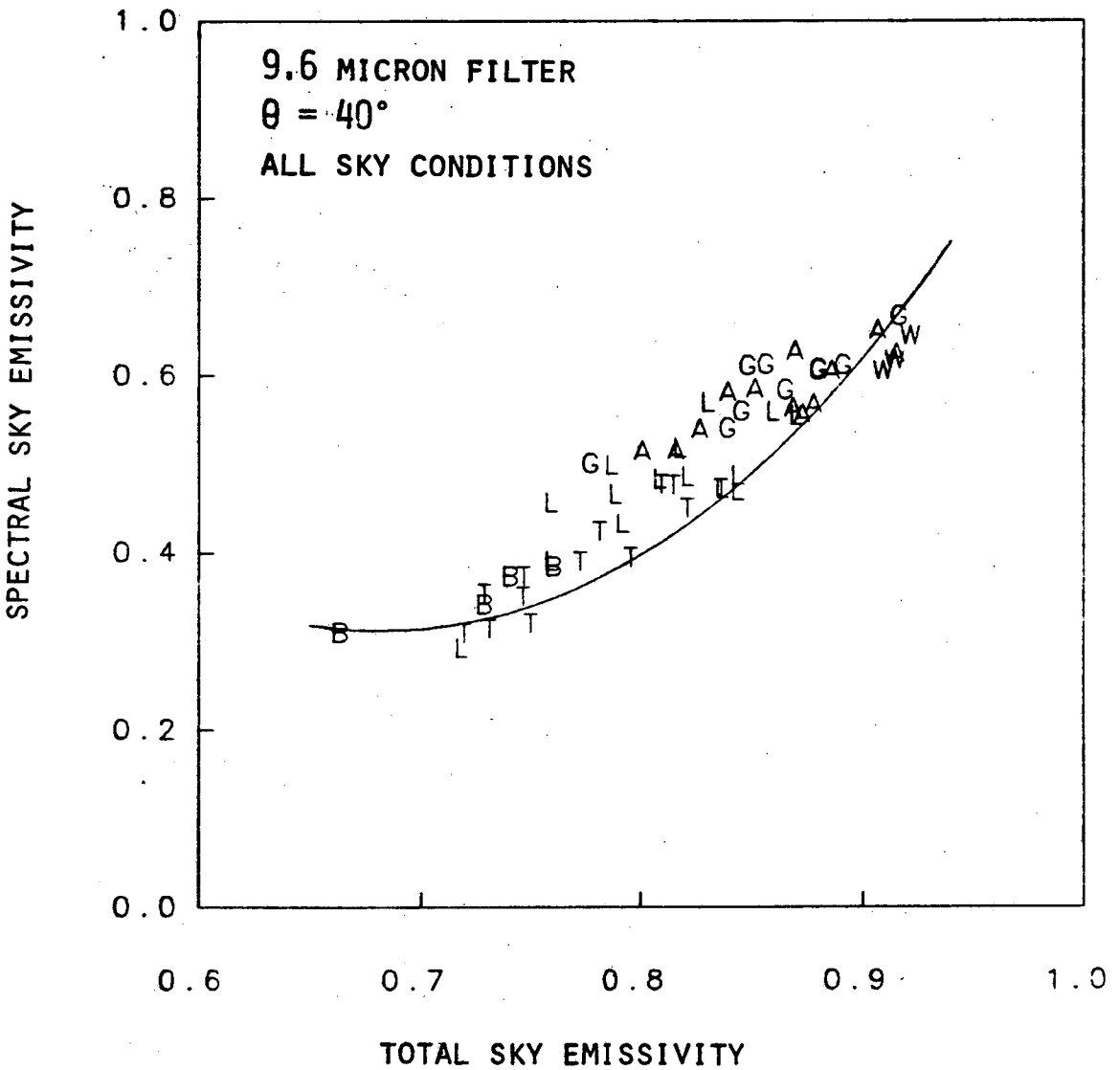
9.6 MICRON FILTER
θ = 40°
ALL SKY CONDITIONS
SPECTRAL SKY EMISSIVITY
TOTAL SKY EMISSIVITY
1.0
0.8
0.6
0.4
0.2
0.0
0.6
0.7
0.8
0.9
1.0

FIGURE 13D

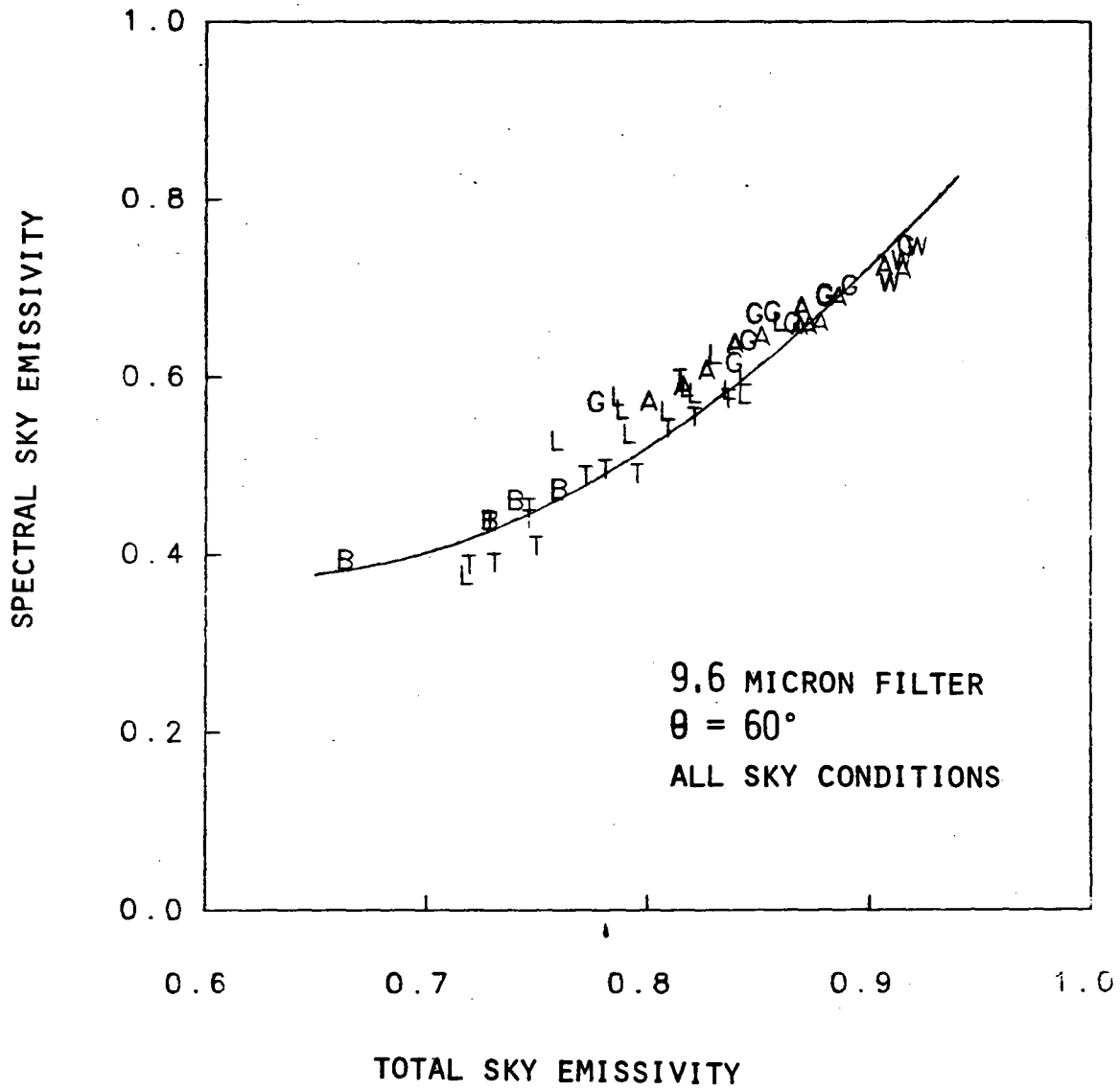
1.0
0.8
0.6
0.4
0.2
0.0
SPECTRAL SKY EMISSIVITY
9.6 MICRON FILTER
θ = 60°
ALL SKY CONDITIONS
0.6
0.7
0.8
0.9
1.0
TOTAL SKY EMISSIVITY

FIGURE 13E

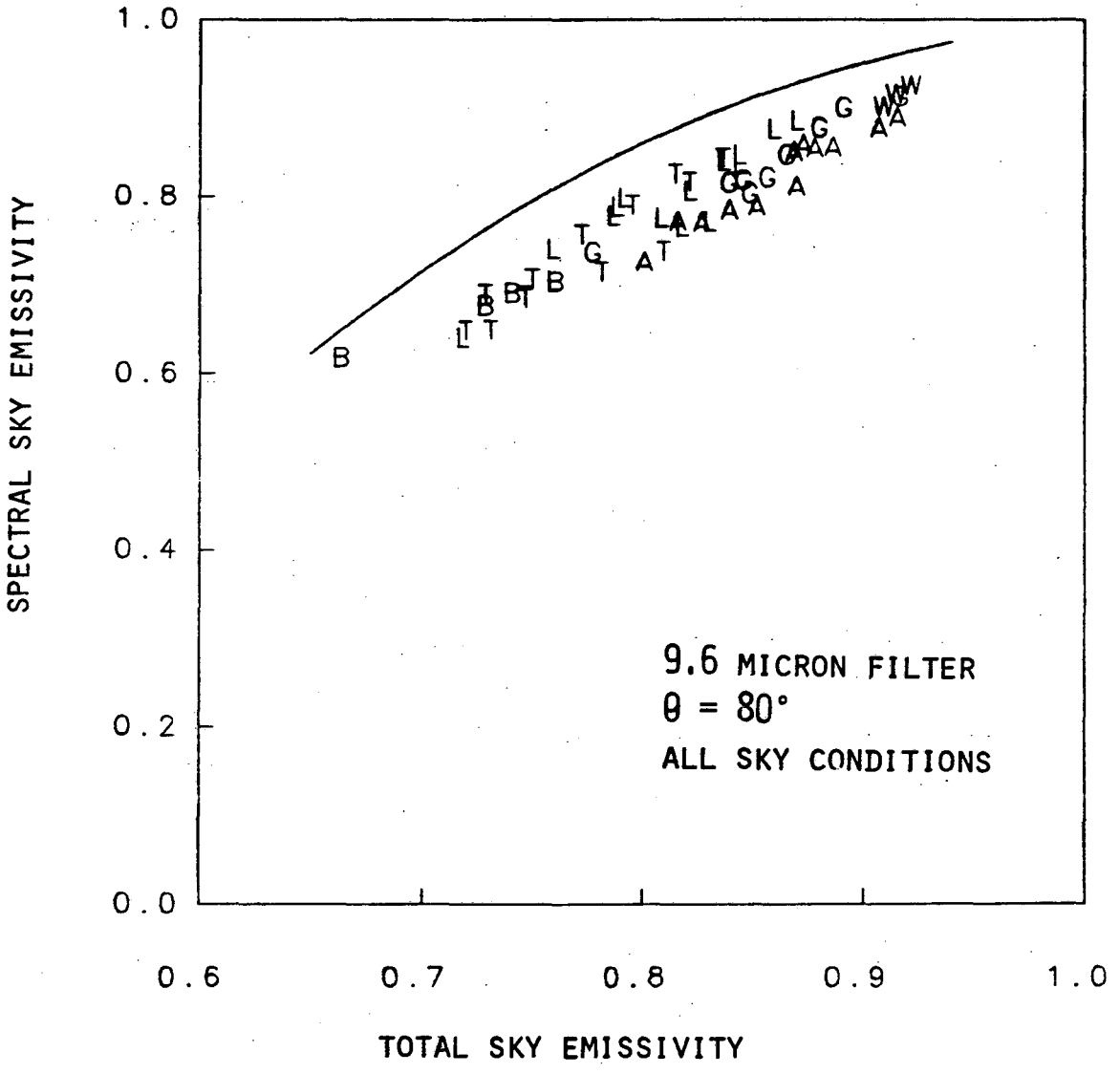
1.0
0.8
0.6
0.4
0.2
0.0
SPECTRAL SKY EMISSIVITY
0.6
0.7
0.8
0.9
1.0
TOTAL SKY EMISSIVITY
9.6 MICRON FILTER
θ = 80°
ALL SKY CONDITIONS

FITURE 13F

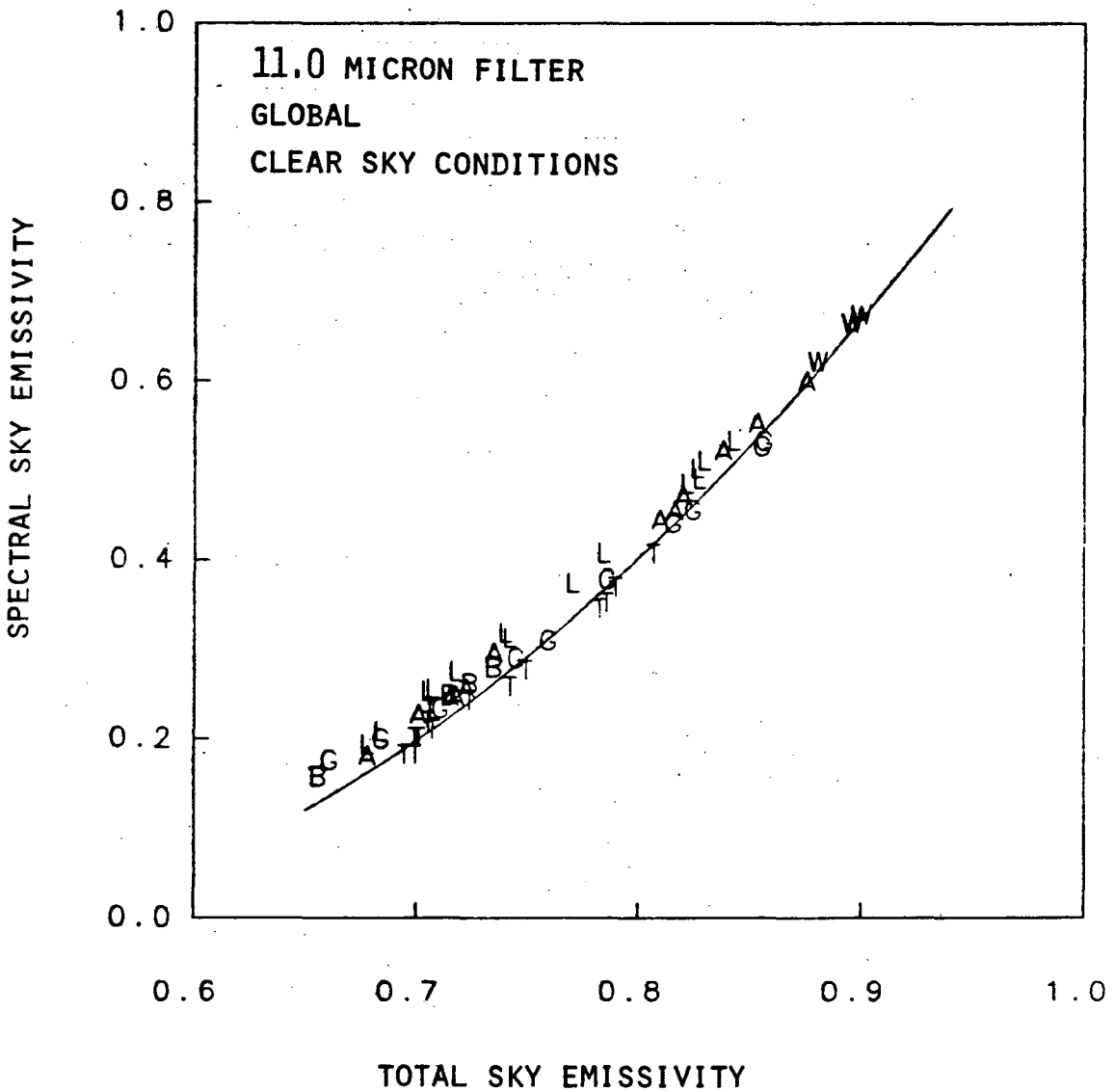
11.0 MICRON FILTER
GLOBAL
CLEAR SKY CONDITIONS
SPECTRAL SKY EMISSIVITY
TOTAL SKY EMISSIVITY
1.0
0.8
0.6
0.4
0.2
0.0
0.6
0.7
0.8
0.9
1.0

FIGURE 14A

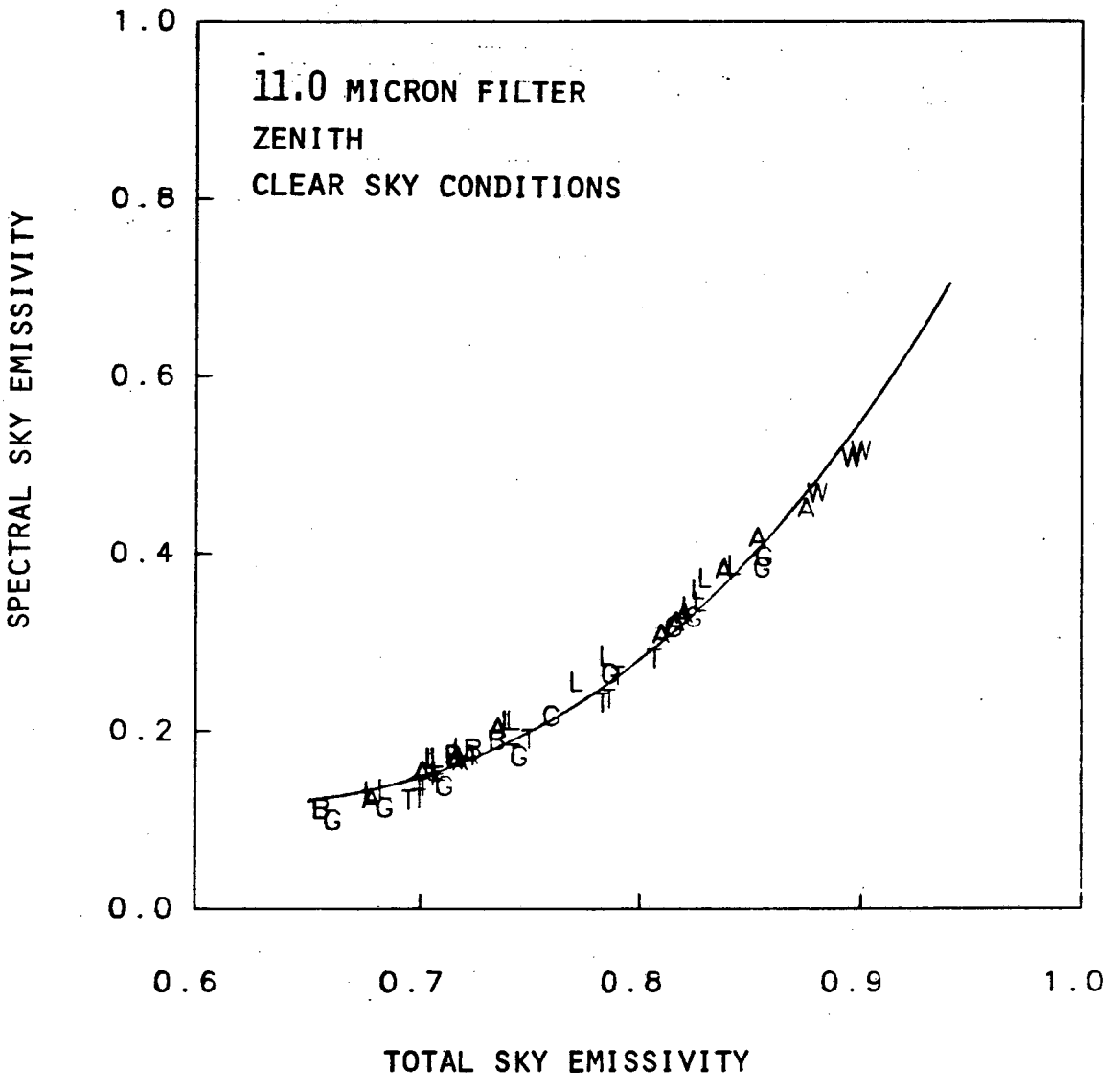
11.0 MICRON FILTER
ZENITH
CLEAR SKY CONDITIONS
SPECTRAL SKY EMISSIVITY
TOTAL SKY EMISSIVITY
1.0
0.8
0.6
0.4
0.2
0.0
0.6
0.7
0.8
0.9
1.0

FIGURE 14B

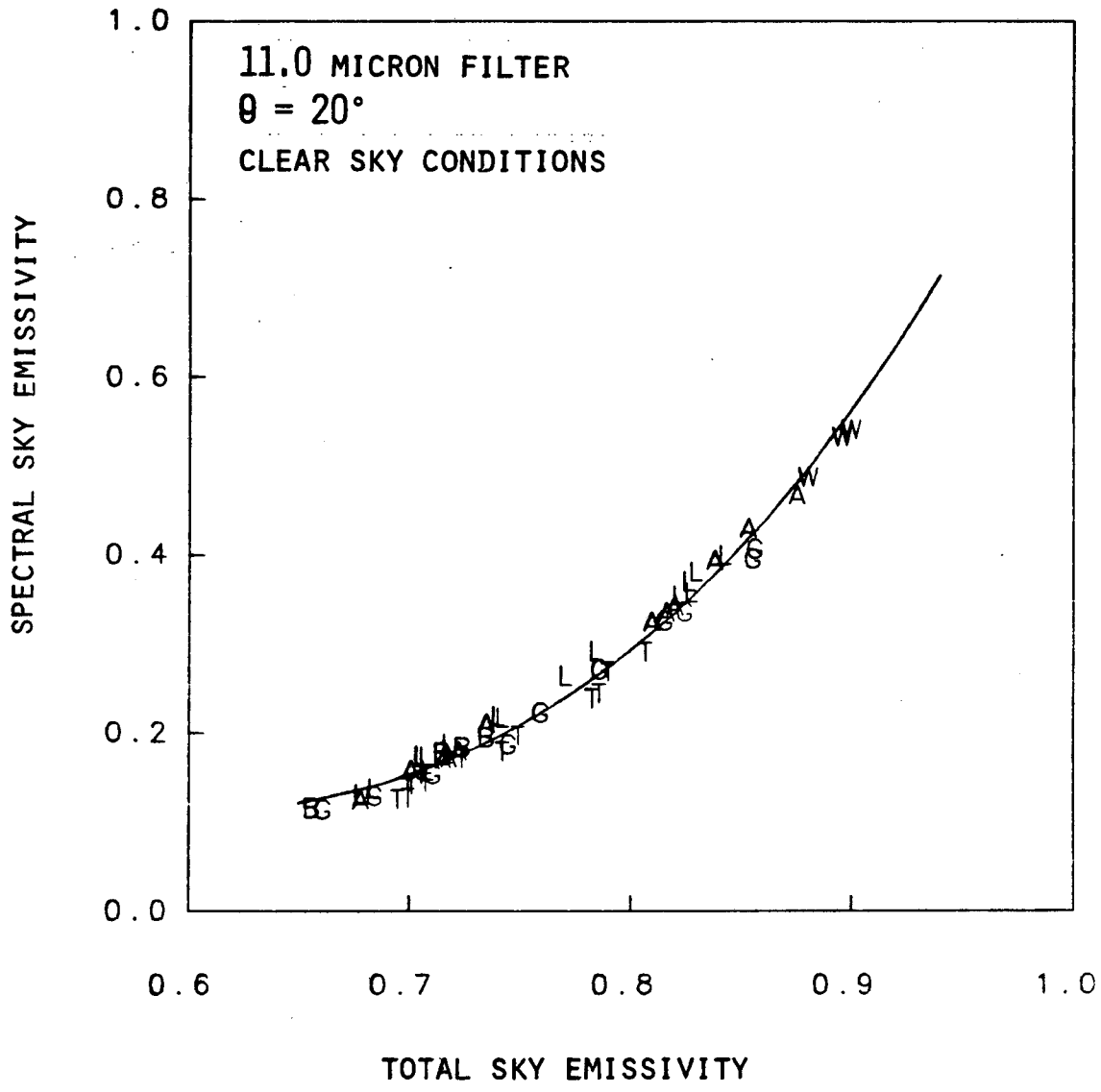
11.0 MICRON FILTER
θ = 20°
CLEAR SKY CONDITIONS
SPECTRAL SKY EMISSIVITY
TOTAL SKY EMISSIVITY
1.0
0.8
0.6
0.4
0.2
0.0
0.6
0.7
0.8
0.9
1.0

FIGURE 14c

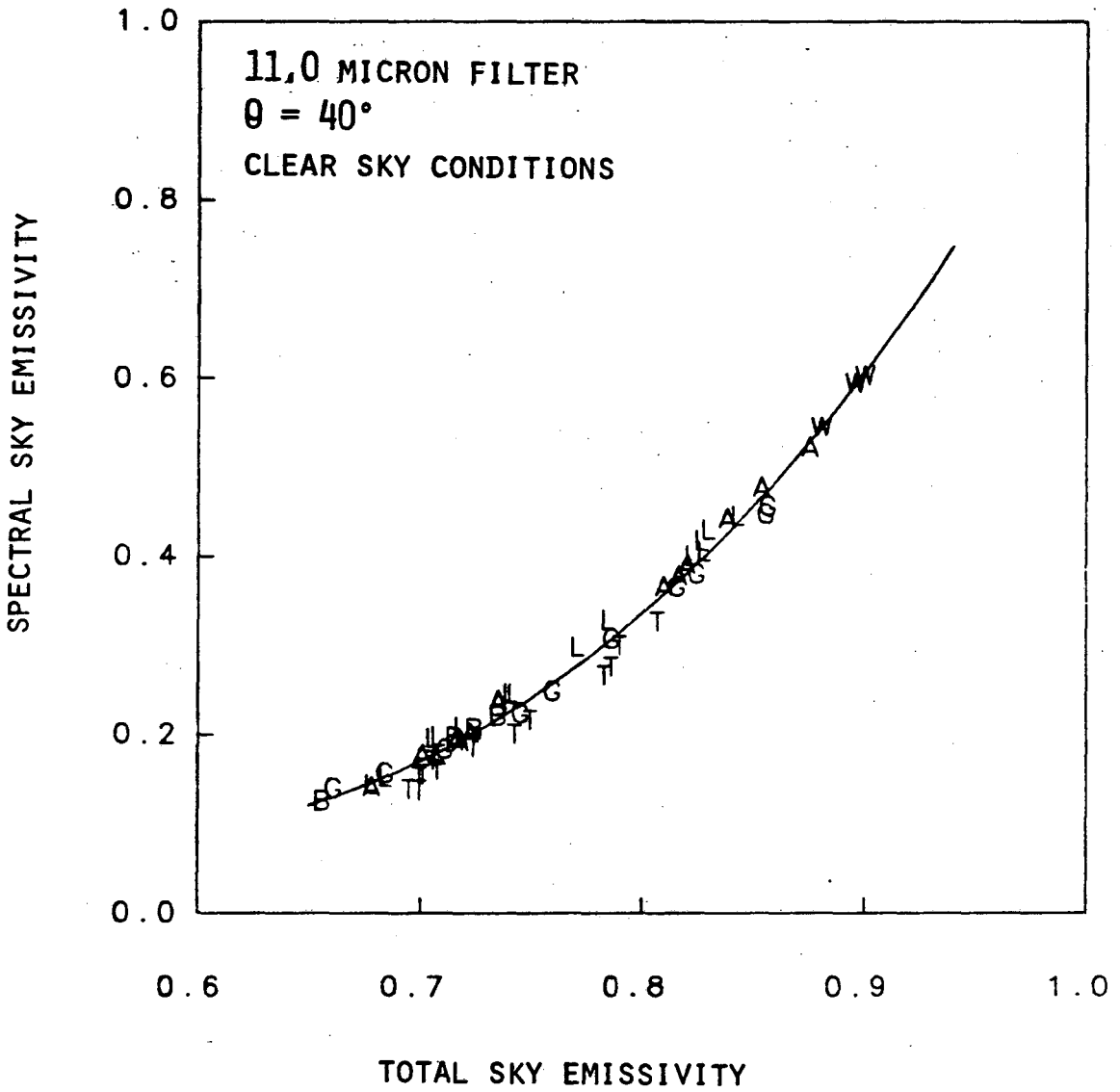
11.0 MICRON FILTER
θ = 40°
CLEAR SKY CONDITIONS
SPECTRAL SKY EMISSIVITY
TOTAL SKY EMISSIVITY
1.0
0.8
0.6
0.4
0.2
0.0
0.6
0.7
0.8
0.9
1.0

FIGURE 14D

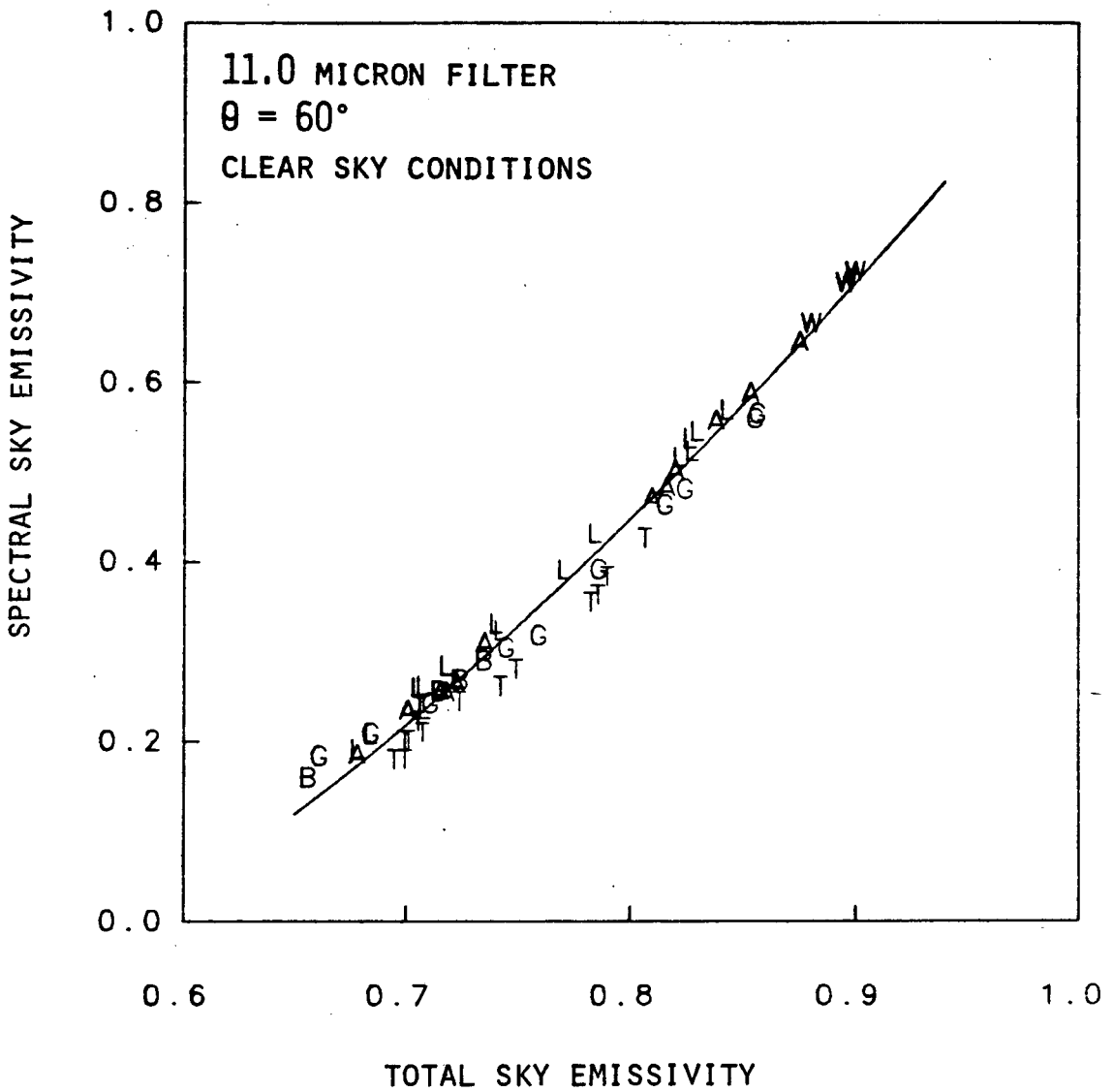
11.0 MICRON FILTER
θ = 60°
CLEAR SKY CONDITIONS
SPECTRAL SKY EMISSIVITY
TOTAL SKY EMISSIVITY
1.0
0.8
0.6
0.4
0.2
0.0
0.6
0.7
0.8
0.9
1.0

FIGURE 14E

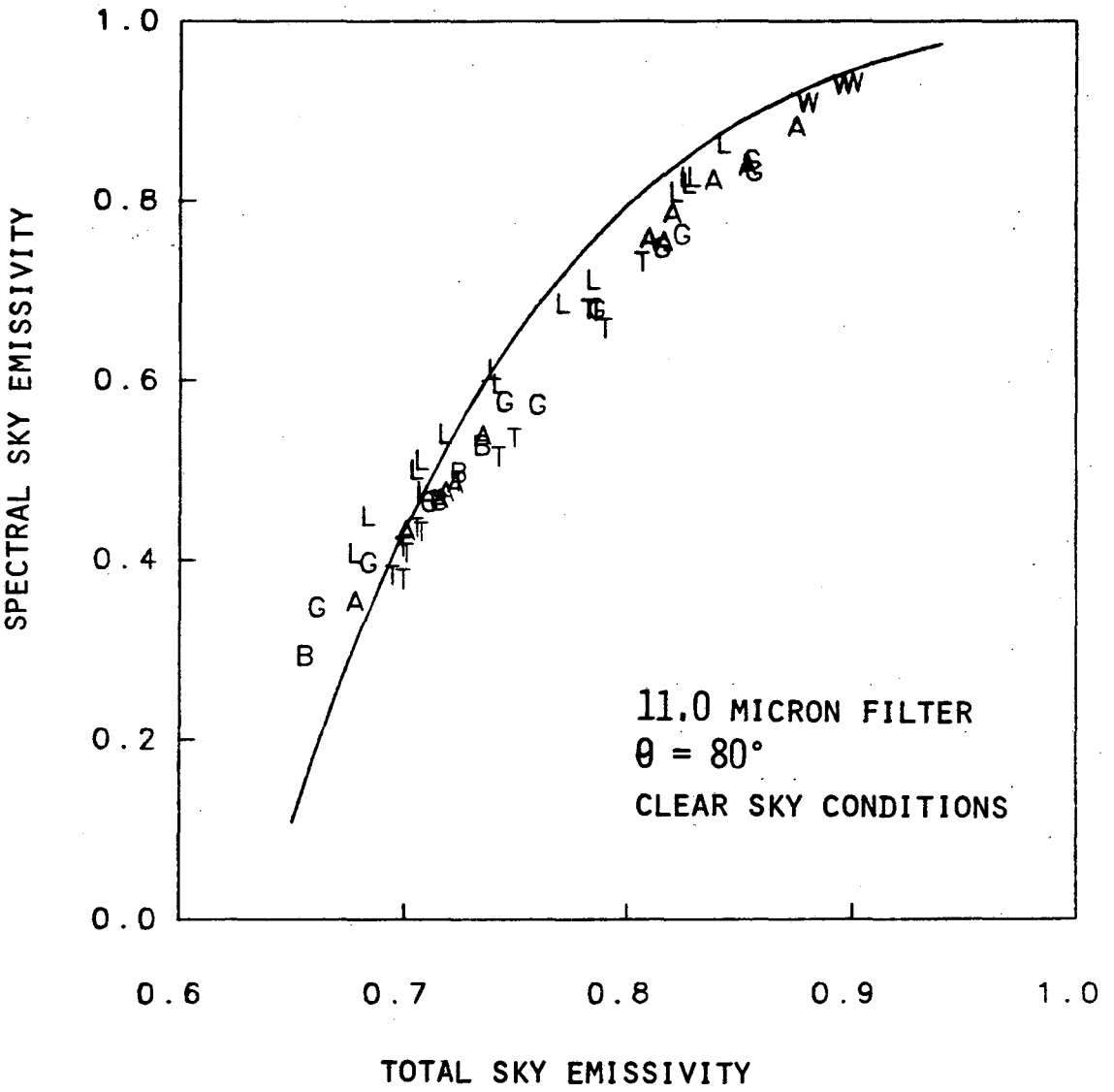
1.0
0.8
0.6
0.4
0.2
0.0
SPECTRAL SKY EMISSIVITY
0.6
0.7
0.8
0.9
1.0
TOTAL SKY EMISSIVITY
11.0 MICRON FILTER
θ = 80°
CLEAR SKY CONDITIONS

FIGURE 14F

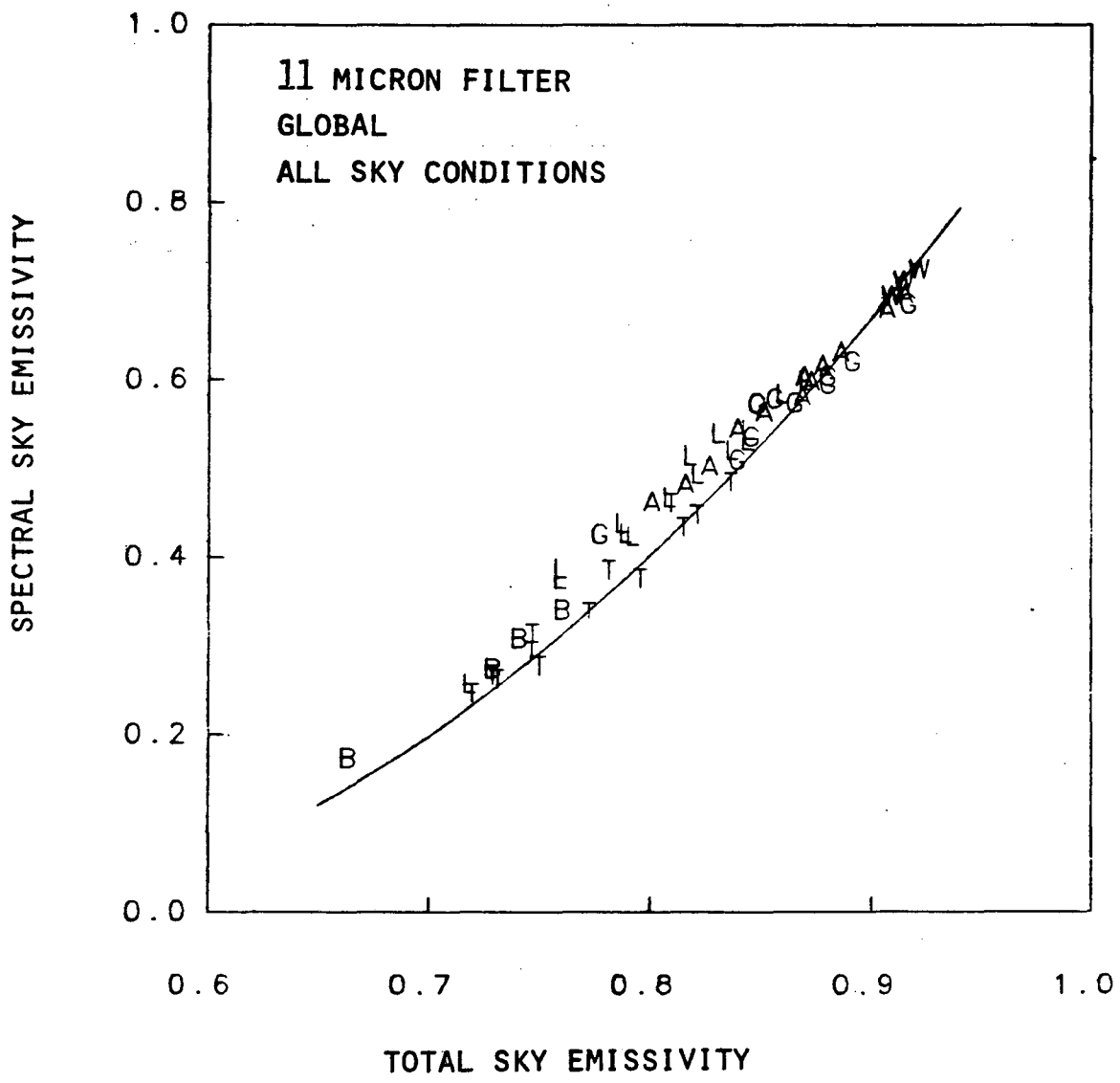
11 MICRON FILTER
GLOBAL
ALL SKY CONDITIONS
SPECTRAL SKY EMISSIVITY
TOTAL SKY EMISSIVITY
1.0
0.8
0.6
0.4
0.2
0.0
0.6
0.7
0.8
0.9
1.0

FIGURE 15A

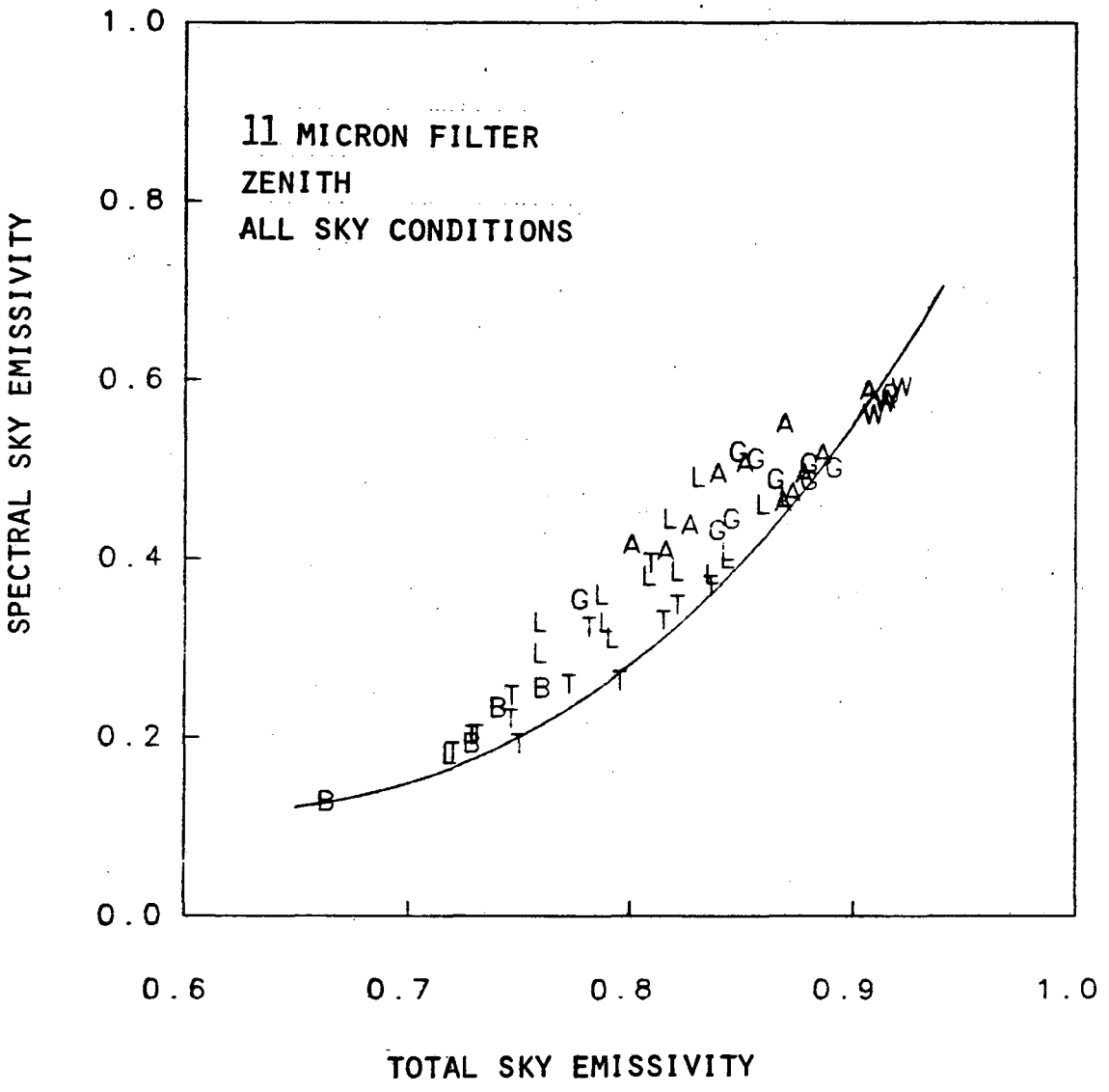
11 MICRON FILTER
ZENITH
ALL SKY CONDITIONS
SPECTRAL SKY EMISSIVITY
TOTAL SKY EMISSIVITY
1.0
0.8
0.6
0.4
0.2
0.0
0.6
0.7
0.8
0.9
1.0

FIGURE 15B

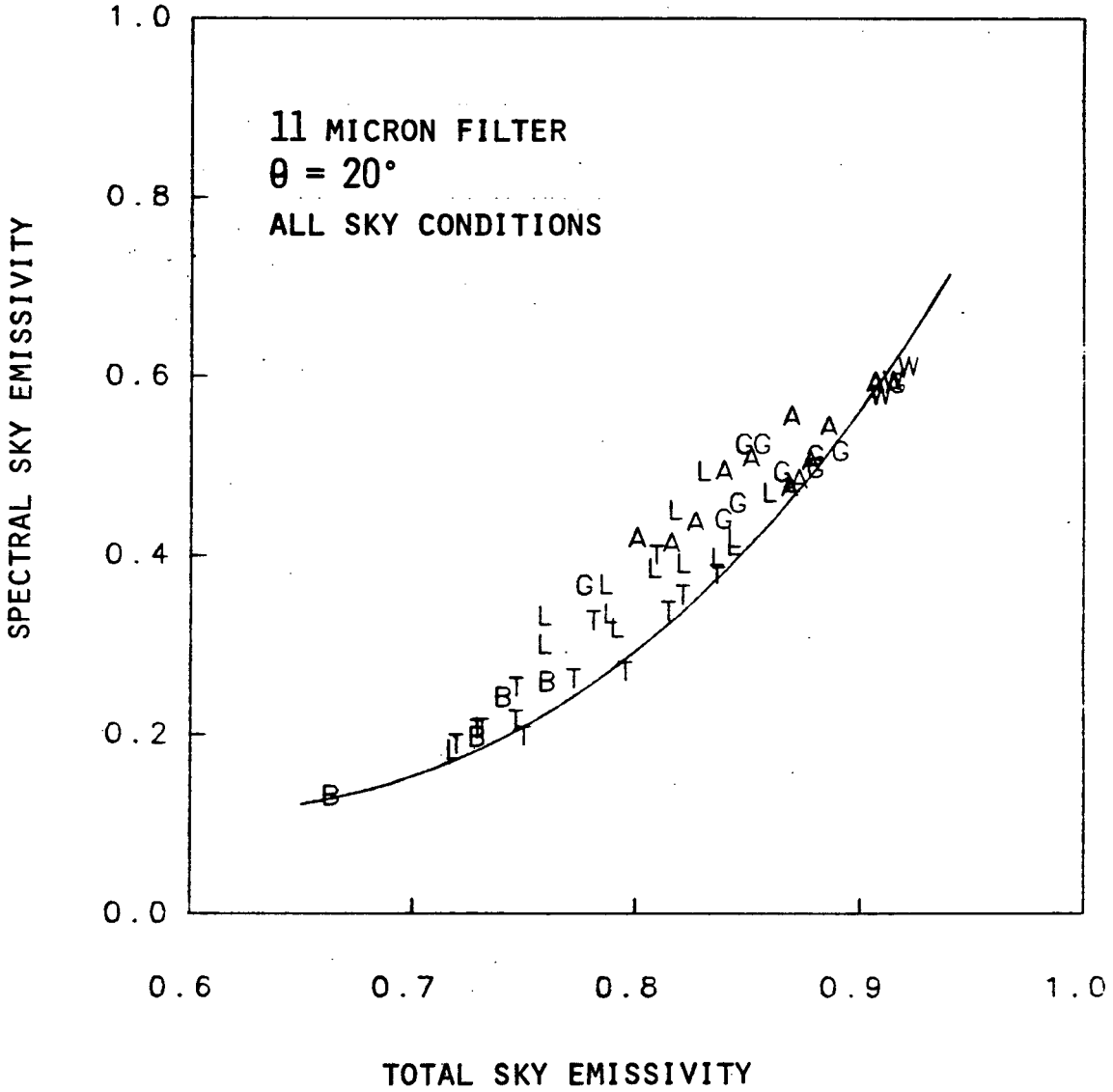
11 MICRON FILTER
θ = 20°
ALL SKY CONDITIONS
SPECTRAL SKY EMISSIVITY
TOTAL SKY EMISSIVITY
1.0
0.8
0.6
0.4
0.2
0.0
0.6
0.7
0.8
0.9
1.0

FIGURE 15c

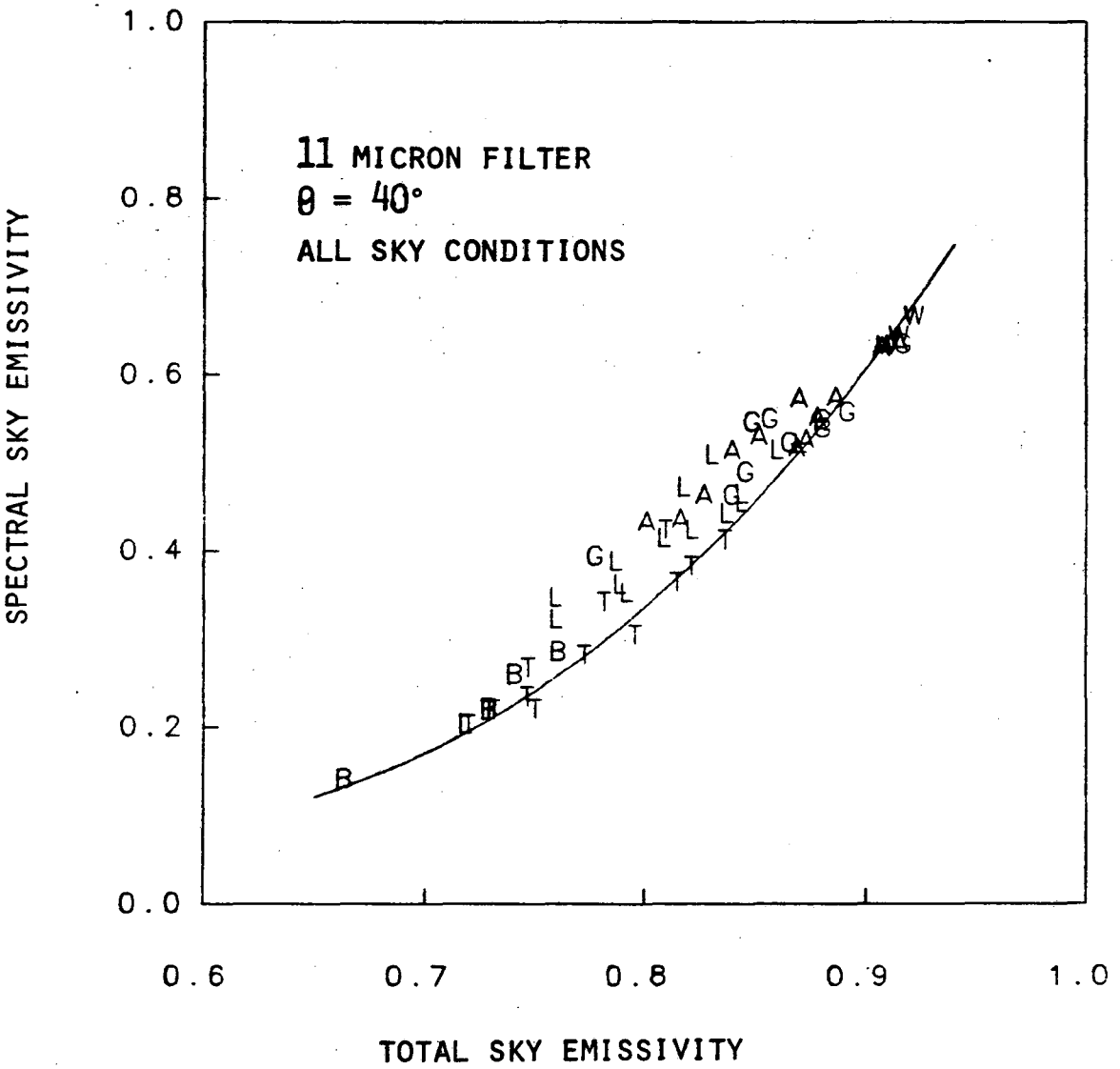
11 MICRON FILTER
θ = 40°
ALL SKY CONDITIONS
SPECTRAL SKY EMISSIVITY
TOTAL SKY EMISSIVITY
1.0
0.8
0.6
0.4
0.2
0.0
0.6
0.7
0.8
0.9
1.0

FIGURE 15D

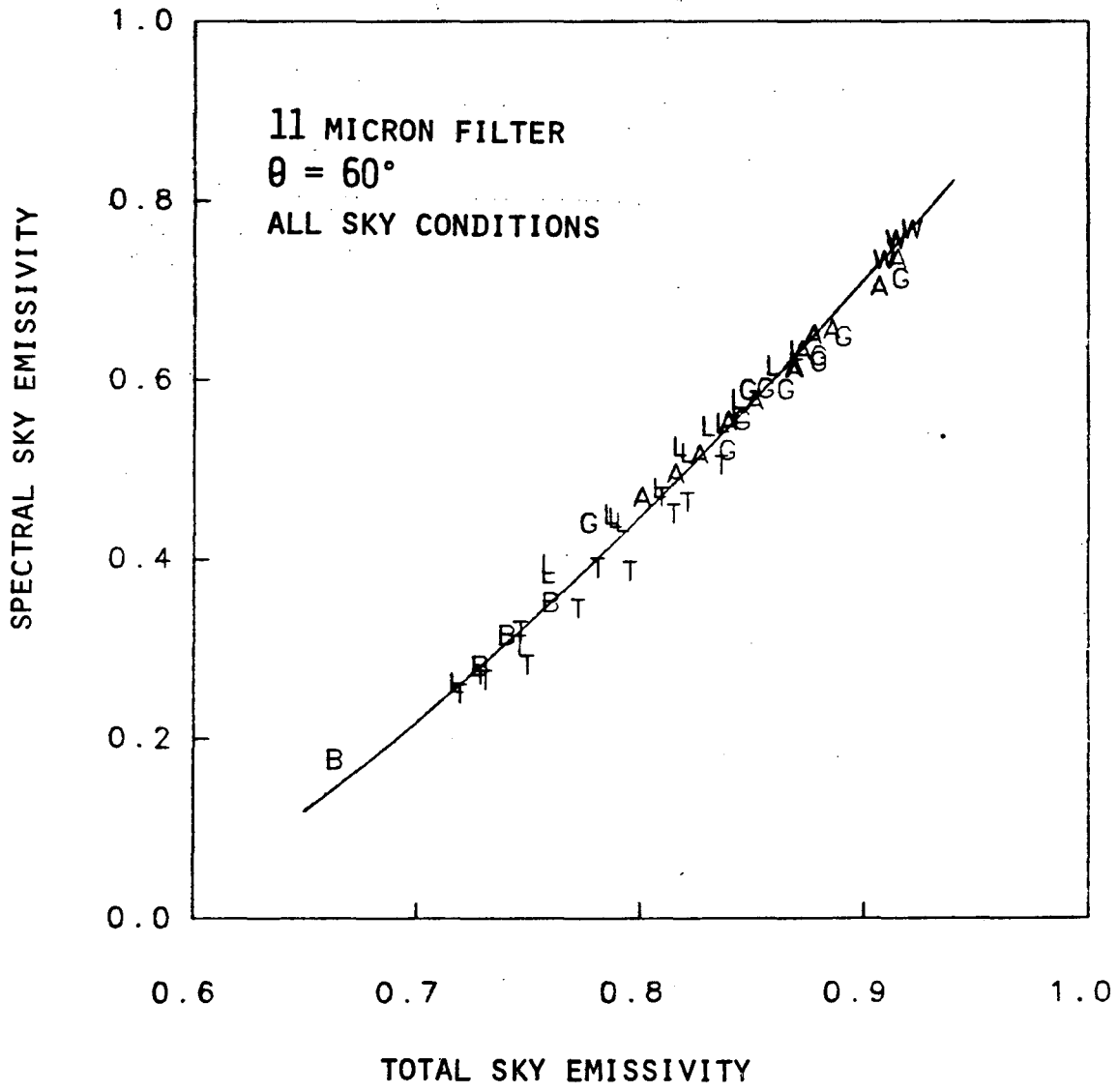
11 MICRON FILTER
θ = 60°
ALL SKY CONDITIONS
SPECTRAL SKY EMISSIVITY
TOTAL SKY EMISSIVITY
1.0
0.8
0.6
0.4
0.2
0.0
0.6
0.7
0.8
0.9
1.0

FIGURE 15E

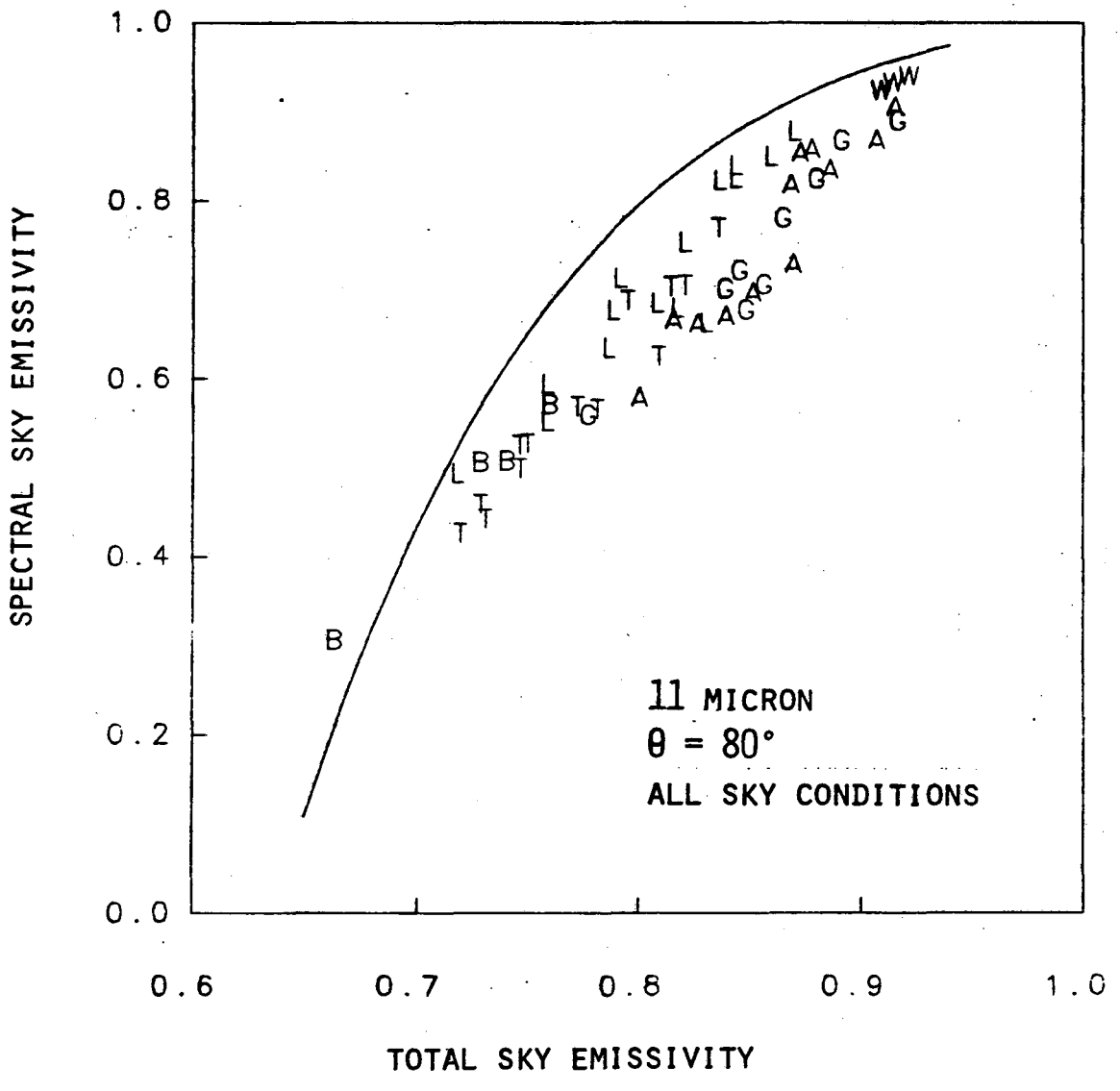
1.0
0.8
0.6
0.4
0.2
0.0
SPECTRAL SKY EMISSIVITY
0.6
0.7
0.8
0.9
1.0
TOTAL SKY EMISSIVITY
11 MICRON
θ = 80°
ALL SKY CONDITIONS

FIGURE 15F

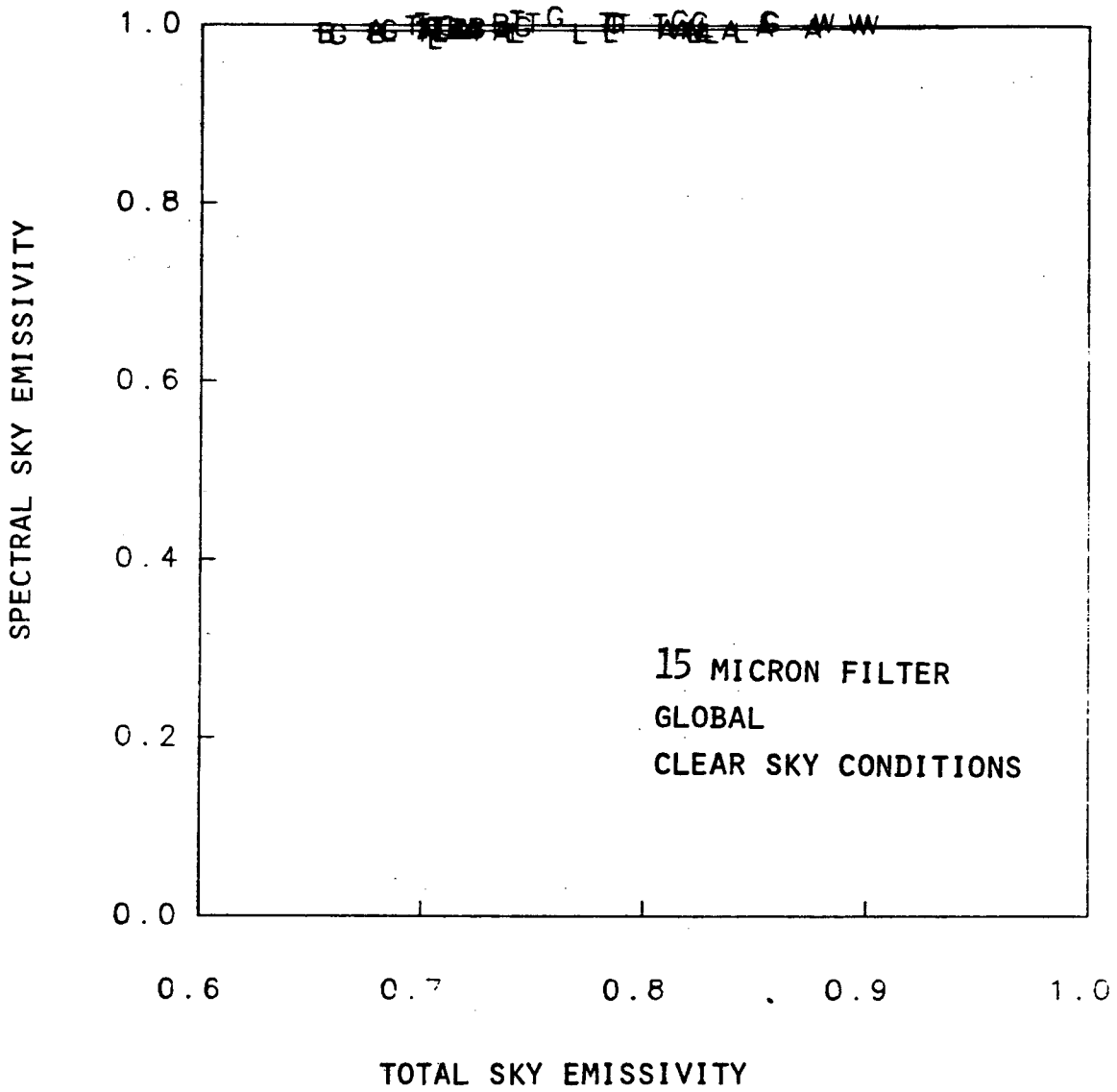
1.0
0.8
0.6
0.4
0.2
0.0
SPECTRAL SKY EMISSIVITY
15 MICRON FILTER
GLOBAL
CLEAR SKY CONDITIONS
0.6
0.8
0.9
1.0
TOTAL SKY EMISSIVITY

FIGURE 16A

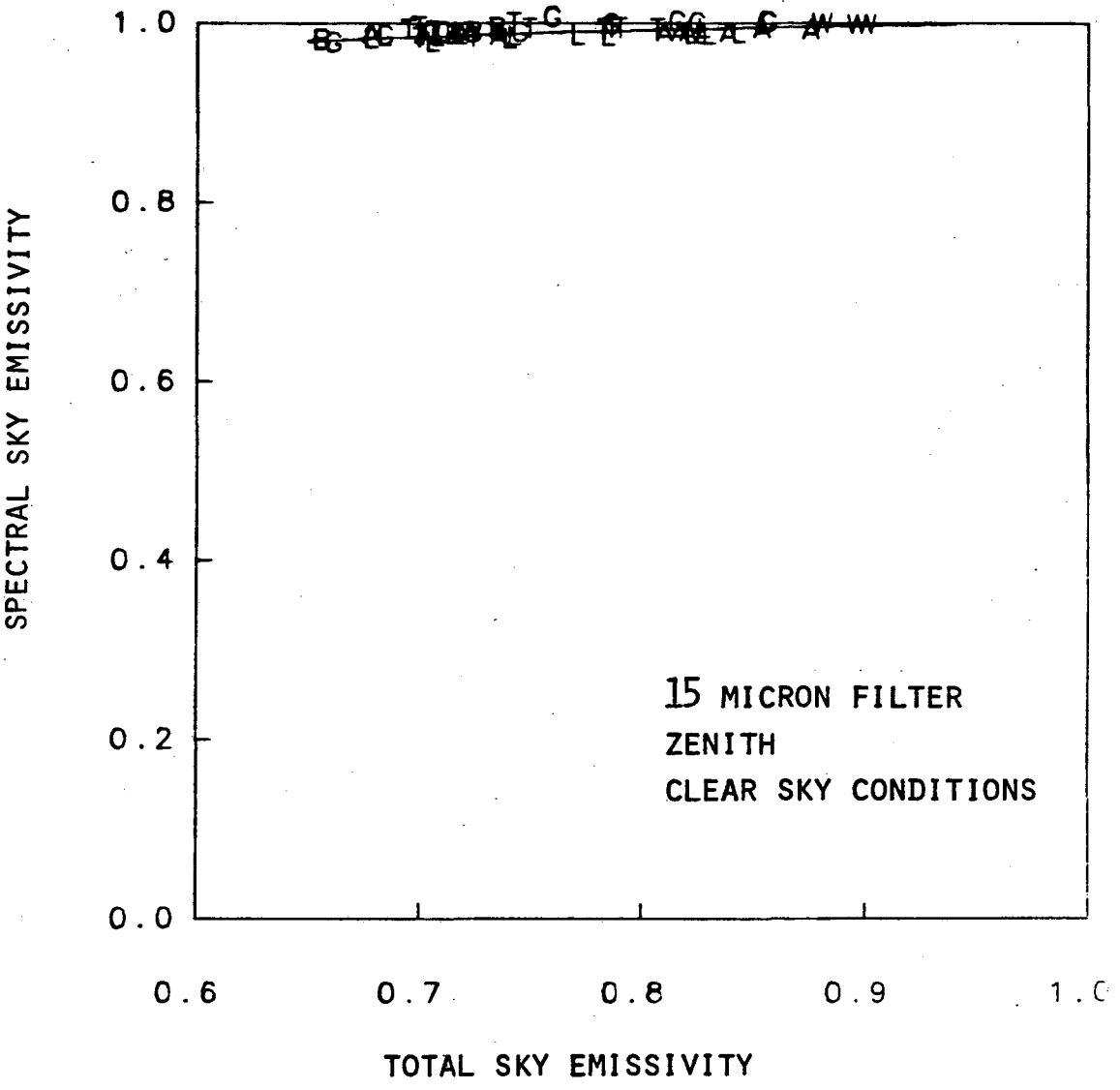
1.0
0.8
0.6
0.4
0.2
0.0
SPECTRAL SKY EMISSIVITY
15 MICRON FILTER
ZENITH
CLEAR SKY CONDITIONS
0.6
0.7
0.8
0.9
1.0
TOTAL SKY EMISSIVITY

FIGURE 16B

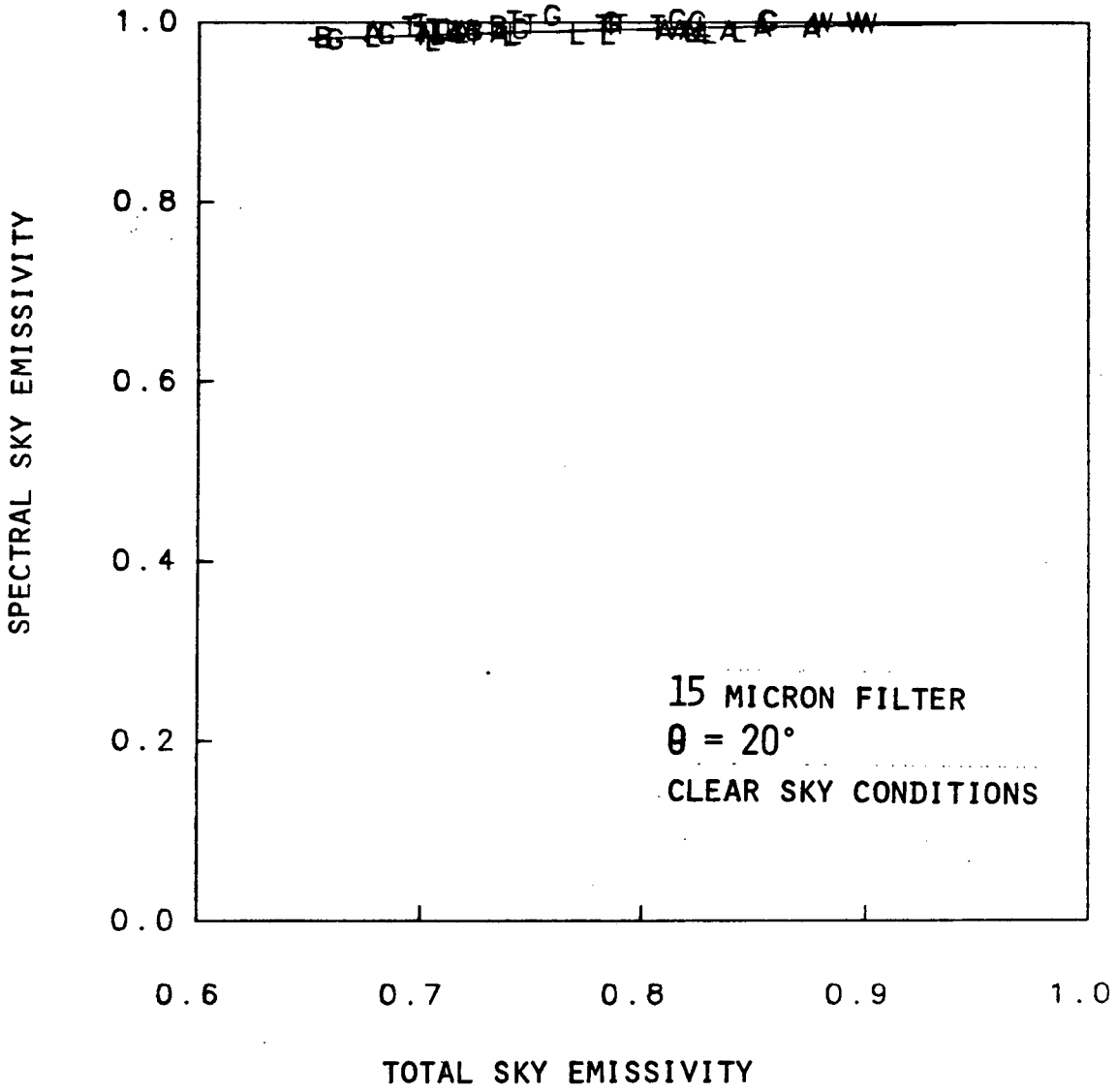
1.0
0.8
0.6
0.4
0.2
0.0
SPECTRAL SKY EMISSIVITY
15 MICRON FILTER
θ = 20°
CLEAR SKY CONDITIONS
0.6
0.7
0.8
0.9
1.0
TOTAL SKY EMISSIVITY

FIGURE 16c

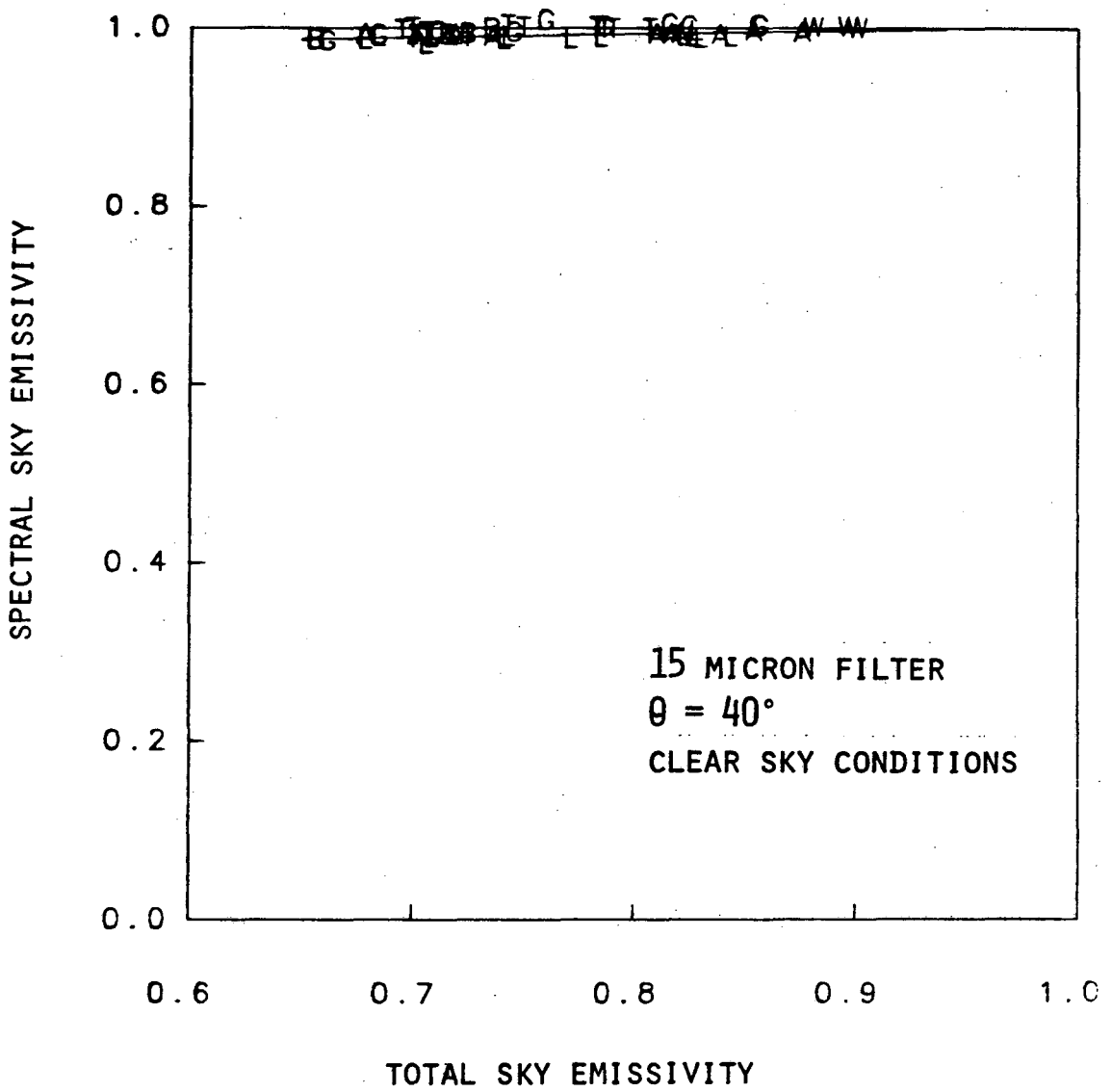
1.0
0.8
0.6
0.4
0.2
0.0
SPECTRAL SKY EMISSIVITY
15 MICRON FILTER
θ = 40°
CLEAR SKY CONDITIONS
0.6
0.7
0.8
0.9
1.0
TOTAL SKY EMISSIVITY

FIGURE 16D

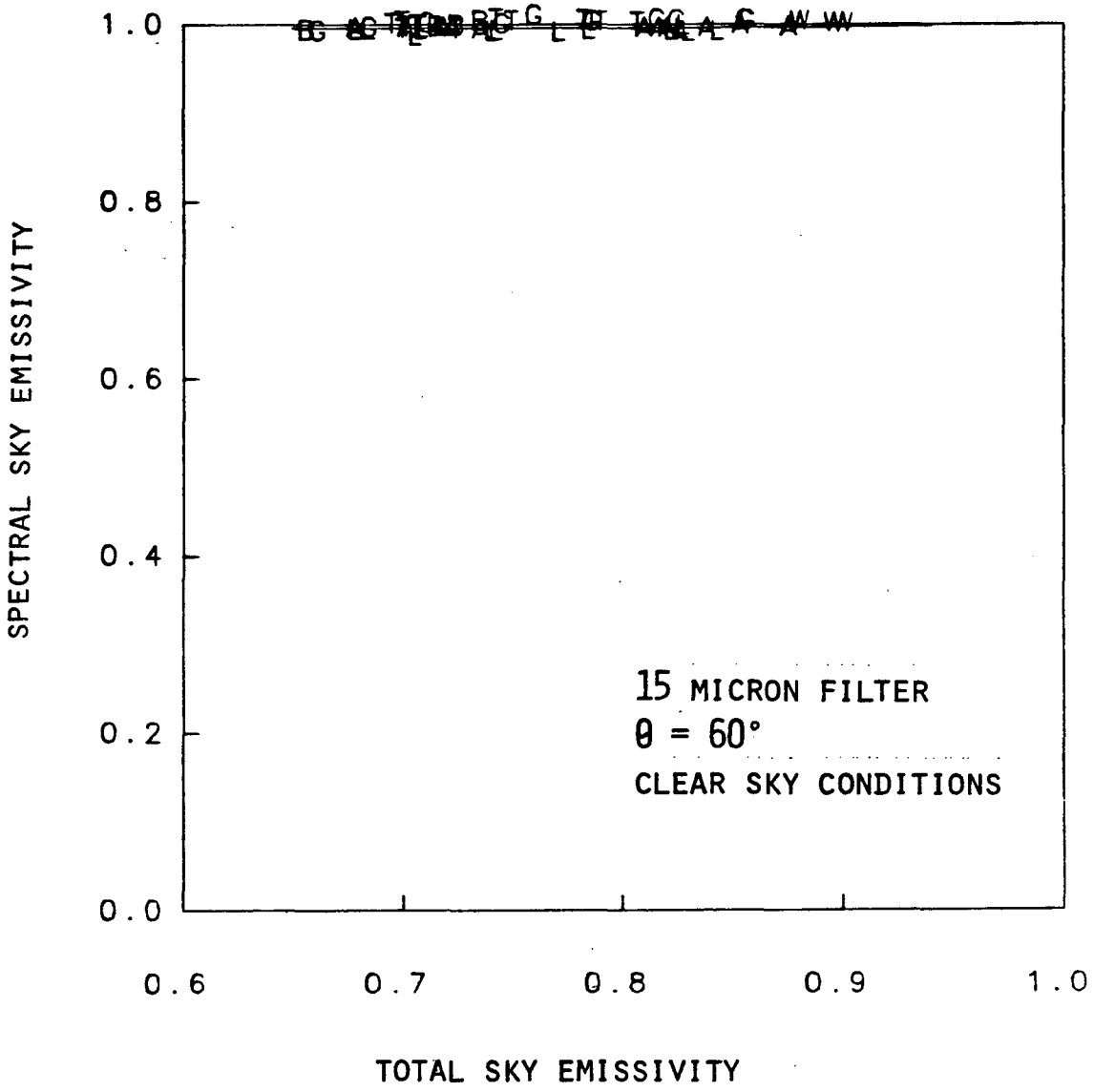
1.0
0.8
0.6
0.4
0.2
0.0
SPECTRAL SKY EMISSIVITY
15 MICRON FILTER
θ = 60°
CLEAR SKY CONDITIONS
0.6
0.7
0.8
0.9
1.0
TOTAL SKY EMISSIVITY

FIGURE 16E

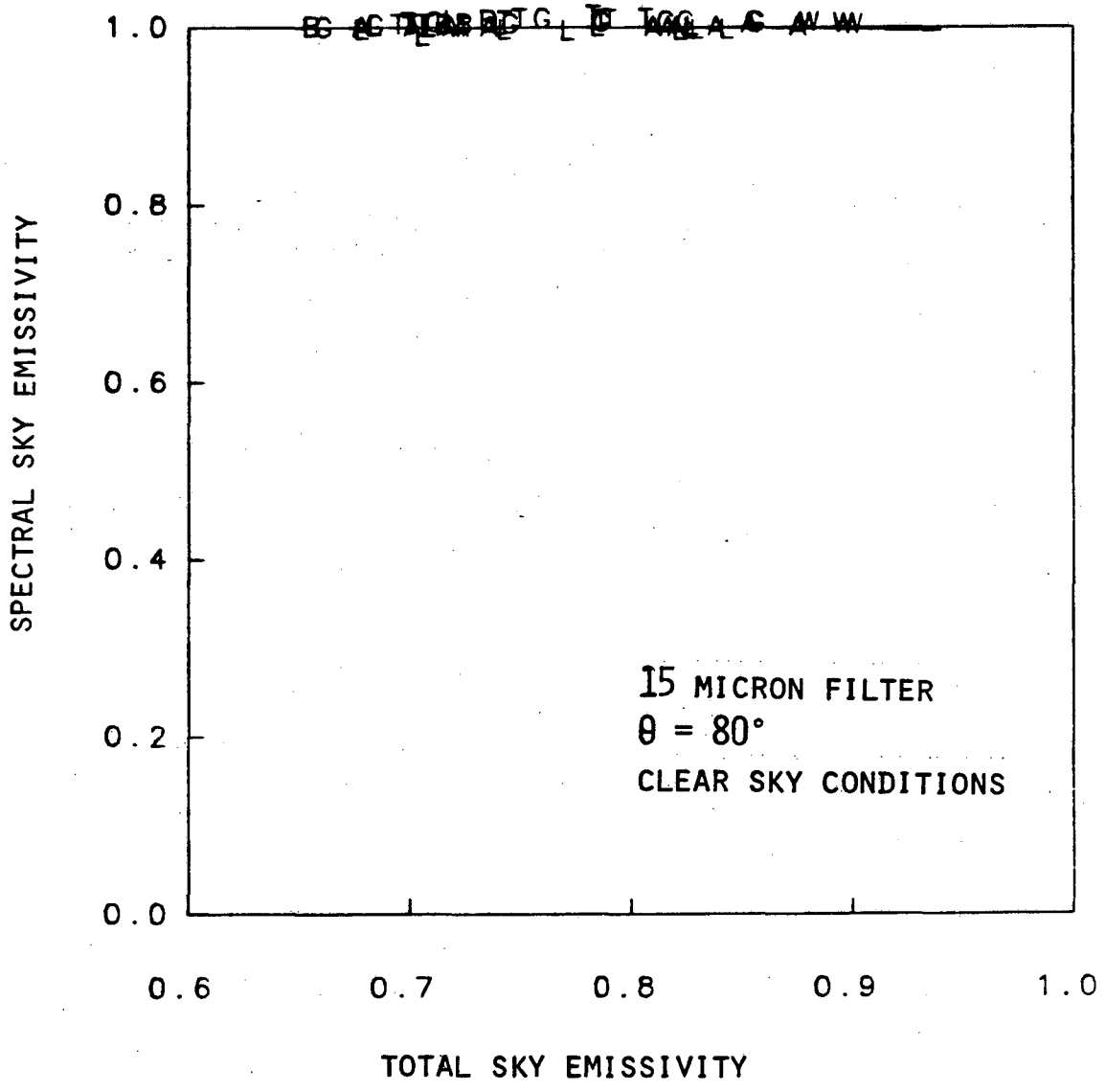
1.0
0.8
0.6
0.4
0.2
0.0
SPECTRAL SKY EMISSIVITY
15 MICRON FILTER
θ = 80°
CLEAR SKY CONDITIONS
0.6
0.7
0.8
0.9
1.0
TOTAL SKY EMISSIVITY

FIGURE 16F

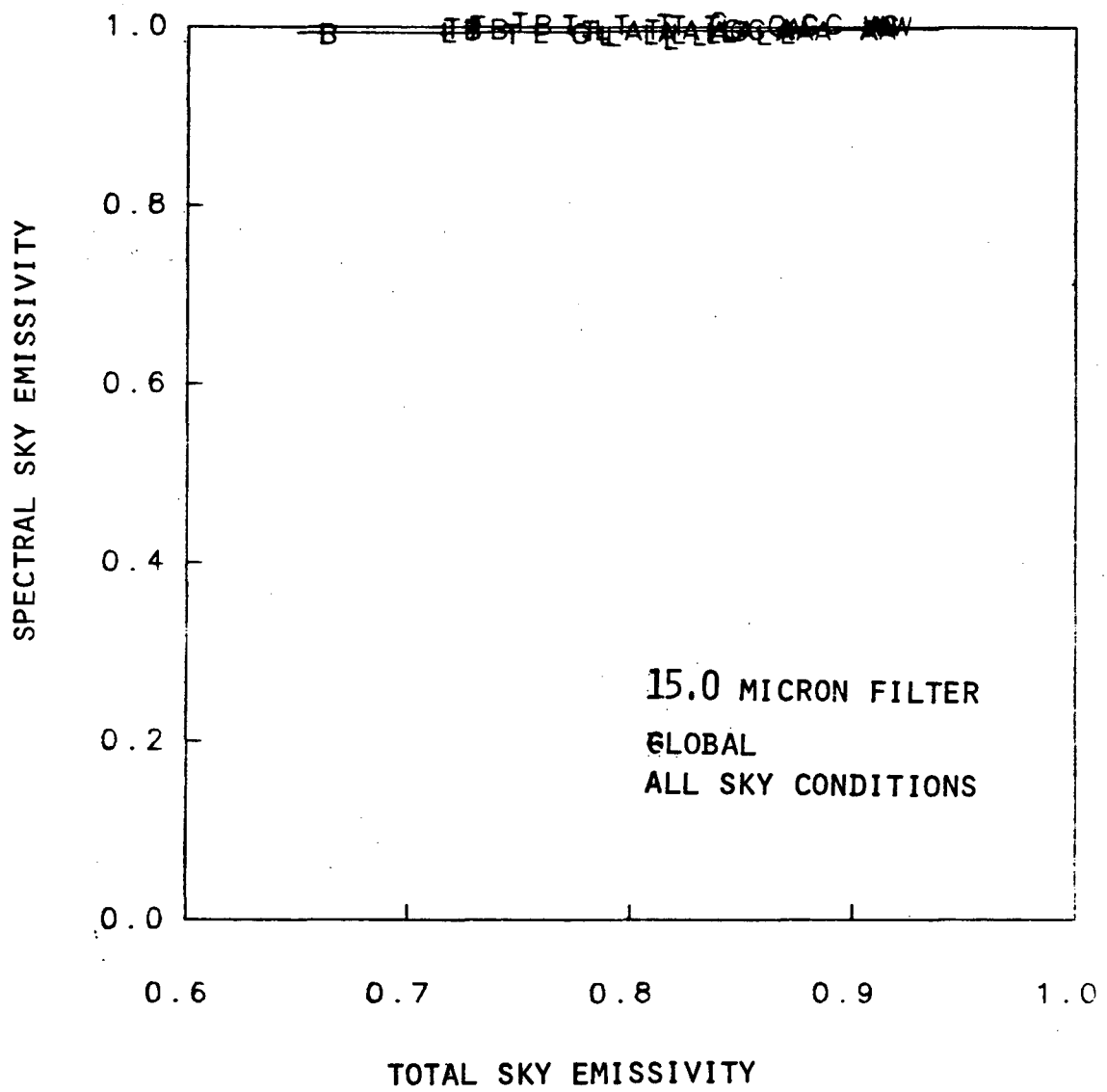
1.0
0.8
0.6
0.4
0.2
0.0
SPECTRAL SKY EMISSIVITY
15.0 MICRON FILTER
GLOBAL
ALL SKY CONDITIONS
0.6
0.7
0.8
0.9
1.0
TOTAL SKY EMISSIVITY

FIGURE 17A

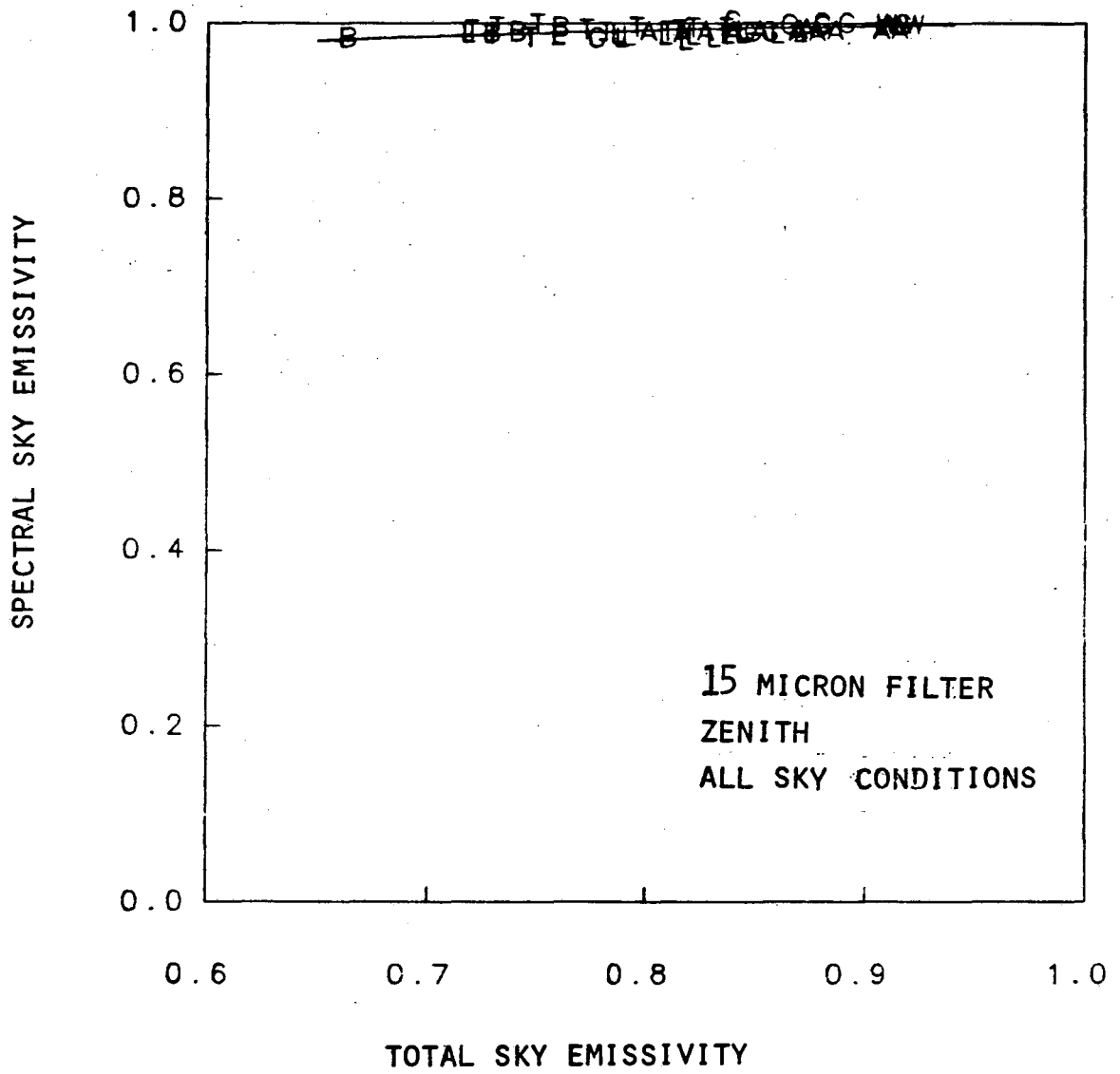
1.0
0.8
0.6
0.4
0.2
0.0
SPECTRAL SKY EMISSIVITY
15 MICRON FILTER
ZENITH
ALL SKY CONDITIONS
0.6
0.7
0.8
0.9
1.0
TOTAL SKY EMISSIVITY

FIGURE 17B

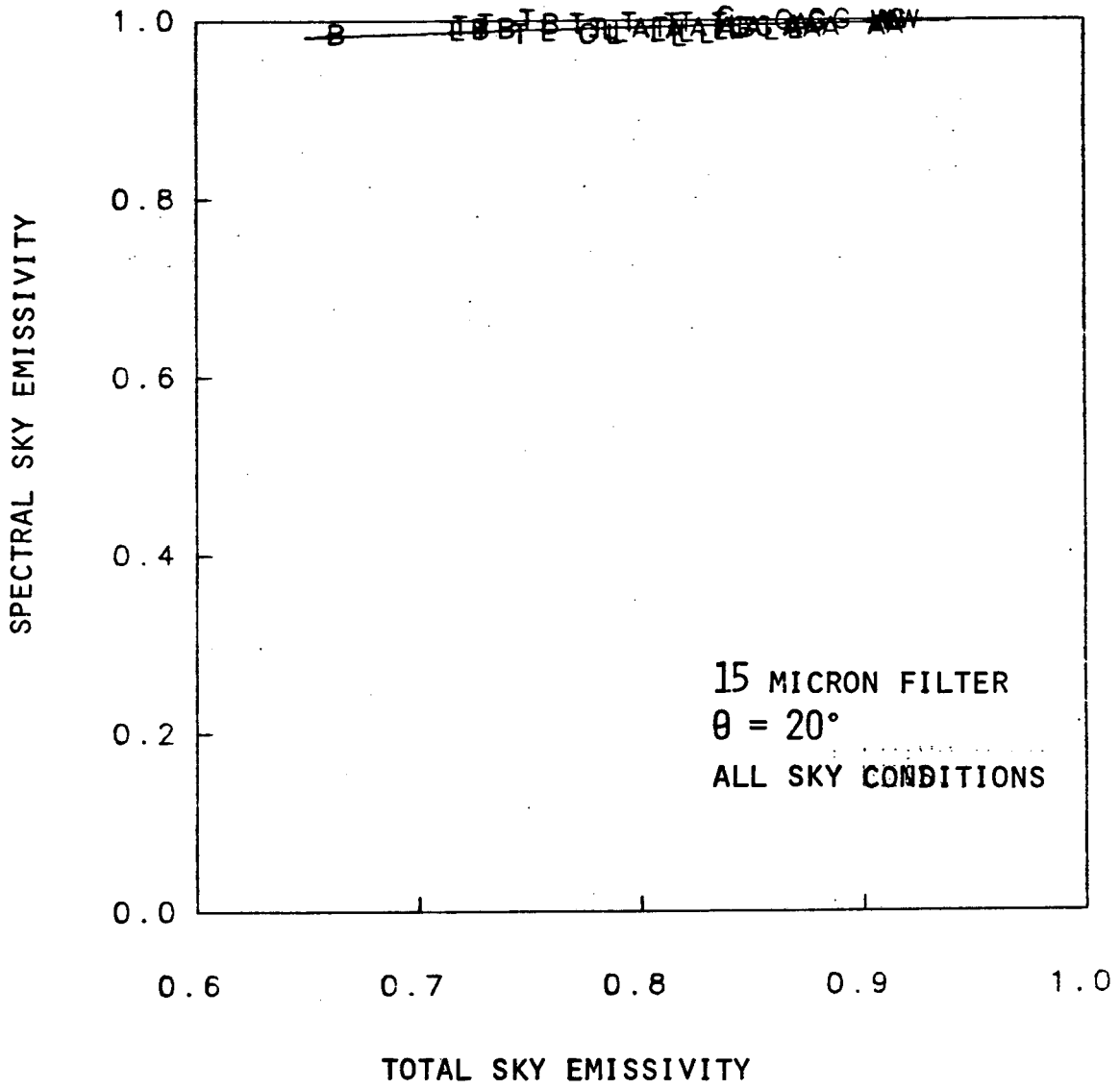
1.0
0.8
0.6
0.4
0.2
0.0
SPECTRAL SKY EMISSIVITY
15 MICRON FILTER
θ = 20°
ALL SKY CONDITIONS
0.6
0.7
0.8
0.9
1.0
TOTAL SKY EMISSIVITY

FIGURE 17c

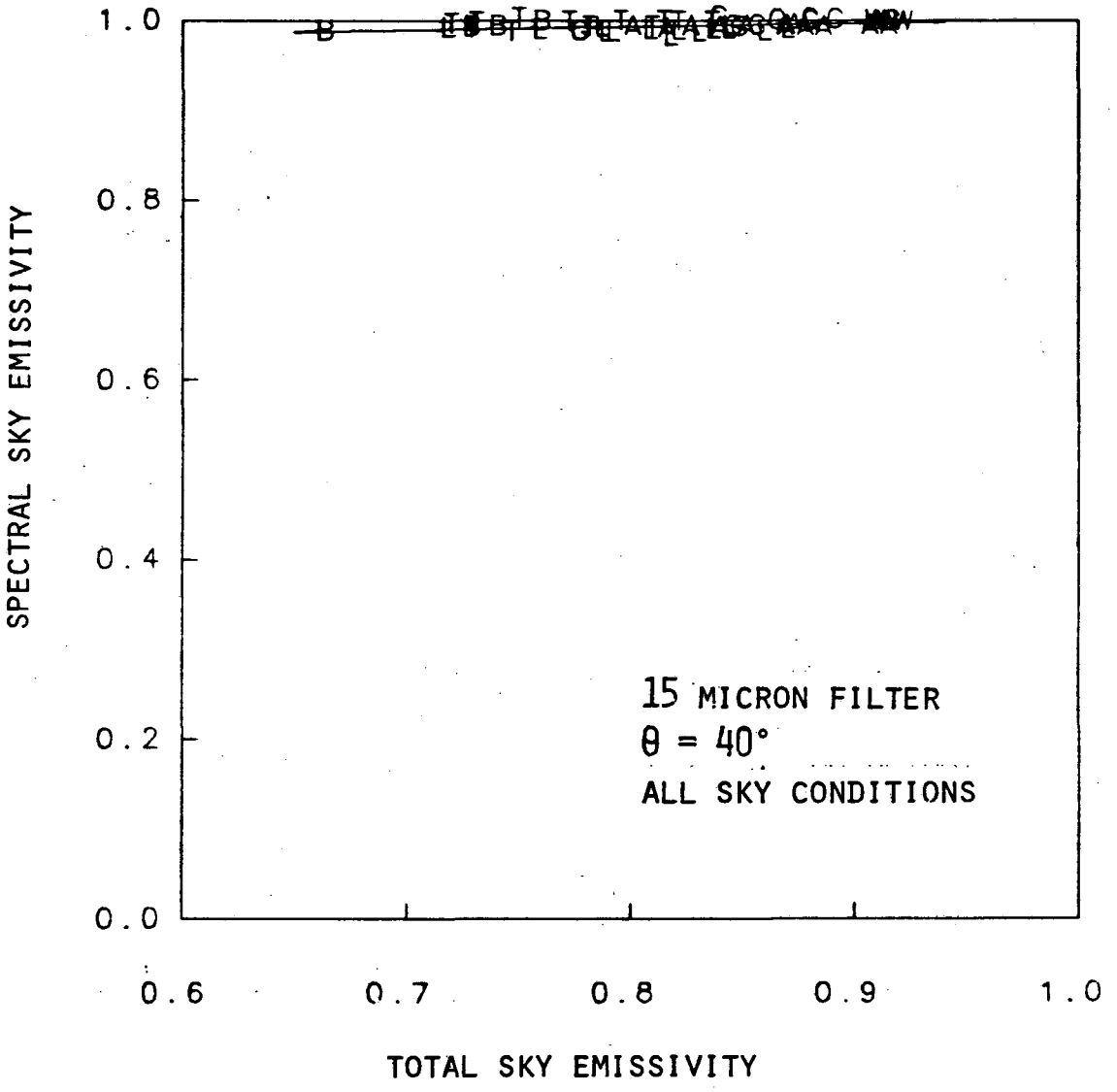
1.0
0.8
0.6
0.4
0.2
0.0
SPECTRAL SKY EMISSIVITY
15 MICRON FILTER
θ = 40°
ALL SKY CONDITIONS
0.6
0.7
0.8
0.9
1.0
TOTAL SKY EMISSIVITY

FIGURE 17D

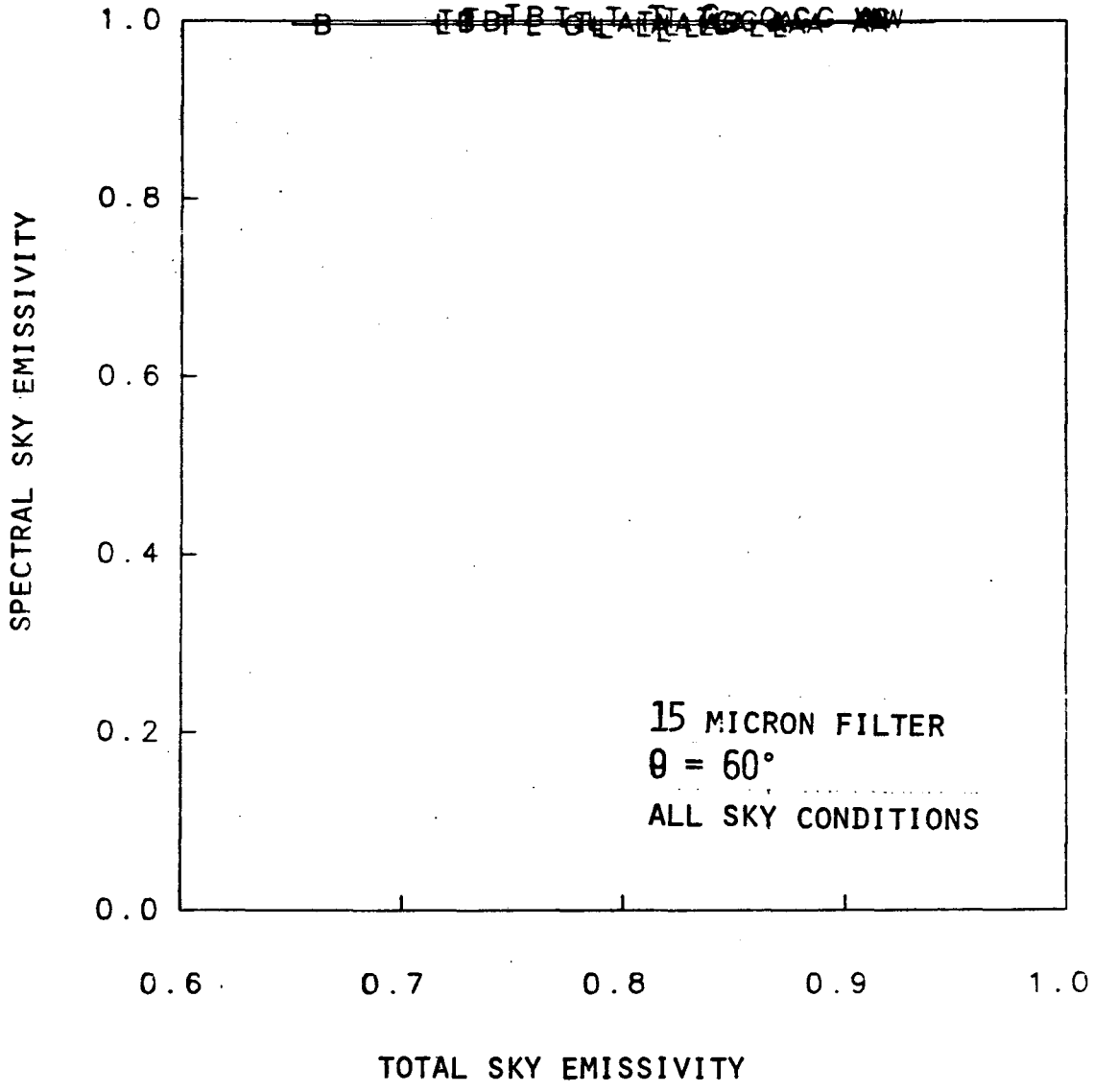
1.0
0.8
0.6
0.4
0.2
0.0
SPECTRAL SKY EMISSIVITY
15 MICRON FILTER
θ = 60°
ALL SKY CONDITIONS
0.6
0.7
0.8
0.9
1.0
TOTAL SKY EMISSIVITY

FIGURE 17E

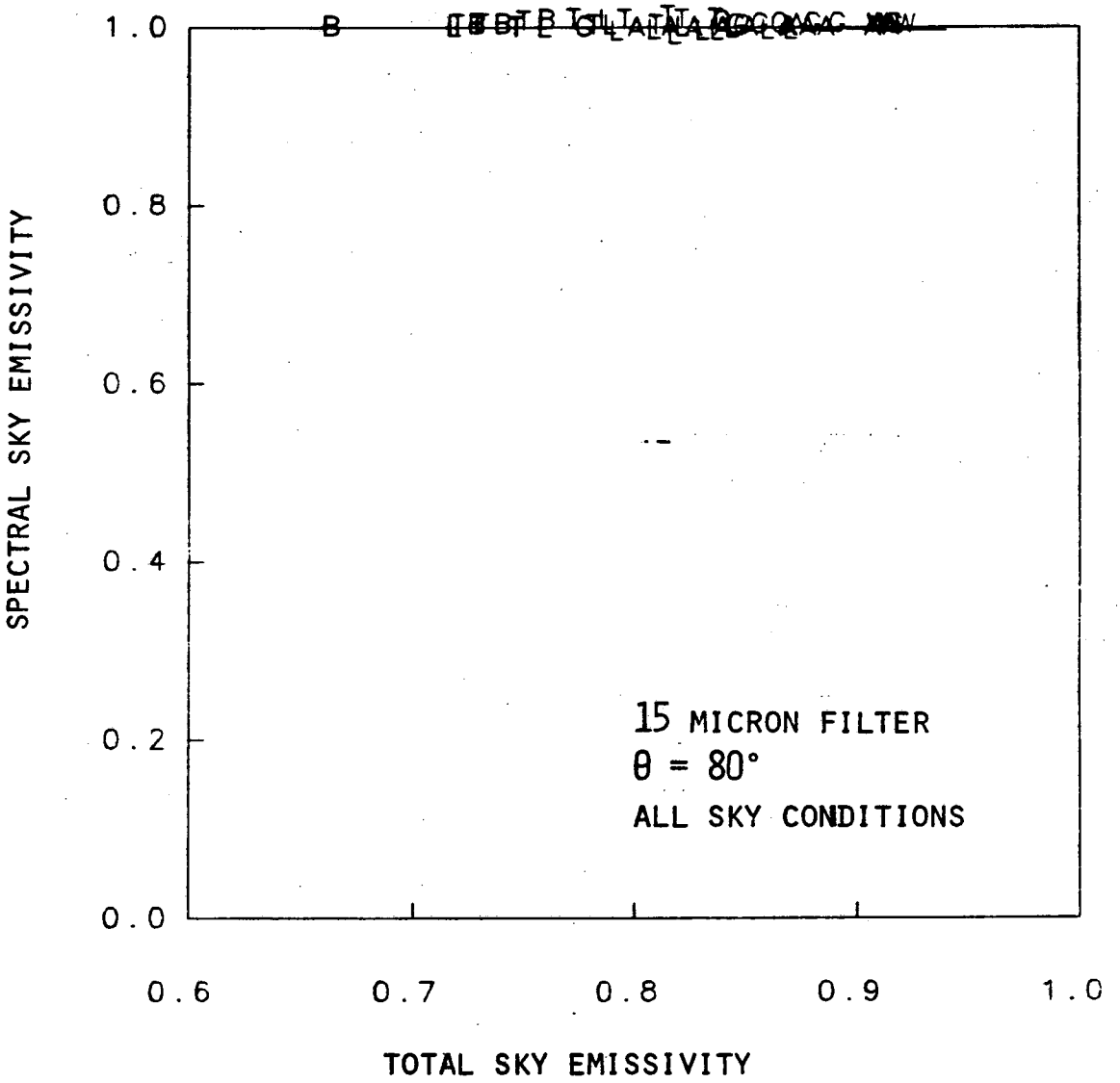
1.0
0.8
0.6
0.4
0.2
0.0
SPECTRAL SKY EMISSIVITY
15 MICRON FILTER
θ = 80°
ALL SKY CONDITIONS
0.6
0.7
0.8
0.9
1.0
TOTAL SKY EMISSIVITY

FIGURE 17F

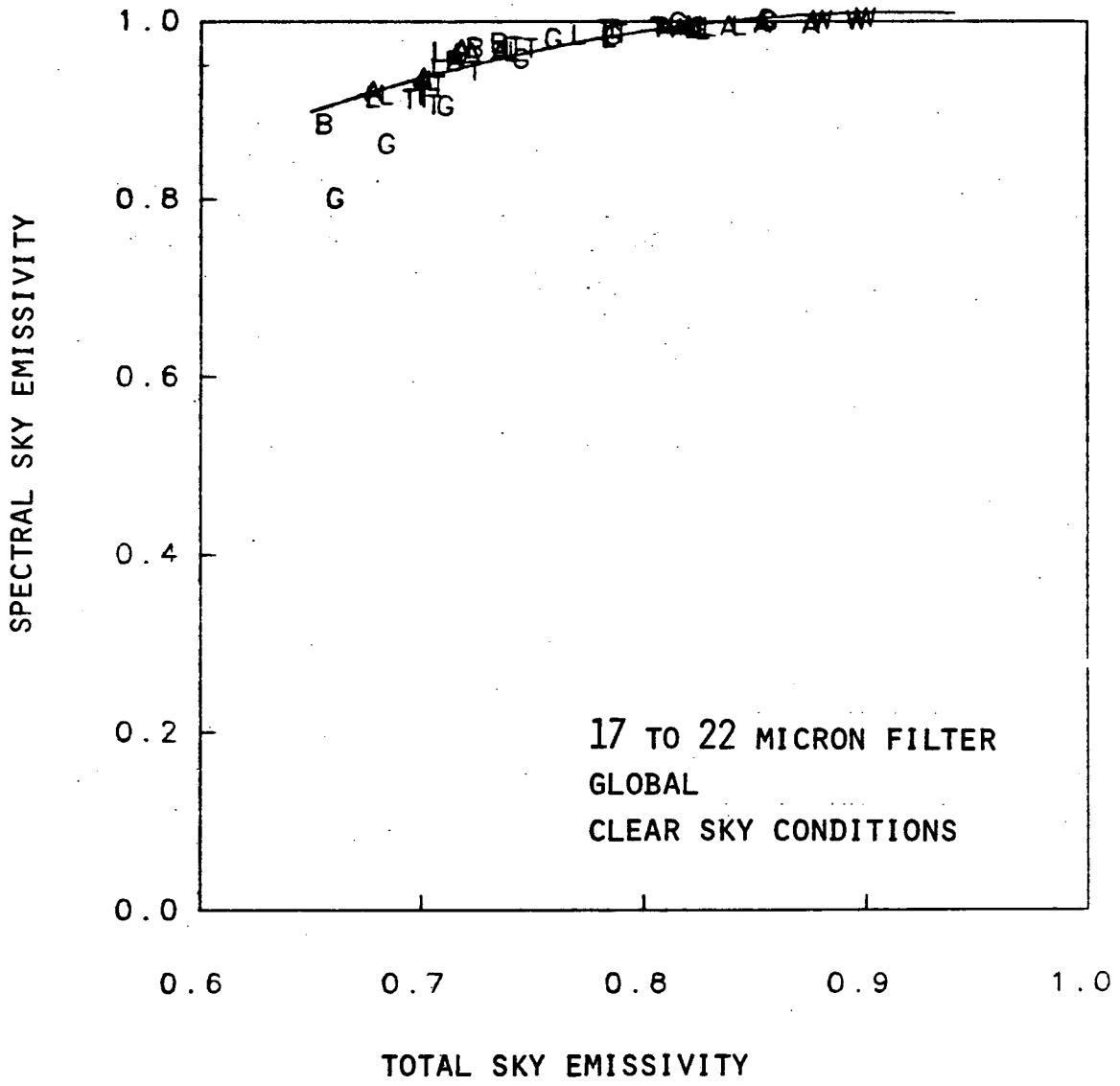
1.0
0.8
0.6
0.4
0.2
0.0
SPECTRAL SKY EMISSIVITY
0.6
0.7
0.8
0.9
1.0
TOTAL SKY EMISSIVITY
17 TO 22 MICRON FILTER
GLOBAL
CLEAR SKY CONDITIONS

FIGURE 18A

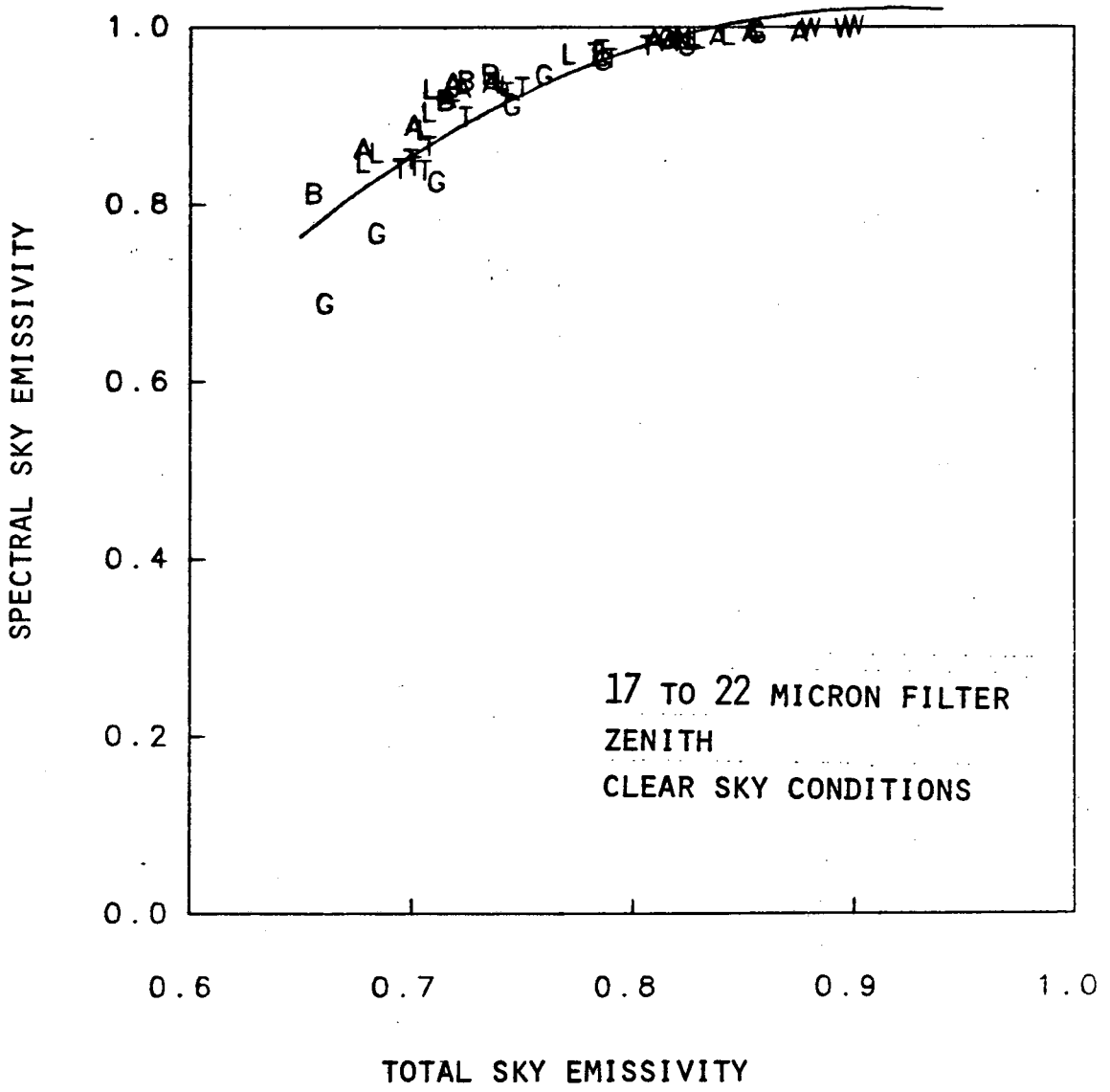
1.0
0.8
0.6
0.4
0.2
0.0
SPECTRAL SKY EMISSIVITY
0.6
0.7
0.8
0.9
1.0
TOTAL SKY EMISSIVITY
17 TO 22 MICRON FILTER
ZENITH
CLEAR SKY CONDITIONS

FIGURE 18B

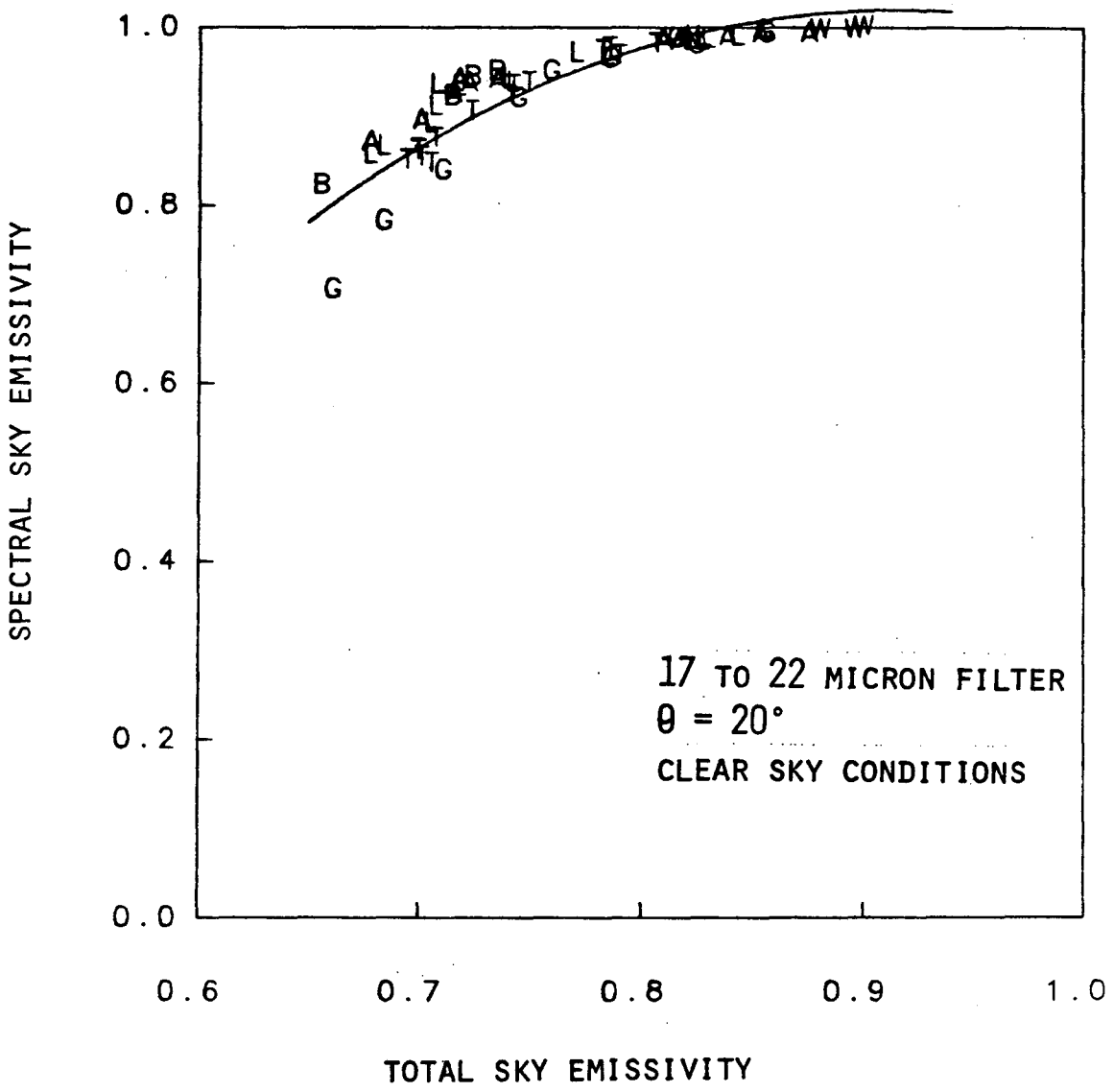
1.0
0.8
0.6
0.4
0.2
0.0
SPECTRAL SKY EMISSIVITY
0.6
0.7
0.8
0.9
1.0
TOTAL SKY EMISSIVITY
17 TO 22 MICRON FILTER
θ = 20°
CLEAR SKY CONDITIONS

FIGURE 18c

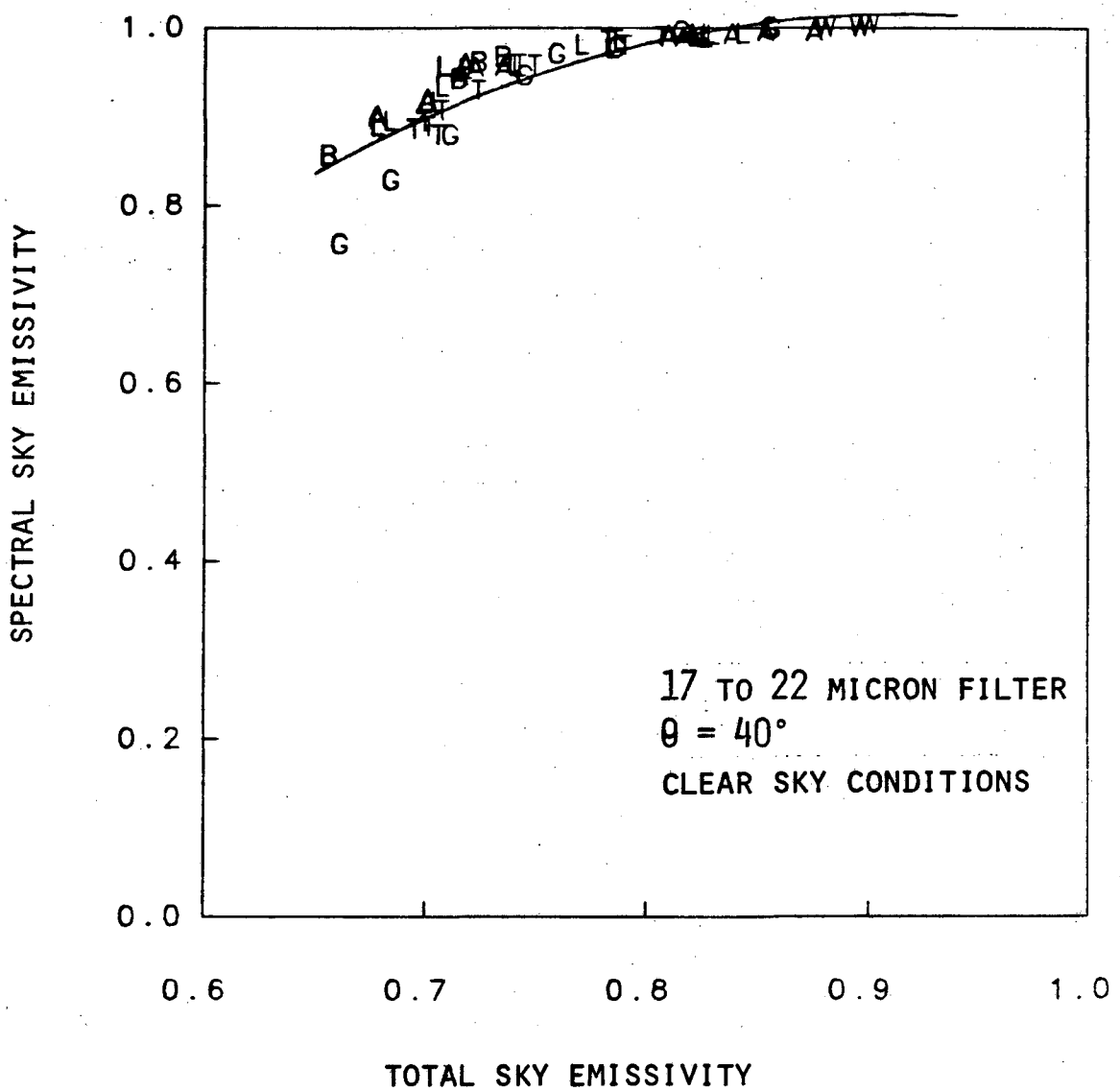
1.0
0.8
0.6
0.4
0.2
0.0
0.6
0.7
0.8
0.9
1.0
SPECTRAL SKY EMISSIVITY
TOTAL SKY EMISSIVITY
17 TO 22 MICRON FILTER
θ = 40°
CLEAR SKY CONDITIONS

FIGURE 18D

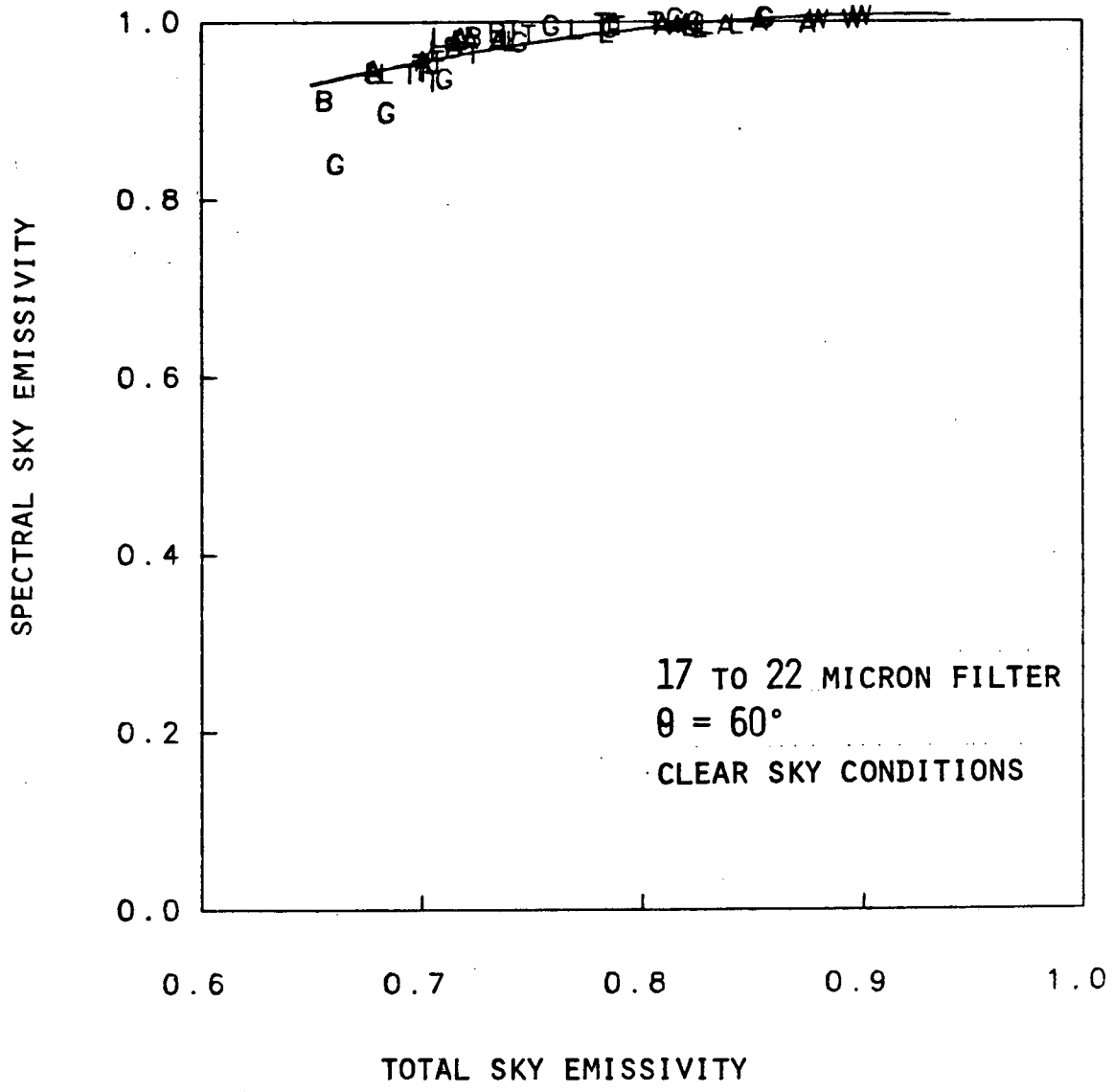
1.0
0.8
0.6
0.4
0.2
0.0
SPECTRAL SKY EMISSIVITY
17 TO 22 MICRON FILTER
θ = 60°
CLEAR SKY CONDITIONS
0.6
0.7
0.8
0.9
1.0
TOTAL SKY EMISSIVITY

FIGURE 18E

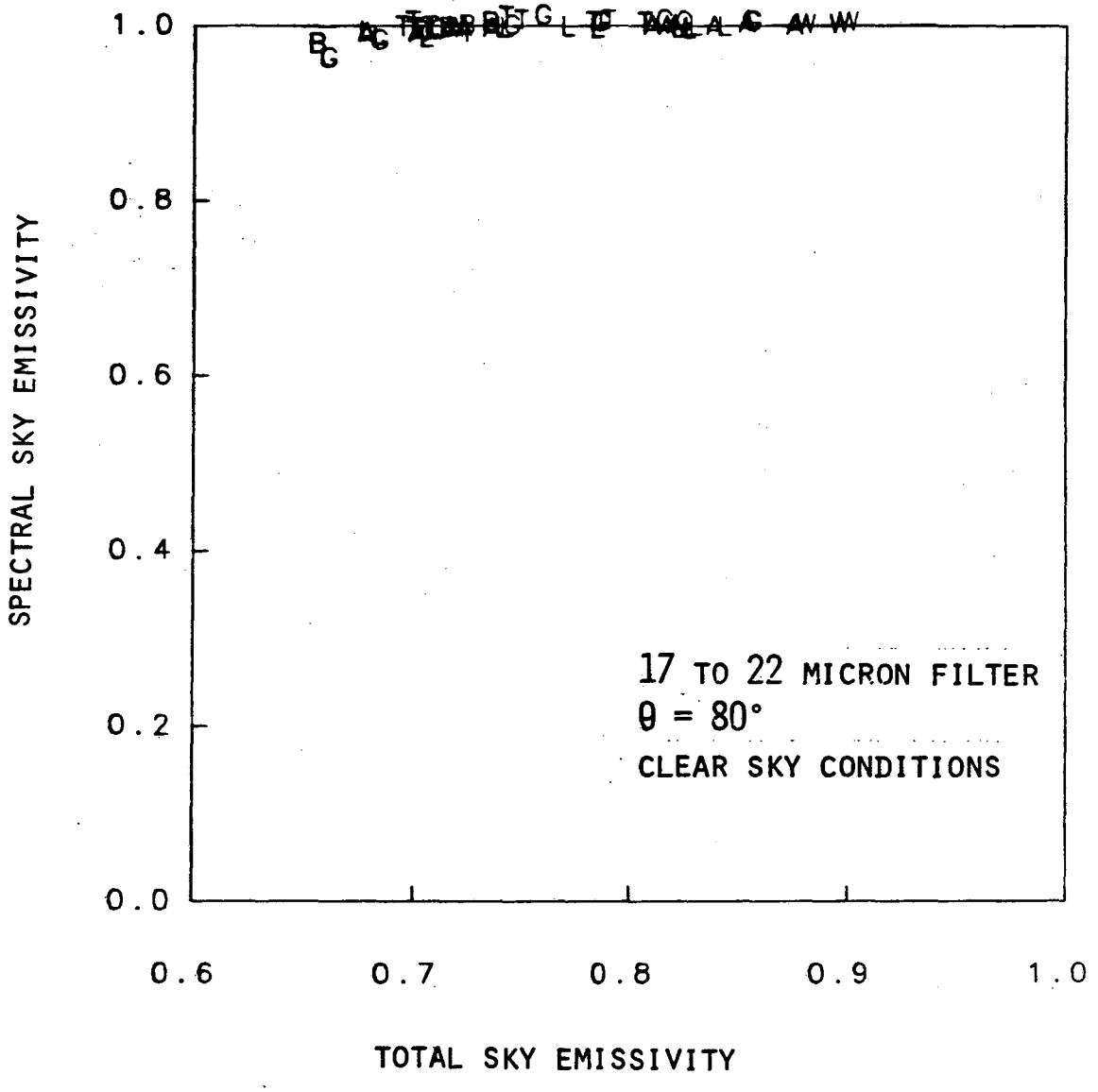
1.0
0.8
0.6
0.4
0.2
0.0
SPECTRAL SKY EMISSIVITY
17 TO 22 MICRON FILTER
θ = 80°
CLEAR SKY CONDITIONS
0.6
0.7
0.8
0.9
1.0
TOTAL SKY EMISSIVITY

FIGURE 18F

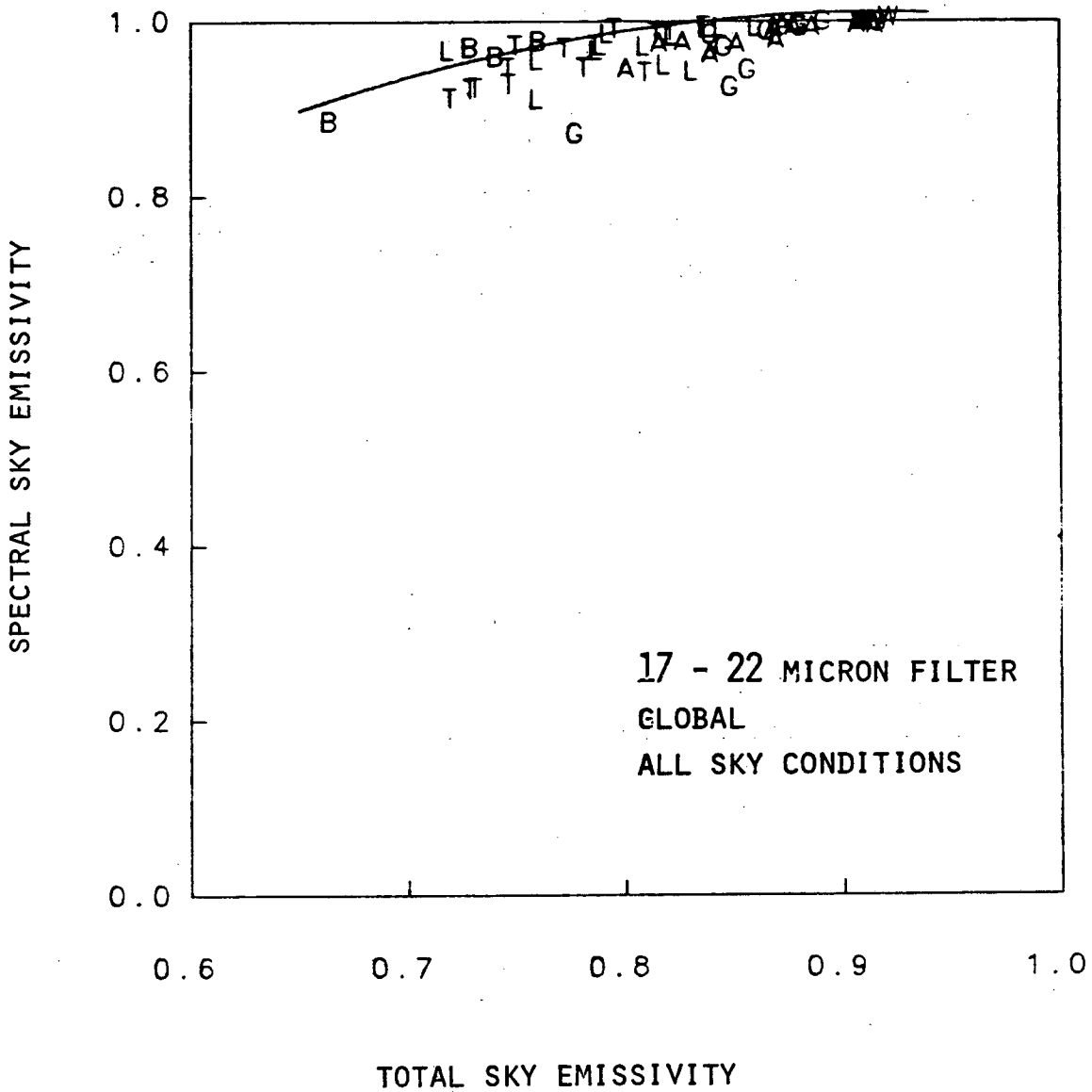
1.0
0.8
0.6
0.4
0.2
0.0
0.6
0.7
0.8
0.9
1.0
SPECTRAL SKY EMISSIVITY
TOTAL SKY EMISSIVITY
17 - 22 MICRON FILTER
GLOBAL
ALL SKY CONDITIONS

FIGURE 19A

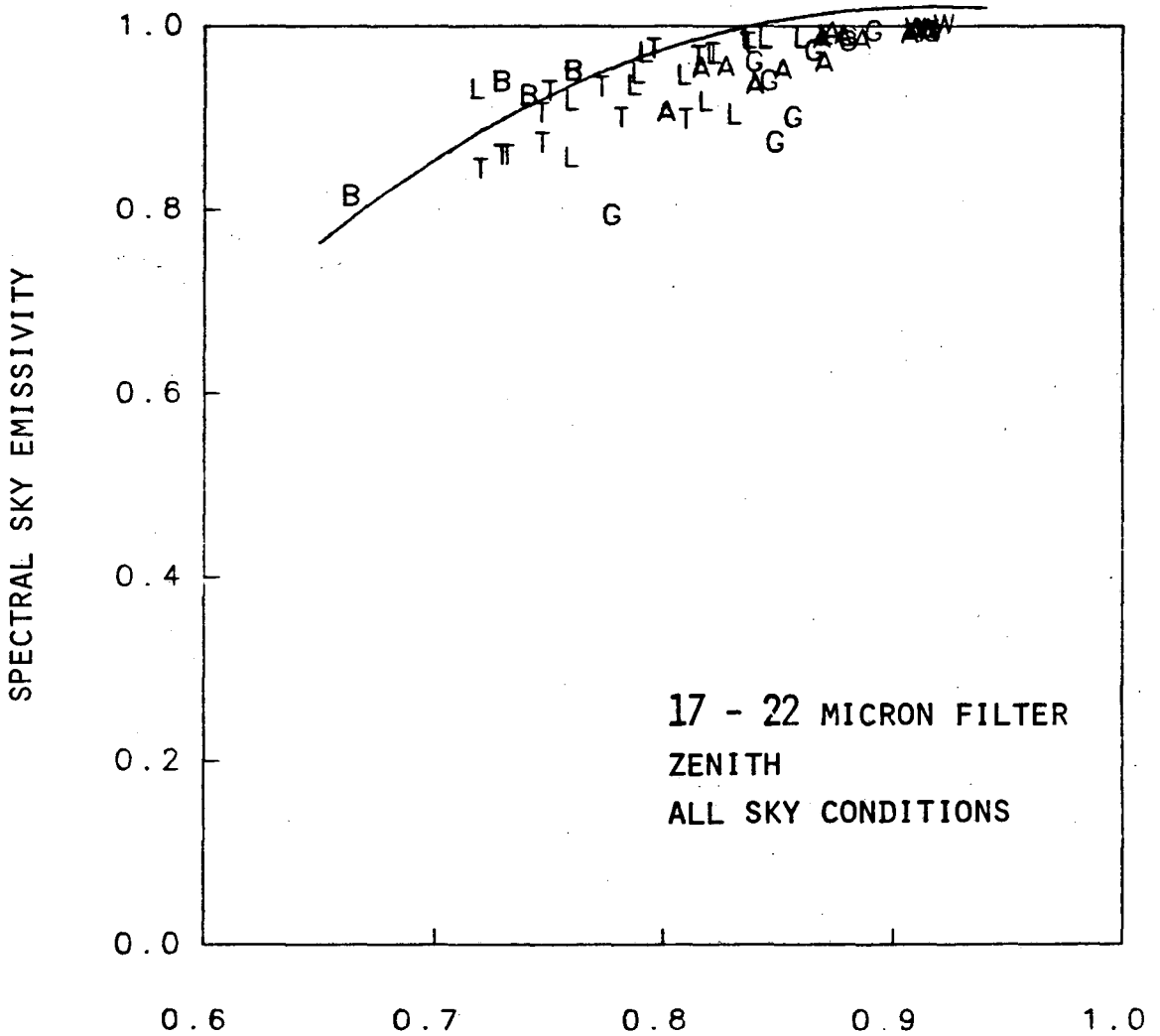
1.0
0.8
0.6
0.4
0.2
0.0
0.6
0.7
0.8
0.9
1.0
SPECTRAL SKY EMISSIVITY
TOTAL SKY EMISSIVITY
17 - 22 MICRON FILTER
ZENITH
ALL SKY CONDITIONS

FIGURE 19B

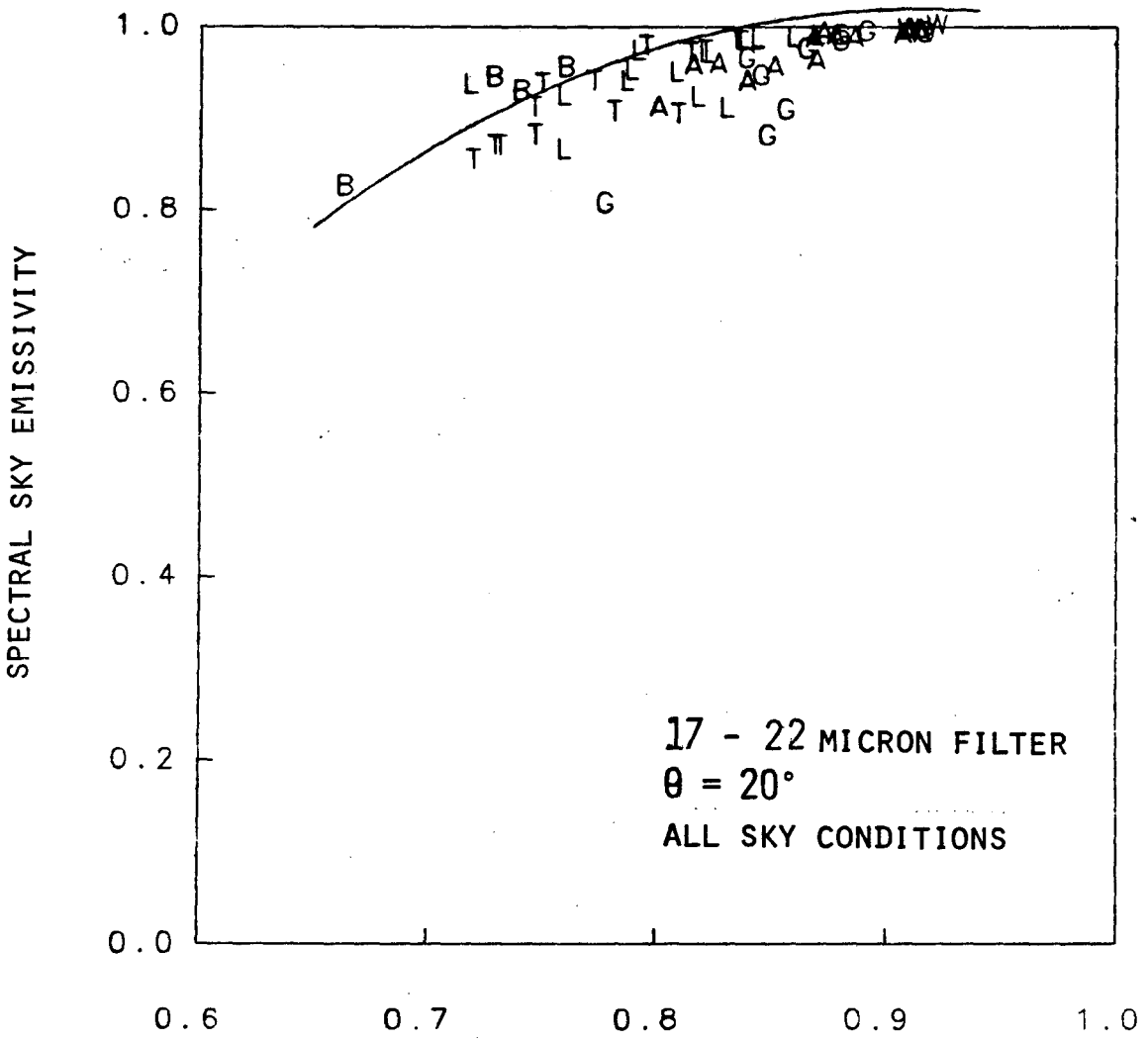
1.0
0.8
0.6
0.4
0.2
0.0
0.6
0.7
0.8
0.9
1.0
SPECTRAL SKY EMISSIVITY
TOTAL SKY EMISSIVITY
17 - 22 MICRON FILTER
θ = 20°
ALL SKY CONDITIONS

FIGURE 19c

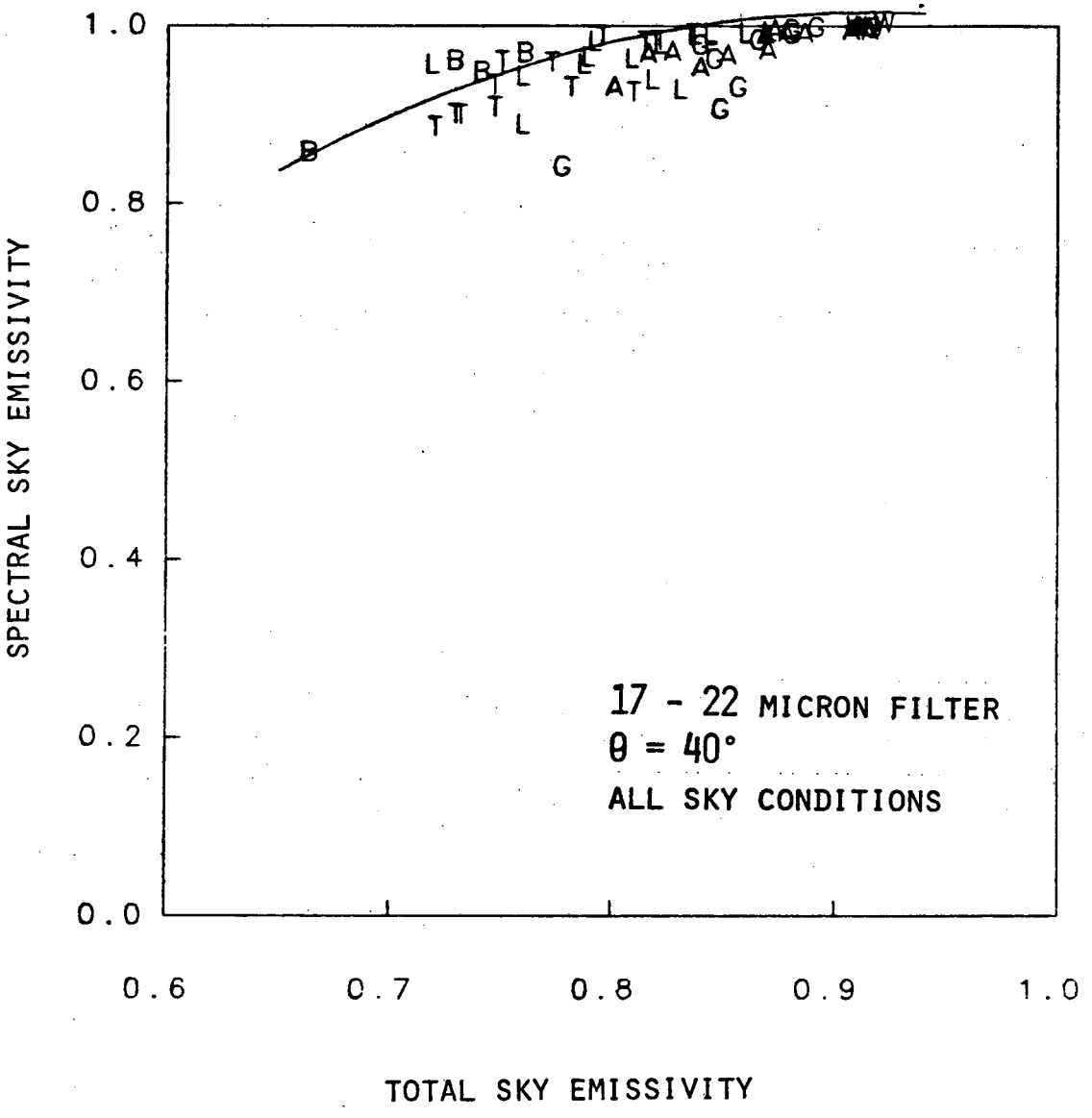
1.0
0.8
0.6
0.4
0.2
0.0
0.6
0.7
0.8
0.9
1.0
SPECTRAL SKY EMISSIVITY
TOTAL SKY EMISSIVITY
17 - 22 MICRON FILTER
θ = 40°
ALL SKY CONDITIONS

FIGURE 19D

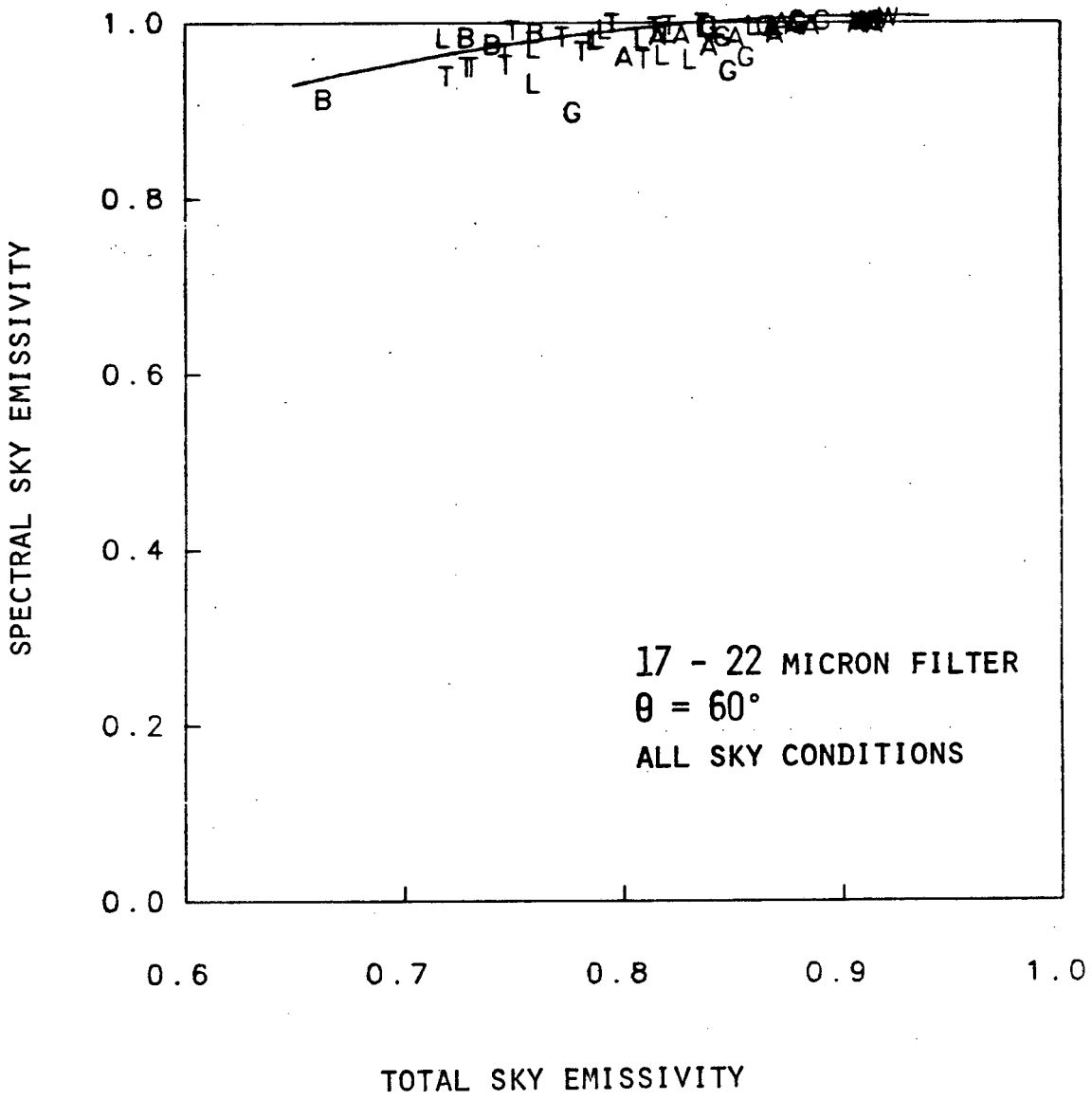
1.0
0.8
0.6
0.4
0.2
0.0
0.6
0.7
0.8
0.9
1.0
SPECTRAL SKY EMISSIVITY
TOTAL SKY EMISSIVITY
17 - 22 MICRON FILTER
θ = 60°
ALL SKY CONDITIONS

FIGURE 19E

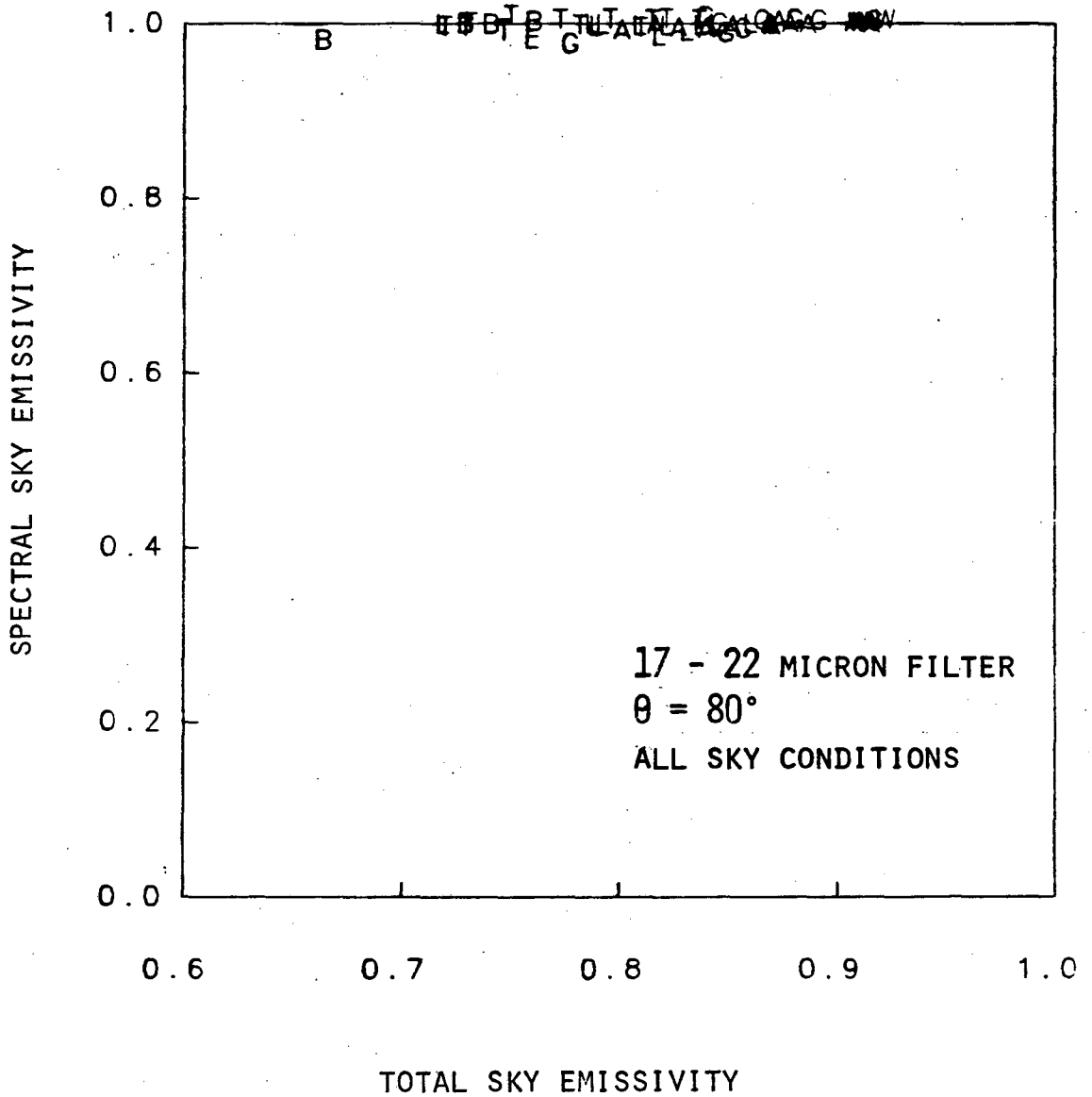
1.0
0.8
0.6
0.4
0.2
0.0
SPECTRAL SKY EMISSIVITY
17 - 22 MICRON FILTER
θ = 80°
ALL SKY CONDITIONS
0.6
0.7
0.8
0.9
1.0
TOTAL SKY EMISSIVITY

FIGURE 19F

This report was done with support from the Department of Energy. Any conclusions or opinions expressed in this report represent solely those of the author(s) and not necessarily those of The Regents of the University of California, the Lawrence Berkeley Laboratory or the Department of Energy.

Reference to a company or product name does not imply approval or recommendation of the product by the University of California or the U.S. Department of Energy to the exclusion of others that may be suitable.

TECHNICAL INFORMATION DEPARTMENT
LAWRENCE BERKELEY LABORATORY
UNIVERSITY OF CALIFORNIA
BERKELEY, CALIFORNIA 94720